NASA CR-54559
PWA FR-2641

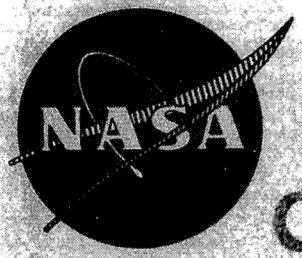

SINGLE STAGE EXPERIMENTAL EVALUATION OF VARIABLE GEOMETRY INLET GUIDE VANES AND STATOR BLADING

PART VI- FINAL REPORT

By
B. A. Jones

Prepared For
National Aeronautics and Space Administration
Contract NAS3-7604

Pratt & Whitney Aircraft DIVISION OF UNITED AIRCRAFT CORPORATION
FLORIDA RESEARCH AND DEVELOPMENT CENTER
BOX 2691, WEST PALM BEACH, FLORIDA 33402

NASA CR-54559
PWA FR-2641

SINGLE STAGE EXPERIMENTAL EVALUATION OF VARIABLE GEOMENTRY INLET GUIDE VANES AND STATOR BLADING

PART VI- FINAL REPORT

By
B. A. Jones

Prepared For
National Aeronautics And Space Administration
15 March 1970

Contract NAS3-7604

Technical Management
NASA Lewis Research Center
Cleveland, Ohio

L. Joseph Herrig,
NASA Program Manager
Fluid System Components Division

Pratt & Whitney Aircraft DIVISION OF UNITED AIRCRAFT CORPORATION
FLORIDA RESEARCH AND DEVELOPMENT CENTER
BOX 2691, WEST PALM BEACH, FLORIDA 33402

ABSTRACT

An analytical and experimental investigation was conducted to determine the extent that variable geometry inlet guide vanes and stators can extend the stable operating range of a supersonic-cruise turbine engine compressor front stage. The variable geometry guide vanes and stators, tested with uniform and distorted inlet flow in a 0.5 hub-tip ratio single-stage compressor, provided efficient, stable operation between the sea level takeoff (SLTO) design point and a Mach 3.0 cruise design point selected at 70% of the SLTO design corrected rotor speed and 54% of the design corrected flow.

TABLE OF CONTENTS

TABLE OF CONTENTS (Continued)

LIST OF ILLUSTRATIONS

LIST OF ILLUSTRATIONS (Continued)

LIST OF ILLUSTRATIONS (Continued)

LIST OF ILLUSTRATIONS (Continued)

LIST OF ILLUSTRATIONS (Concluded)

SINGLE STAGE EXPERIMENTAL EVALUATION OF STATOR BLADING AND VARIABLE GEOMETRY INLET GUIDE VANES PART VI - FINAL REPORT

B. A. JONES

PRATT & WHITNEY AIRCRAFT
FLORIDA RESEARCH AND DEVELOPMENT CENTER

SUMMARY

An analytical and experimental investigation was conducted with a single-stage compressor to determine the extent that variable geometry inlet guide vanes and stators can extend the stable operating range of supersonic cruise Mach number turbine engine compressor front stages. Velocity diagrams were analyzed for two design operating conditions: sea level takeoff (SLTO) and a supersonic cruise Mach number of approximately 3.0 at altitude. A variable camber inlet guide vane, rotor, and two variable-geometry stator configurations (designated Stator A and Stator B) were designed, fabricated, and tested with uniform inlet flow over a range of rotor speeds from 50 to 110% of the SLTO design corrected rotor speed. Overall performance tests with circumferential and radial inlet flow distortions were conducted on the stage with Stator B.

The compressor stage had a rotor hub-tip ratio of approximately 0.5 and a rotor tip diameter of approximately 43 inches, and in general resembled the front stage of a supersonic cruise engine compressor. The variable geometry guide vanes were designed with 63-Series airfoils and comprised a fixed forward segment and two articulated flaps. The rotor was designed with circular arc airfoils and had a tip inlet relative Mach number of 1.15. The variable geometry stators were designed with 65-Series airfoils. Stator A was designed with a fixed forward segment and an adjustable flap, whereas Stator B was designed with two adjustable segments that permitted variation of both the leading and trailing edge metal angles.

The Stator A and Stator B stage SLTO and cruise configurations met or exceeded their respective SLTO and Mach 3.0 cruise design overall performance goals. At 70% of the SLTO design corrected rotor speed and corresponding corrected flow (approximately equivalent to a Mach 3.0 cruise flight condition), the variable geometry features of the guide vane and Stators A and B provided a 7.2-point improvement in efficiency over that obtained with the SLTO (fixed geometry) configuration. Also, the cruise configuration permitted efficient, stable operation at lower flows than those attainable at equal rotor speeds with the SLTO configuration.

The Stator A configuration, with one adjustable segment, provided better blade element performance than that obtained with the Stator B configuration which had two adjustable segments.

Both the radial and circumferential inlet flow distortion caused a large loss of Stator B stage stall margin. For distorted inlet flow conditions, the variable camber inlet guide vane restored more than half of the stall margin degradation due to inlet flow distortion.

INTRODUCTION

Compressors for advanced supersonic cruise aircraft must operate efficiently over a wide range of flow and rotor speed. As cruise flight speed increases above Mach 1.0, it becomes increasingly difficult to meet prescribed performance levels at both sea level takeoff (SLTO) and cruise operating conditions with a fixed-geometry compressor. The problem arises primarily from the compressor inlet temperature increase due to ram compression at supersonic cruise Mach numbers; if the compressor is maintained at the same mechanical speed to limit stresses, the corrected speed is significantly reduced. The associated changes in corrected flow (and blading incidence angles) and pressure ratio cause compressor front stages to operate closer to their stall limit, and rear stages to operate closer to their maximum flow limit relative to their respective SLTO operating conditions. The stage matching problem at supersonic cruise conditions is thus more critical for the front stages than for the rear stages. Adequate stall margin must be provided in the inlet stages to prevent the onset of rotating stall. At supersonic flight speeds the inlet flow becomes distorted, which adds to the possibility of stage stall and compressor surge.

One method that can be used to increase the stable operating range of compressor stages involves the use of variable geometry blading to accommodate the blade element velocity triangle changes at off-design operating conditions. The extent that variable geometry inlet guide vanes and variable geometry stator blade rows can extend the stable operating range of a typical Mach 3.0 cruise engine compressor front stage, and an evaluation of the mechanical aspects of variable geometry hardware required for this purpose, were the subject of the analytical and experimental investigation reported herein.

Reference 1 presents the results of a preliminary analysis of the effectiveness of variable-geometry guide vanes to control rotor inlet flow conditions. The results of this analysis indicate trends of rotor incidence and flow rematching at off-design conditions that can be expected with various mathematically-described rotor inlet swirl patterns. Details of the design analysis and aerodynamic design of the variable geometry blading and test rig for the program reported herein are presented in reference 2. The results of the reference 2 design analysis support some of the important trends noted in reference 1.

The variable geometry inlet guide vane and stator investigation was accomplished in three steps. Initially, a meanline analysis was performed to select the type of stage, characterized by rotor prewhirl distribution, that would be best suited for the employment of variable geometry features. An aerodynamic design analysis was subsequently performed to define the blade element velocity triangles at specified SLTO and cruise operating conditions. Finally, a variable camber inlet guide vane, rotor, and two variable geometry stator configurations

(designated Stator A and Stator B) were designed, fabricated, and tested with uniform inlet flow over a range of corrected rotor speeds from 50 to 110% of the SLTO corrected design rotor speed. The stage with Stator B was used for subsequent overall performance tests with radially and circumferentially distorted inlet flow.

The variable camber inlet guide vanes were designed to provide zero prewhirl at the SLTO design point and a near-linear distribution of 35 degrees hub prewhirl to 20 degrees tip prewhirl at the cruise design point. The two variable geometry stator configurations were designed to turn the flow to the near-axial direction at the SLTO design point, and to provide an average swirl of 27.5 degrees into a hypothetical second stage rotor at the cruise design point. The rotor was designed with a tip relative inlet Mach number of 1.15, and a pressure ratio of 1.35. The rotor inlet hub-tip ratio was approximately 0.5 and the rotor tip diameter was approximately 43.0 inches.

Experimental results obtained with the Stator A and Stator B stage configurations are detailed in references 3 and 4, respectively. Reference 5 presents the results obtained with the Stator B configuration with inlet flow distortion. Reference 6 presents the results of exploratory tests, performed in an annular cascade as part of the design effort, of two variable geometry guide vane configurations and a stator having a leading edge slot for improved flow turning at high off-design incidence.

This report summarizes the analytical and experimental results of the overall program with specific reference to the prescribed SLTO and cruise design performance objectives.

DESIGN APPROACH

The design selections for the variable geometry stage were accomplished in the following steps:

1. Analysis of stage types for the application of variable geometry features.

2. Analysis of SLTO design point vector diagrams and blade geometry.

3. Analysis of the cruise design point vector diagrams and evaluation of cruise design point geometry requirements for rematching blade rows at the cruise design point conditions.

4. Selection of variable geometry features to satisfy cruise geometry requirements.

Stage Type Analysis

Preliminary evaluation of stage types characterized by rotor prewhirl indicated that a zero prewhirl SLTO design point stage would produce the largest change of rotor incidence per degree change in prewhirl at off-design conditions (figure 4a of reference 2). For the analysis reported herein, the flowpath geometry and SLTO performance of a high cruise Mach number production engine compressor front stage were used. For cruise performance analysis, a corrected rotor speed of 70% of the SLTO design corrected speed, and a corrected flow corresponding to a flight Mach number of approximately 3.0 at 65,000 ft altitude were specified. The SLTO design point rotor inlet swirl angle at the meanline diameter was varied from -30 to +30 degrees without regard to the influence of swirl distribution on axial velocity distribution (i.e., the meanline axial velocity was maintained constant over the range of meanline swirl angles). Both the SLTO guide vane exit swirl angle, and a 25-degree increase in guide vane exit swirl angle over that for SLTO were considered in the cruise condition analysis.

The stage type analysis showed that: (1) operation at rotor speed and flow typical of Mach 3.0 cruise conditions with a fixed-geometry front stage may be unstable, (2) an increase in rotor inlet swirl angle at cruise conditions tends to restore the rotor inlet relative air angle to the stable operating region, and (3) as mentioned above, the most effective change in cruise relative air angle produced by a change in swirl angle is obtained when the SLTO design point swirl is zero. These observations are generally consistent with the results of the reference 1 analysis. A more complete discussion of this stage type analysis is given in reference 2.

SLTO Design Point Analysis

The SLTO design operating point was based on the following specified rotor design conditions:

1. Tip inlet relative Mach number of approximately 1.1

2. Tip diffusion factor between 0.3 and 0.4

3. Pressure ratio, 1.35

4. Constant hub-to-tip exit total pressure.

The stage flowpath geometry, blade row solidities, and blade thickness ratios and chord lengths were similar to those for the front stage of a state-of-the-art supersonic cruise Mach number engine compressor.

The stage flowpath geometry is shown in figure 1. The flowpath model for vector diagram analysis is shown in figure 2, and streamline diameters for design and experimental data reported herein are presented in table 1.

The 63-Series airfoil sections were selected (on the basis of the cruise operation turning requirements discussed in the following section) for the inlet guide vane design, and the data presented in reference 7 was used as a guideline for the selection of guide vane leading and trailing edge angles. A guide vane loss coefficient of 0.134, constant across the span, was used in the vector diagram analysis. This relatively high loss coefficient was selected to account for the anticipated effect of surface irregularities of the uncambered guide vane on loss. The rotor blades were comprised of circular arc airfoil sections. A photograph of the rotor assembly is shown in figure 3; a part-span shroud was located at 40% span from the tip to avoid stall flutter. The stator vanes were comprised of 65-Series airfoil sections and were designed to turn the stage exit flow to the near-axial direction. Pratt & Whitney Aircraft experimental data correlations of loss coefficient, incidence angle, and Mach number for circular arc and 65-Series airfoils, and the NASA deviation angle calculation method of reference 8 were utilized in the rotor and stator blading design. The resulting SLTO design point conditions and predicted overall performance are listed in table 2. Design point blade element velocity diagram data and geometry details for the guide vane, rotor, and stator are presented in tables 3 through 8. Incidence and deviation angles, and leading and trailing edge metal angles for the 65-Series airfoil stators are referred to equivalent circular arc meanline distributions. For the 63-Series airfoil inlet guide vanes, leading and trailing edge metal angles are based on tangents to the meanline at 0.5 and 95 percent chord locations, respectively. Performance variables are defined in Appendis A; symbols are defined in Appendix B.

Cruise Design Point Analysis

The cruise design point rotor speed was arbitrarily selected at 70% of the SLTO design corrected rotor speed. This rotor speed and the corresponding weight flow of 143.3 lb/sec were selected to be typical of the requirements for a cruise Mach number of approximately 3.0. Velocity diagrams calculated for the specified cruise conditions were combined with the SLTO blading geometries to determine the extent of blade section incidence mismatch and the approximate magnitude of blade row geometry change required to satisfy the cruise velocity diagrams. The incidence angle mismatch results thus obtained are summarized in figure 4 for the rotor, stator, and a hypothetical second stage rotor.

Inlet Guide Vane Exit Air Angle Distribution

Inlet guide vane and stator exit air angle distributions required to restore the first and second stage rotor blade incidence angles to acceptable levels were analyzed. The analysis of inlet guide vane swirl distributions indicated that the rotor tip incidence angle is relatively insensitive to swirl angle change compared to the hub section sensitivity. This observation is illustrated in figure 5, where rotor incidence angle at 10 and 90% span locations is plotted as a function of hub swirl angle for 20 and 30 degrees of tip swirl angle. Tip and hub section low-loss incidence angle ranges are indicated on the figure. For an increase in swirl angle from zero to a linear distribution of 37 degrees at the hub to 30 degrees at the tip, the hub incidence was decreased from 17 degrees (90% span in figure 4) to -8 degrees (figure 5) whereas the tip incidence was decreased from 7.5 degrees to 4.8 degrees. It is apparent from the shape of the curves in this figure that further increases in either tip or hub swirl to decrease rotor tip incidence angles will result in a hub choking limitation.

The composite of linear swirl distributions in figure 5 embodies a variety of tangential velocity distributions. In this respect, some qualitative comparisons can be made with the results of the reference 1 analysis. Swirl distributions of interest for comparative purposes from the present investigation are the 45-degree hub - 20-degree tip and the 10-degree hub - 30-degree tip distributions, since these extremes roughly approximate the B/r and Dr tangential velocity distributions of reference 1, as shown in figure 6. The trends of incidence angle change noted in figure 5 for these two swirl distributions are similar to those obtained in the reference 1 analysis for the Dr and B/r tangential velocity distributions, as shown in figure 7. Reference 1 shows that the relative sensitivity of rotor hub and tip incidence angles to swirl angle change is caused primarily by the redistribution of axial velocity to satisfy radial equilibrium conditions.

For the B/r tangential velocity distribution, the axial velocity is approximately constant from hub to tip. Since the B/r distribution has a higher hub swirl relative to the tip swirl (figure 6), a choking limitation is reached in the hub region before large changes in tip incidence can be achieved (figures 5 and 7). If the hub swirl is reduced relative to the tip swirl (constant Dr distribution) to alleviate the hub choking condition, the tip axial velocity decreases relative to the hub axial velocity. This change in axial velocity also limits the reduction in tip incidence angle that can be achieved. However, the use of guide vane turning reduces the axial velocity ratio across the rotor tip section and thereby reduces the blade loading in this region; thus a somewhat higher stalling incidence angle can be achieved.

The final selection of inlet guide vane swirl distribution to rematch the rotor at cruise operating conditions included the effects of streamline curvature and radial entropy gradients. Additional

criteria that were used in the analysis for the selection of the cruise swirl distribution were: (1) acceptable levels of rotor hub and tip loading in terms of static pressure rise coefficient; (2) acceptable level of stator exit axial velocity; and (3) equal hub and tip rotor exit absolute air angle change between SLTO and cruise design points. The latter criterion was a mechanical design consideration for the variable leading edge geometry Stator B.

The inlet guide vane swirl distribution (35-degree hub - 20-degree tip) that was selected as a result of all of the above considerations is compared in figure 8 with the tangential velocity distributions that were analyzed in reference 1. It is seen in the figure that the selected swirl distribution roughly approximates the B/r distribution, even though the C, Dr, and Er^2 type distributions (see reference 1) were considered to be more attractive than the B/r distribution from the standpoint of potential range improvement and the degree of mechanical complexity. This selection of swirl distribution was influenced by the foregoing criterion which concerns the relative change in rotor hub and tip section exit air angle. Curves of rotor hub and tip exit air angle are shown as functions of swirl distribution in figure 9. Points of intersection of the rotor hub and tip curves were considered to represent acceptable swirl distributions provided that the other criteria for the selection of swirl distribution were satisfied. Thus, the point of intersection at β_1 (hub) = 40 degrees (β_1 (tip) = 30 degrees) was unacceptable because of the rotor hub choking limitation (figure 5). Note that this point is closest to the B/r distribution indicated in figure 9. The point of intersection at β_1 (hub) = 35 degrees (β_1 (tip) = 20 degrees) provides a better rotor hub incidence angle, as seen in figure 5. The change in rotor tip incidence angle for the 35-degree hub - 20-degree tip swirl distribution is only one degree less than the incidence change for the 40-degree hub - 30-degree tip swirl distribution. The C, Dr, and Er^2 tangential velocity distributions indicated in figure 9 result in large differences in the rotor hub and tip exit air angles.

Stator Exit Air Angle Distribution

A similar analysis was performed to select the stator exit swirl distribution that could restore the hypothetical second-stage rotor incidence angles to their stable operating range. With first-rotor prewhirl set at the 35-degree hub - 20-degree tip distribution, second-stage rotor hub and tip incidence angles were evaluated as functions of stator exit air angle, as shown in figure 10. The radial distributions of stator exit axial velocity were modified as required for the various stator exit air angle distributions to satisfy simple radial equilibrium. A stator exit air angle distribution of approximately 29 degrees hub - 26.5 degrees tip was selected within the low-loss incidence region indicated in figure 10. This radial variation of incidence angle is consistent with that attainable from simple blade geometry changes.

Cruise Design Point Velocity Diagrams and Predicted Performance

With the inlet guide vane and stator exit air angles established as described in the foregoing paragraphs, cruise velocity diagrams were calculated for the specified cruise corrected rotor speed and flow conditions. It is noted that the loss for a variable geometry stator in the cruise configuration was assumed to be the same as the loss for a conventional stator designed for the same air turning. The resulting cruise design point velocity diagram data for the inlet guide vane, rotor, and stators are summarized in tables 3, 5, and 7, respectively.

Predicted overall performance for the cruise design point is presented in table 2.

Variable Geometry Selections

Criteria for the selection of variable geometry features for the inlet guide vanes and stators included consideration of aerodynamic shape in the SLTO and cruise configurations, and mechanical design complexity.

Inlet Guide Vane Geometry

Two candidate inlet guide vane configurations were evaluated in an annular cascade (reference 6). One configuration had a fixed forward segment and two articulated flaps (variable camber). The other configuration had three flap sections that resembled a venetian blind. The variable camber configuration was selected on the basis of lower losses in the uncambered (zero swirl) position. Although the variable camber guide vane design was mechanically more complex than a conventional single-flap guide vane, it provided relatively smooth meanline coordinate distributions over the required range of camber angles.

Hub, midspan, and tip sections of the variable camber inlet guide vane in the SLTO and cruise configuration are shown in figure 11. The design camber of the inlet guide vanes was less than that required for the total desired turning. This was done to minimize surface irregularities when the vanes are uncambered for SLTO operating conditions (zero swirl). The total desired turning for operation at cruise conditions was obtained by cambering the vanes past the design camber. A slot between the two flap segments in the cruise configuration can be noted in figure 11. This slot was provided to aid flow turning at the high camber angles. The slot width increases with increasing camber angle.

Blade element geometry details for the design camber (basic airfoil) inlet guide vane and for the cruise configuration of the inlet guide vane are presented in table 4. Additional details of the aerodynamic and mechanical design of the variable camber inlet guide vane are given in reference 2. A photograph of the guide vanes installed in

the test rig is shown in figure 12. Details of the guide vane actuation linkage are illustrated in figure 13. Actuation of the two flap segments was synchronized through a single actuation lever.

Stator Geometry

Two variable geometry stator configurations were designed. Stator A consisted of a fixed-position leading edge segment and a flap. Stator B was divided into two rotatable segments that permitted changes to both the leading and trailing edge metal angles. Hub, midspan, and tip sections of Stator A and Stator B are shown in figures 14 and 15, respectively.

Both stator configurations were designed with the same camber angle distribution for SLTO operating conditions. For cruise operating conditions the Stator A flap was reset 26 degrees; the Stator B forward segment was reset 9 degrees and the Stator B rear segment was reset 26 degrees. Because of the stationary forward segment, Stator A was required to operate with very high incidence angles at cruise conditions. In the initial design (reference 6) a slot was incorporated near the leading edge of the stationary segment to improve flow turning at cruise operating conditions. Exploratory tests conducted at NASA-Lewis Research Center, however, indicated that the slot would not be required for the cruise operating conditions; therefore, Stator A was tested without a slot.

Photographs of the two stator assemblies are shown in figures 16 and 17. Two actuation levers were required for the independent control of leading and trailing edge metal angles of Stator B; one actuation lever was required for Stator A.

Blade element geometry data for Stator A and Stator B in their cruise configuration are presented in table 8. Additional information concerning the aerodynamic and mechanical design of the two stator configurations in presented in reference 2.

Incidence Angle Distributions for Cruise Configuration

The predicted incidence angle distributions for the rotor, stator, and hypothetical second-stage rotor at the specified cruise operating conditions are compared with their respective predicted low-loss incidence ranges in figure 18. The tip region incidence of the rotor is seen to be about 2 degrees above the upper limit of low-loss incidence. This was not considered of serious consequence because of the relatively low rotor tip loading and inlet Mach number at cruise conditions. The incidence angles for Stator A having the fixed position leading edge are seen to be outside of the predicted low-loss region over all but 2% of the span at the hub. The incidence angles for Stator B and the second rotor are within the low-loss incidence angle range across the entire span.

TEST RIG, INSTRUMENTATION, AND PRECEDURES

Test Rig

The Pratt & Whitney Aircraft (FRDC) single-stage compressor test rig (figure 19) was used for the variable geometry blading test program. The test rig comprises a bellmouth inlet section; inlet guide vane, rotor, and stator vane assemblies; and an exhaust diffuser system. The exhaust system was designed with a series of radial flow vanes for overboard dumping of part of the airflow to accommodate flowrates up to 330 lb/sec using the existing compressor test stand exhaust system. Flow was controlled by means of 24 motor-driven throttle vanes located upstream of the overboard dump section. The stationary leading edge segments of the inlet guide vanes and eight struts in the exhaust case supported the rotor. The rotor was driven by a free turbine that was powered by the exhaust of a J75 slave engine.

The compressor test facility used for this program is shown schematically in figure 20. The compressor rig inlet duct contains a flow measuring orifice and inlet throttle valve. There is a 10:1 area contraction from the plenum to the compressor rig inlet.

Instrumentation

The instrumentation utilized for the Stator A, Stator B, and the distortion tests is described in detail in references 3, 4, and 5, respectively. A general description of the instrumentation is given here to identify the source of measurements for the calculated performance variables.

Weight flow was measured by means of a flat plate orifice located in the test facility inlet duct. Stall limit flow was measured with close-coupled fast response transducers while operating the compressor into and out of the stall.

Rotor speed was measured by means of an electromagnetic sensor mounted adjacent to a 60-tooth gear on the rotor shaft. Gear tooth passing frequency was displayed as rpm on a digital counter.

Inlet total pressure and temperature were measured with Kiel head total pressure probes and half-shielded total temperature probes located in the inlet plenum. Stage (stator) exit total pressure was measured with 16-tube circumferential rakes located at 10, 30, 50, 70, and 90 percent of the span. For circumferential inlet flow distortion, two radial rakes were installed ahead of the guide vanes and two sets of stator exit rakes were utilized to measure total pressures in and out of the

distorted flow region. Stage exit total temperature was obtained by means of four radial temperature rakes spaced approximately 90-degrees apart.

Total pressure behind the inlet guide vane was measured by means of circumferential rakes similar to those behind the stators. Total pressure behind the rotor was measured with two 20-degree wedge traverse probes and checked by means of two radial rakes with Kiel head sensing elements. The rakes and traverse probes were positioned approximately one-half of a guide vane gap apart at approximately diametrically opposite circumferential positions.

Static pressures behind each blade row were measured by means of 8-degree wedge traverse probes and four approximately equally-spaced static pressure taps on the inner and outer walls. Air angle measurements were obtained from two 20-degree wedge traverse probes located behind each blade row.

Three Kistler high-frequency-response transducers were located 30 and 60 degrees apart at 10% span from the tip behind the rotor to measure the number, size, and rotational speed of rotating stall cells.

Bellmouth static pressure, rotor speed, and selected stage exit pressures were recorded on tape using high-response instrumentation to aid in the determination of stall transient characteristics.

Steady-state pressures were measured by a scannivalve system, automatically recorded on punch cards, and subsequently stored on tape for data processing. Traverse probe and transient data were recorded on tape in digital form. Temperatures were indicated on precision potentiometers and manually recorded.

Test Procedures

Each of the two stage configurations, Stator A and Stator B, was operated at 50, 70, 80, 100, and 110% of the SLTO design corrected rotor speed in the SLTO configuration and at 50, 70, 80, and 100% of the SLTO design corrected rotor speed in the cruise configuration. Stator B was also tested at 50, 70, 80, and 100% of SLTO design corrected rotor speed at an intermediate setting of the inlet guide vane and stator halfway between the SLTO and cruise configurations. Approximately six data points, evenly spaced between maximum flow and near-stall conditions, were obtained at each rotor speed. At each speed and flow setting, data from the fixed instrumentation were recorded and then the traverse probes were immersed to the hub; traverse data were recorded as the probes were withdrawn at a travel rate of 2.0 in./min. Stall transient measurements were obtained at each rotor speed while operating the stage into and out of stall to define the stall point.

For the inlet flow distortion tests with the Stator B stage, overall performance data were obtained for the SLTO and cruise configurations at 70, 80, and 100% of the SLTO design corrected rotor speed. Four data points were recorded at each rotor speed. Stall transient measurements were obtained for these tests also.

Data Reduction Procedures

Definitions of overall and blade element performance variables are given in Appendix A. Total pressures and temperatures at each axial station were mass averaged to obtain pressure ratio and efficiency. The mass average temperature determined from stage exit temperature and flow distributions was used as the rotor exit average temperature.

Blade element velocity diagram data were calculated for the blade row leading and trailing edges for the streamline segments shown in figure 2. Angular momentum, continuity, and radial equilibrium were preserved in the translation of measured quantities from the axial measuring stations to the blade row leading and trailing edges. Rotor loss coefficients were calculated on the basis of as-measured quantities because of their sensitivity to slight errors in calculated static pressure near wide-open discharge and stall conditions. Inlet guide vane and stator loss coefficients were calculated using selected free-stream pressures from the respective downstream wake probe data as the upstream pressures. Because of occasional incorrect pressures in the guide vane wakes due to leaky rake tubes, and the associated manual effort required to calculate loss coefficient, guide vane losses were calculated for only the 70 and 100% of SLTO design corrected rotor speed conditions.

DISCUSSION OF RESULTS

Overall Performance

The assessment of the effect of variable geometry inlet guide vane and variable geometry stators on overall performance is presented for the Stator B stage configuration. The overall performance results obtained with the Stator A stage (reference 3) were somewhat clouded by a rotor tip rub early in the test program. The rotor shroud was modified for the Stator B test (reference 4) and no further problems were encountered. The overall performance and stall limit of the Stator B stage is therefore considered to be the best representation of SLTO and cruise configuration performance, and the stall limit improvement achievable with variable geometry for this investigation.

Overall Performance for SLTO Configuration

Pressure ratio and adiabatic efficiency are presented as functions of corrected weight flow for the Stator B stage in its SLTO configuration in figure 21. The overall performance of the Stator B stage at design flow conditions was slightly better than the predicted performance. The measured pressure ratio and adiabatic efficiency for design corrected rotor speed and flow are 1.35 and 91%, respectively, compared to corresponding predicted values of 1.32 and 85%.

The difference between measured and predicted pressure ratio is consistent with the corresponding difference in efficiency and is attributable to two causes: (1) guide vane losses were not as high as assumed in the design, and (2) slightly high rotor incidence angle compared to design incidence. The relatively high value of inlet guide vane loss coefficient, 0.134, was assumed for design analysis purposes to allow for possible influence of airfoil surface irregularities on profile loss (reference 2). The measured inlet guide vane loss coefficient was approximately 0.025. The difference between assumed and measured guide vane loss accounts for about 2 out of the 6-point difference between measured and predicted efficiency for the Stator B stage. The rotor incidence angle over the inner 30% span was about 1 degree larger than the design incidence. This resulted in a slight increase in rotor work at design flow.

Overall Performance for Cruise and Intermediate Configurations

Overall performance of the Stator B stage in its cruise configuration and intermediate configuration (half way between SLTO and cruise) is presented in figures 22 and 23, respectively. The stall limit line and pressure ratio and efficiency characteristics for 70 and 100% design corrected rotor speed conditions obtained with the SLTO configuration are included in figures 22 and 23 for comparative purposes. Cruise design pressure ratio and efficiency goals for the cruise configuration were slightly exceeded. A pressure ratio of 1.155 was achieved at cruise corrected flow compared to the predicted value of 1.129. The corresponding efficiency was about 2 points greater than the predicted value of 88.3. At the cruise design point the cruise configuration provided an increase of approximately 7 percentage points over the efficiency obtained with the SLTO configuration. Also, the stall-free operating range between the cruise design point corrected flow and the indicated stall limit flows for 70% of design corrected rotor speed conditions is larger for the cruise configuration. With respect to the SLTO design corrected flow of 265 lb/sec, the variable geometry features provided an 11% increase in stall-free flow range over that obtained with the SLTO configuration (i.e., a fixed geometry stage). With respect to the cruise design corrected flow of 143.3 lb/sec, the stall-free flow range was nearly doubled.

Neither the efficiency characteristics nor the stall limit line of the SLTO configuration were appreciably changed by the intermediate

configuration, as shown in figure 23. Maximum flow, however, was substantially reduced as indicated by comparison with the two SLTO configuration speedlines in the figure.

Rotating Stall Characteristics

The stage stall transient characteristics, and rotating stall patterns are discussed in references 3 and 4. The variable geometry features of the stage had no apparent affect on the rotating stall characteristics during stall transients. The development of only one rotating stall zone was observed in each of the tests. Rotational speed of the stall zones varied between about 45 and 65 percent of the SLTO corrected rotor speed. The size of the stall zone varied between 20 and 60% of the annulus area (circumferentially) at incipient stall conditions, and grew in size to between 40 and 80% of the annulus during operation in deep stall. Because the three fast response Kistler transducers were located at 10% span from the tip in anticipation of the initiation of rotating stall in the tip region, the radial extent of the rotating stall zones was not measured. During one stall transient the measured size of the rotating stall zone diminished to 9% of the annulus area (circumferentially) just prior to recovery.

Operation of the Stator A and B stages in deep stall was fairly stable, and blade vibration amplitudes were low. For the SLTO configurations at 70% of SLTO design corrected rotor speed, rotating stall was not detected at flow rates below about 80% of the incipient stall flow.

Analysis of Mass Flow Reduction With Variable Geometry Guide Vanes

The reduction in incipient stall weight flow attainable with the variable camber inlet guide vanes between the SLTO zero tip swirl and cruise 20-deg tip swirl conditions was shown in figure 22. The mass flow reduction as a function of guide vane turning at a constant tip incidence angle was evaluated for comparison with the results of the reference 1 analysis. The reference flow condition for zero guide vane turning was arbitrarily selected at the peak efficiency for 70% of SLTO design corrected rotor speed conditions. Flowrates obtained with the intermediate and cruise settings of the guide vane (reference 4) were evaluated at the same rotor speed and tip incidence angle. The reduced mass flow as a percent of the reference mass flow is shown in figure 24 as a function of guide vane tip turning angle. For 5 degrees of tip turning the mass flow was reduced to 92 percent of the reference flow and for 19 degrees of tip turning the mass flow was reduced to 84 percent of the reference flow. For guide vane turning angles less than 20 degrees, the reduction in mass flow is greater than that calculated for the B/r tangential velocity distribution from reference 1. The average experimental tangential velocities for β_{1tip} = 5 degrees (figure 25) are higher than for B/r = constant. Therefore, a larger mass

flow reduction would be expected relative to that calculated for the B/r distribution. For β_{1tip} = 19 degrees, the experimental tangential velocities are between those of the B/r and C distributions. As noted in figure 24, the flow decrease is nearly that indicated for B/r = constant. The experimental rate of change in mass flow with increasing inlet guide vane tip turning, however, is similar to that of the C distribution. The experimental results in general support the trends indicated in the reference 1 analysis.

Blade Element Performance

Variable Camber Inlet Guide Vane Performance

Inlet guide vane exit air angle at the hub, midspan, and tip sections are shown in figures 26 and 27 as a function of inlet guide vane exit Mach number for the various rotor speed conditions. Figure 26 corresponds to the SLTO configuration and figure 27 corresponds to the cruise configuration. Inlet guide vane exit Mach number was selected as an independent variable to show the influence on guide vane turning, if any, of rotor-induced static pressure field between the guide vane and rotor. Results are presented for the Stator B stage test. Stator A stage inlet guide vane data are omitted because of the rotor tip rub that occurred with this configuration and the resulting variation in tip clearance during the test. This variation in tip clearance is thought to have caused irregularities in the tip region air angle data that are not present in the Stator B stage data.

With the exception of the 110% rotor speed data in figure 26, the guide vane exit air angles at the hub and midspan sections are within ±2.5 degrees of zero swirl. At the tip section the exit air angle is seen to increase with decreasing Mach number at each rotor speed. This variation in air angle with Mach number increases with increasing rotor speed, and is most pronounced at the rotor near-stall conditions, as indicated by the dashed line drawn through the near-stall data points. A similar variation of exit air angle with Mach number and rotor speed is not apparent at the other span locations.

Inlet guide vane exit air angles for the cruise configuration, figure 27, also indicate more variation in the tip region than in the midspan or hub regions, with the variation increasing as rotor speed increases. The amount of variation, however, is less than that for the SLTO configuration. The representative average turning achieved with the guide vane in the cruise configuration is considered to be 30.5 degrees at the hub, 26 degrees at midspan, and 20 degrees at the tip.

Inlet guide vane turning angle, $\theta = \beta_0 - \beta_1$, is shown in figure 28 as a function of camber angle for the hub (σ = 1.41), midspan, (σ = 1.08) and tip (σ = 0.75) sections. Design values for the basic and

modified airfoil sections (reference 2) are indicated. Also shown in the figure are the design values for a relatively high camber 63-series inlet guide vane that was used for the compressor stage reported in reference 9.

The data in figure 28 are seen to diverge slightly from the design values of turning as camber angle increases. The reference 9 data for σ = 1.21, 1.11, and 1.02 correlate favorably with the variable camber inlet guide vane data for σ = 1.08. Figure 29 shows the variable camber inlet guide vane trailing edge metal angle distribution that will produce the desired air angle distribution, based on extrapolation of the data in figure 28. A constant hub-to-tip change in camber by means of the variable geometry features can match the desired SLTO and cruise swirl angles within approximately 1 degree at all span locations.

Average values of inlet guide vane loss coefficient from references 3, 4 and 9 are presented as a function of air turning angle in figure 30. The data indicate an increase in loss coefficient from about 0.025 at zero degrees turning to 0.035 at 35 degrees of turning. There appears to be no significant differentiation between hub (90% span), midspan, and tip (10% span) losses.

Rotor Blade Element Performance

A convenient source of representative rotor blade element performance characteristics is provided by the data for the Stator B stage intermediate configuration reported in reference 4. These characteristics, loss coefficient, diffusion factor, and deviation angle as functions of incidence angle are repeated in figures 31a through 31e. The rotor data obtained with this configuration are consistent within the set and they are in favorable agreement with the respective design values. Examination of the data in reference 4 indicated that the rotor loading (diffusion factor) and inlet relative Mach number distributions with incidence angle were not appreciably affected by rotor prewhirl between the intermediate and SLTO configuration prewhirls at SLTO corrected rotor speed, or between the intermediate and cruise configuration prewhirls at cruise corrected rotor speed. These data were thus utilized to evaluate the spanwise distributions of loss coefficient for the following configurations and operating conditions:

1. SLTO configuration; SLTO design corrected rotor speed and flow

2. SLTO configuration; Cruise corrected rotor speed and flow

3. Cruise configuration; Cruise corrected rotor speed and flow

4. Intermediate configuration; SLTO and cruise corrected rotor speed and flow

The incidence angle distributions for these conditions were obtained from interpolation of incidence-flow curves for the appropriate configurations. The incidence angle distribution thus obtained for the SLTO

configuration at SLTO design corrected rotor speed and flow conditions, and the corresponding loss coefficient distribution derived from the data in figures 31a through 31e, are shown in figure 32. The interpolated experimental data agree favorably with the corresponding design incidence angle and predicted loss coefficient distributions. The rotor inlet relative Mach number at 10 percent span from the tip for the interpolated data in figure 32 is 1.04 compared with a design value of 1.10. This slightly lower experimental value of Mach number at SLTO design corrected flow conditions is due to the rotor prewhirl produced by the inlet guide vane in its intermediate position.

When the SLTO configuration was operated at cruise corrected rotor speed and flow conditions, the rotor incidence angles and corresponding loss coefficients across the span were substantially larger than the design low-loss incidence angles and predicted losses for cruise conditions, as shown in figure 33.

Restoration of the incidence angles to the low-loss operating range at cruise conditions by means of the variable camber inlet guide vanes (increased rotor prewhirl) produced the reduction in incidence angle and the corresponding reduction in loss coefficient shown in figure 34. The tip incidence angle (10% span) was reduced 2.8 degrees and the hub incidence angle (90% span) was reduced 9.3 degrees. The relative reduction in incidence angle at the hub and tip is generally consistent with the analyses in references 1 and 2. The experimental values of incidence angle in the hub region in figure 38 are larger than the design values because the axial velocities in this region were lower than the corresponding design values (references 2 and 4). The experimental loss coefficients, with the exception of the midspan value, are in good agreement with the predicted values. The relatively high midspan loss (noted in figures 33 and 34 but not in figure 32) is attributed to the rotor part-span shroud wake, which may have been displaced radially inward when the SLTO and cruise configurations were operated at cruise conditions.

The performance of the Stator B stage intermediate configuration operating as a fixed-geometry stage at the SLTO and cruise corrected rotor speed and flow conditions is illustrated in figure 35. As noted in the figure, the experimental incidence angles with respect to the design incidence angles are low for the SLTO operating conditions and high for the cruise operating conditions. The corresponding loss coefficients are high compared to the predicted values, particularly for the cruise operating conditions.

Stator Blade Element Performance

Stator A and Stator B blade element data from references 3 and 4 (loss coefficient, deviation angle, and diffusion factor as functions of incidence angle) are presented in figures 36a through 36e for the SLTO configuration and figures 37a through 37e for the cruise configuration. Data

obtained with the Stator A and B SLTO configurations at SLTO and cruise corrected rotor speed are included in figures 36a through 36e; data obtained with the Stator A and B cruise configurations at cruise corrected rotor speed are included in figures 37a through 37e.

Incidence angle data from references 3 and 4 were interpolated to determine the incidence angle distributions for the stator SLTO configurations operating respectively at SLTO and cruise corrected rotor speed and flow, and for the stator cruise configurations operating at cruise corrected rotor speed and flow. The incidence angles thus determined are indicated in figures 36a through 36e and figures 37a through 37e. Spanwise loss coefficient distributions were subsequently established for these configurations and operating conditions.

Stator Performance For SLTO Configuration at SLTO Conditions. - Incidence angle and loss coefficient distributions for the Stator A and Stator B SLTO configurations operating at SLTO corrected rotor speed and flow are shown in figure 38. The experimental incidence angles are within approximately 1.5 degrees from the design incidence angles between 10 and 90 percent span.

The experimental loss coefficients agree favorably with the design loss coefficients, with the exception of the Stator B hub region which indicates a relatively high loss compared to the Stator A hub loss. The Stator B losses at 90 percent span from the tip were consistently high relative to the corresponding Stator A losses, as noted in figure 36e. Comparison of the Stator A and Stator B wakes at 90 percent of span from the tip (figure 39) indicates a much larger wake for Stator B.

The major difference between the Stator B and Stator A SLTO configurations that could have caused the observed difference in hub loss is the cavity between the forward and rear airfoil segments of Stator B (figure 15). This cavity was anticipated as a possible path for secondary flow from tip-to-hub during the design of Stator B (page 24 of reference 2). A 0.015-in. slot was therefore provided between the forward and rear airfoil segments in the SLTO configuration to maintain a high velocity component over the rear segment leading edge and thereby reduce the tendency for spanwise secondary flow in the cavity. If this slot was too small to do the job it was intended to do, the cavity would provide a convenient path for the flow of low energy air from the outer wall boundary layer to the hub wall. At the hub wall this low energy air would mix with the hub wall boundary layer flow and cause a relatively large hub wake. This might explain the relatively large Stator B hub wake in figure 39.

Stator Exit Air Angle For SLTO Configurations at SLTO Conditions. - Stator A and B exit air angles are compared in figure 40 with the predicted stator exit air angle distribution for the SLTO configurations operating at SLTO corrected rotor speed and flow conditions. The Stator B exit air angles are about 2 degrees below the predicted exit air angles over most of the span whereas the Stator A air angles are 4 to 6 degrees above the predicted air angles over the span. Since the losses of Stator A and Stator B are of similar magnitude except in the hub region

(figures 36a through 36e) it is suspected that the relatively high air angles for the Stator A SLTO configuration are due to an instrumentation error. A 4-to-6 degree error in Stator A exit air angle would not influence the evaluation of either overall or stator blade element performance; an error in stator exit air angle would, however, slightly affect the evaluation of incidence angle for a hypothetical second stage rotor.

Stator Performance For SLTO Configuration at Cruise Conditions. - When the Stator A and Stator B SLTO configurations were operated at the cruise corrected rotor speed and flow conditions, the resulting incidence angles over most of the span were substantially larger than the low-loss incidence angles that were predicted for a stator having variable leading edge metal angle capability, as shown in figure 41. The low-loss incidence angle distribution shown in figure 41 was predicted for the Stator B cruise configuration (as shown in figure 18).

Operation at the high incidence angles shown in figure 41 caused the high loss coefficients shown in the lower half of the figure. The Stator B hub loss remained high relative to the Stator A hub loss.

Second-Stage Rotor Incidence For SLTO Configuration at SLTO Conditions. - Incidence angles calculated for a hypothetical second stage rotor, based on Stator B exit conditions, are shown in figure 42. The calculated incidence angles vary from 3 degrees below to 5 degrees above the predicted incidence angles at the tip (10% span) and hub (90% span), respectively. The difference between calculated and predicted incidence angles in figure 42 is primarily due to the difference between measured and predicted Stator B exit axial velocities, shown in figure 43.

Second-Stage Rotor Incidence For SLTO Configuration at Cruise Conditions. - Approximately 30 degree hub - 25 degree tip swirl distribution is required at cruise operating conditions to provide a low-loss incidence distribution for the hypothetical second-stage rotor. Since the air turning for the stator SLTO configuration operating at cruise corrected rotor speed was about the same as the turning for SLTO design corrected rotor speed (zero stator exit swirl), the resulting second-stage rotor incidence angles are high. Calculated incidence angles for the second-stage rotor, based on Stator B exit conditions, are compared with the upper limit of the low-loss incidence range ($\bar{\omega}'_{lim} = \bar{\omega}'_{min} + 0.02$) in figure 44. The calculated incidence angles vary from about 2 degrees within the low loss range at the tip to about 10 degrees above the low loss range at the hub. Thus the second stage would be expected to have poor efficiency and very little, if any, stable operating range at cruise conditions if preceded by a fixed-geometry front stage.

Effect of Stator Variable Geometry on Cruise Performance. - Stator A in its cruise configuration had the same leading edge metal angle distribution as in the SLTO configuration, and the hinged flap was rotated to reduce camber and provide the desired exit swirl distribution (figure 14). Consequently, Stator A was required to operate with high

incidence angles at cruise conditions. Stator B in its cruise configuration could be matched to the flow at the leading edge and provide the desired exit swirl by means of the two adjustable segments (figure 15).

The incidence angle and loss coefficient distributions obtained with Stators A and B in their cruise configuration at cruise corrected rotor speed and flow conditions are presented in figure 45. Stator A, because of its fixed leading edge, is seen to retain a high level of incidence angle relative to the design low-loss incidence distribution. The Stator B incidence angles are close to the design curve except at midspan, where the incidence angle is approximately 4 degrees above the design curve. The relatively high midspan incidence was caused by a relatively low midspan axial velocity, which may have resulted from the rotor part-span-shroud wake.

The incidence distribution obtained with the Stator A and B SLTO configurations (figure 41) is repeated in figure 45 to show the changes in incidence angle caused by the stator variable geometry. The Stator A cruise configuration incidence angles actually increased due to improved rotor air turning in the cruise configuration.

Although the incidence angles for the Stator A cruise configuration are suggestive of very high losses, the measured losses were substantially reduced from those obtained with the SLTO configuration operating at cruise conditions (repeated from figure 41), as shown in the lower half of figure 45. Conversely, the losses obtained with the Stator B cruise configuration, which was rematched to the stator inlet flow over most of the span, were of the same magnitude as those obtained with the SLTO configuration operating at cruise conditions.

Analysis of Stator A and B Cruise Configuration Losses. - One of the most significant results of the variable geometry stator investigation was the favorable performance obtained with the Stator A cruise configuration operating with very high off-design incidence angles. Midspan loss coefficient and diffusion factor as functions of incidence angle are shown for the SLTO and cruise configuration in figure 46. At approximately 6 degrees incidence angle the flap rotation from SLTO to cruise position reduced the overall loading from a diffusion factor of 0.45 to 0.12. As incidence angle was increased further the diffusion factor increased to a value of 0.34 and the loss coefficient decreased to a value of 0.06 at the cruise design incidence angle of 12.2 degrees. At the cruise design incidence angle the cruise configuration loss coefficient was about one-half that of the SLTO configuration. As noted in figure 45, the Stator A cruise configuration loss at cruise corrected rotor speed and flow are less than half the loss for the SLTO configuration over most of the span.

The high loss of the Stator B cruise configuration relative to that of the Stator A cruise configuration over the range of incidence angle

at cruise corrected rotor speed were apparent in figures 37a through 37e. The cause of the large difference in loss levels of the two stators configurations was investigated by examining their respective midspan surface velocity distributions. The velocity distributions were calculated using an incompressible potential flow calculation and applying the Karmen-Tsien correction for compressibility (reference 10, page 258). The velocity distributions thus obtained are compared in figure 47.

Examination of the Stator A suction surface velocity distribution indicates flow decelaration over the forward segment and acceleration over the front half of the flap. Although the maximum-to-minimum velocity ratio for the forward segment indicates probable boundary layer separation (because the velocity ratio is much greater than the limiting value of 2.0 suggested in reference 11), the proximity of the flap in its uncambered position and the acceleration of flow over the flap are favorable conditions for reattachment of the separated boundary layer. Conversely, the velocity distribution on the pressure surface of Stator A in figure 47 indicates acceleration of the flow up to the flap hinge chordal location and subsequent deceleration. The local negative velocity gradient is conducive to rapid boundary layer growth, increased wake size, and increased loss. The observed net result, however, was a smaller wake (and lower loss) than that obtained with the SLTO configuration at the same high incidence angle, as shown in figure 48 .

The velocity distributions on the suction and pressure surfaces of the rear segment of the Stator B configuration (figure 47) are indicative of a high negative incidence angle condition. Since the flow angle at the leading edge of the rear airfoil is governed primarily by the pressure surface of the forward airfoil, the high negative incidence condition would prevail over the operating range of the combined airfoil segments. Thus, the Stator B loss would be expected to be relatively high over the entire operating range. It is apparent from the Stator B test results that extreme care must be exercised in the design of tandem-like variable geometry stators to properly match the leading edge of the rear airfoil in its off-design configuration. Although potential flow calculations were not used in the design analysis for the Stator B configuration (reference 2), this type of analysis can be useful in the design of tandem airfoil blade rows as discussed in references 12 and 13.

Effect of Stator Variable Geometry on Hypothetical Second-Stage Rotor Incidence. - As mentioned previously, the hypothetical second-stage rotor required a 30 degree hub - 25 degree tip prewhirl distribution at cruise corrected rotor speed and flow for stable, efficient operation. Both Stator A and Stator B, in their cruise configurations, provided approximately the required cruise design exit swirl distribution, as indicated in the upper half of figure 49. The corresponding incidence angle distributions for the hypothetical second-stage rotor are shown in the lower half of figure 49. The incidence angles are within 3 degrees of the cruise design incidence angles between 10 and 90% span. The change in incidence angle provided by the stator variable geometry can be noted by comparison with the incidence angles repeated from figure 44 for the

SLTO configuration. It may be noted that the change of incidence angle in the hub region is greater than the change of incidence in the tip region due to the stator exit axial velocity redistribution that accompanies the change in stator exit swirl to satisfy radial equilibrium. This result is similar to the analytical and experimental results discussed previously for the test rotor.

Influence of Variable Geometry Features on Performance With Inlet Flow Distortion

The Stator B stage was tested with 360-degree radial and 90-degree circumferential distortion to assess the interaction between distortion and the stage variable geometry features. The radial distortion covered approximately the outer 40% of the annulus area. The intensity of the distortion $(P_{max} - P_{min})/P_{max}$, was 6.7 percent at design equivalent rotor speed. This level of distortion was obtained with a 0.028-inch diameter screen wire on a 4 mesh. The distortion screens were located 9.7 inches upstream of the inlet guide vane leading edge. Details of this investigation are presented in reference 5.

Stall limit curves for the SLTO and cruise configuration with undistorted and distorted inlet flow are summarized in figure 50. For both configurations the loss in stall margin with radial distortion is not greatly different from the loss in stall margin with circumferential distortion. Inspection of these results indicates areas of similarity with the results of other investigators. Figure 51 shows the relative attenuation of the radially and circumferentially-distorted inlet total pressure profile. The radially distorted inlet profile is completely attenuated whereas the circumferentially-distorted profile shows little attentuation through the stage. Although the stall lines were substantially suppressed by radial distortion, the stall limit pressure ratios and maximum flows at design speed were not reduced as much by radial distortion as they were by circumferential distortion, as shown in figure 50. These results are qualitatively consistent with the data presented in references 14 and 15.

The influence of an increase in inlet guide vane turning angle on the stage stall limit line is shown in figure 52. At a constant flow, the stall limit lines are restored more than halfway to the stall limit with undistorted flow due to improvement of the rotor incidence angle. Rotor tip (10% span) incidence angles are shown as a function of corrected flow in figure 53 for undistorted and radially distorted inlet flow and $\beta_{1_{tip}} = 20$ degrees. At a corrected flow of 200 lb/sec the distorted total (and static) pressure caused an increase of 2 degrees in tip incidence angle for $\beta_{1_{tip}} = 0$. Increasing the tip swirl angle from zero to 20 degrees caused a 3-degree reduction of incidence angle. Similar results are presented in reference 15. Thus, variable geometry inlet guide vanes offer a possible means of controlling the tolerance to anticipated or known distorted inlet conditions. It would of course be necessary to schedule an increase in rotor speed with any increase in rotor prewhirl in order to maintain the required pressure ratio and corrected flow at a particular operating condition.

Effect of Single-Stage Range Improvement on Multistage Compressor

It is of interest to note the range and stall margin improvement that a variable geometry front stage can provide for a multistage compressor. The Stator B stage configuration was matched to the last seven stages of the eight-stage compressor of reference 16. Pressure ratio-flow characteristics were calculated at design corrected rotor speed and 70% of design speed for the Stator B front stage in its SLTO and cruise configuration. The pressure ratio-flow coefficient data of reference 17 were used for these calculations. For the cruise configuration calculations, the work of the second stage was reduced in accordance with the increased Stator B exit swirl angle. Compressor maps for the SLTO and cruise configurations based on the two corrected rotor speeds mentioned above are shown in figure 54. An assumed SLTO design point, and a corresponding operating point for Mach 3.0 cruise at approximately 60,000 feet altitude are indicated. The cruise operating point is on the 70% speed line of the SLTO configuration. The stall margin* for the SLTO configuration at the specified cruise operating conditions is 4.4%. To attain the desired cruise pressure ratio and corrected flow with the cruise configuration it is necessary to increase the corrected rotor speed from 70 to approximately 73% of design corrected speed. The stall margin for the eight-stage compressor with the front stage in its cruise configuration is 17.2%.

Associated with the stall margin improvement due to variable geometry shown in figure 54, there is a substantial improvement in efficiency. The efficiency gain at cruise operating conditions due to the variable geometry features of the Stator A and Stator B stages is illustrated in figure 55. Adiabatic efficiency is shown as a function of corrected weight flow. At design corrected flow (143.3 lb/sec), the cruise configurations provide a 7-point increase in efficiency over the SLTO configurations. Thus, the use of variable geometry inlet guide vanes and stator in a compressor front stage can improve stage matching to increase both the stable operating range and efficiency.

* Stall margin is defined as the difference between the slope of line A and the slope of line B or C in figure 54. These lines represent constant turbine inlet temperature operating conditions for a fixed-geometry turbine. The significance of this definition of stall margin is discussed in Appendix C of reference 5.

CONCLUDING DISCUSSION

The extent that variable geometry inlet guide vanes and stator blade rows can extend the efficient, stable operating range of a typical supersonic Mach number turbine engine compressor front stage was investigated. Trends of rotor incidence angle and flow change with changes in guide vane swirl that were established in the preliminary analysis of reference 1 and the design analysis of reference 2 were substantially supported by the experimental results of the program. Control of rotor tip incidence by means of guide vane turning was found in these analyses to be more difficult than control of rotor hub incidence because of the redistribution of axial velocity with swirl change. It is therefore important that radial equilibrium including streamline curvature and radial entropy gradients be accounted for in any design study for a particular application since these factors will influence the axial velocity distributions. Although the tip incidence at off-design conditions was not fully restored to the predicted low loss value, for a sample case the variable camber inlet guide vane sufficiently rematched the rotor inlet flow at the prescribed cruise conditions to achieve a 7.2-point improvement in calculated efficiency. The variable camber inlet guide vane also permitted efficient, stable operation at lower flows for a given rotor speed than those attainable with a fixed geometry (SLTO configuration) guide vane. It should be noted that pressure ratio as well as flow was reduced due to the inlet guide vane swirl in the cruise configuration. The variable geometry stators provided the desired flow rematching of a hypothetical second stage rotor at cruise conditions.

Of the two stator configurations that were evaluated, Stator A with a fixed forward segment and movable rear flap demonstrated superior performance over that of the Stator B configuration which had independently-adjustable leading and trailing edge metal angles. Analyses of the Stator A suction surface velocity distribution indicated a steep negative velocity gradient over the fixed forward segment followed by a favorable (accelerating flow) velocity gradient over the flap. The favorable gradient permitted recovery of the suction surface boundary layer. Conversely, the pressure surface velocity distribution of the rear segment of Stator B indicated a steep negative pressure gradient due to a high negative incidence angle and no apparent opportunity for boundary layer recovery. Although a more detailed design analysis (that used potential flow calculations as a guideline) for a two-part (tandem) stator could probably lead to a more satisfactory configuration, the Stator A results indicate that independent control of leading and trailing edge metal angle is not necessary to achieve a wide range of stator operation. For a range of flap angles, Stator A demonstrated low-loss operation between incidence angles of about -12 and 16 degrees and corresponding exit air angles between zero and 26 degrees. Slight compromise to the Stator A SLTO configuration design might lead to an even larger low-loss operating range. It should be noted that a variable stagger stator would not be expected to produce the same result as the

Stator A configuration because the change in leading edge metal angle would cause large negative incidence angles and probably pressure surface boundary layer separation.

The mechanical design of variable geometry blade rows requires analysis simultaneously with the aerodynamic design to ensure that the flap angles and hinge lines are compatible with mechanical limitations. In a particular application these considerations may lead to off-design swirl distributions that may not appear to be the most desirable from a solely aerodynamic design point of view.

In summary, it is concluded that the variable geometry inlet guide vanes and stators that were evaluated in this investigation provided the desired flow control and velocity diagram adjustment for efficient operation between SLTO and cruise conditions for a supersonic cruise engine compressor front stage.

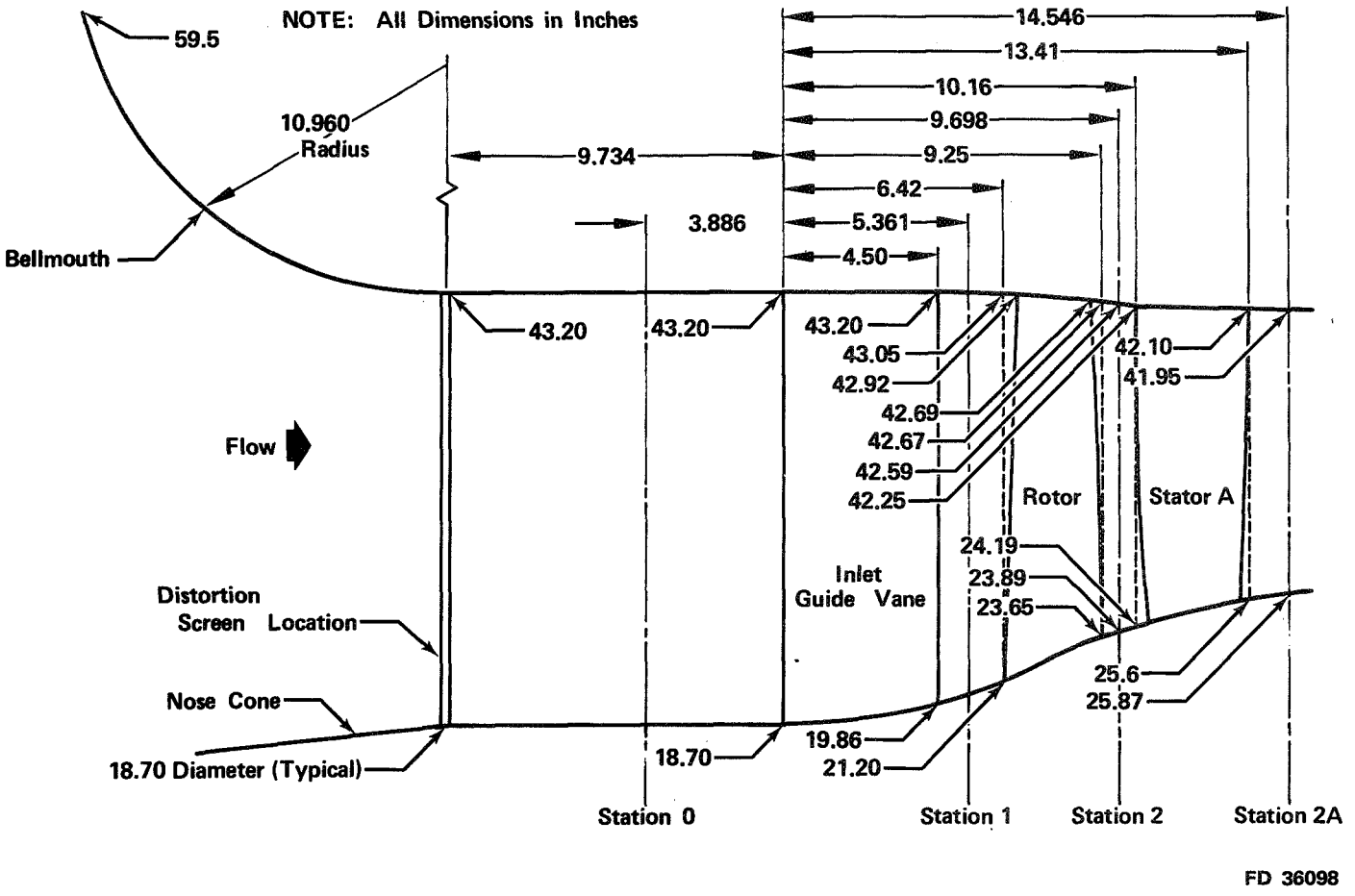

Figure 1. Stage Flowpath Geometry

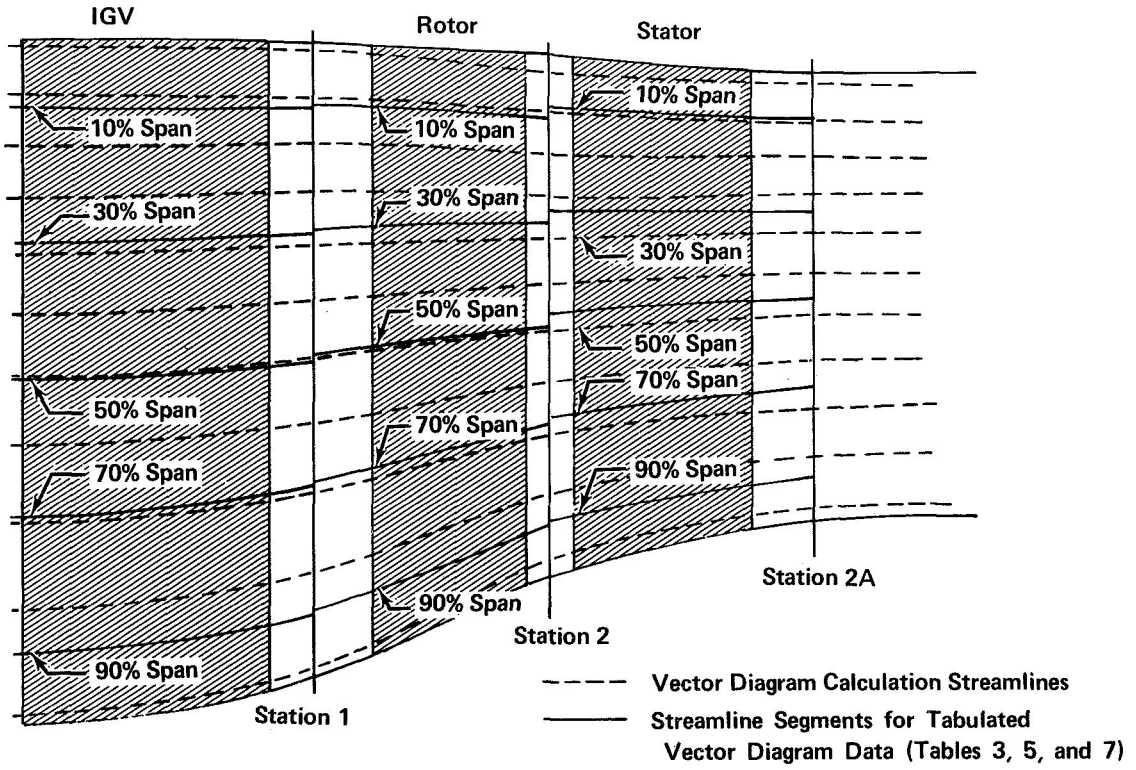

Figure 2. Flowpath Model for Vector Diagram Analysis

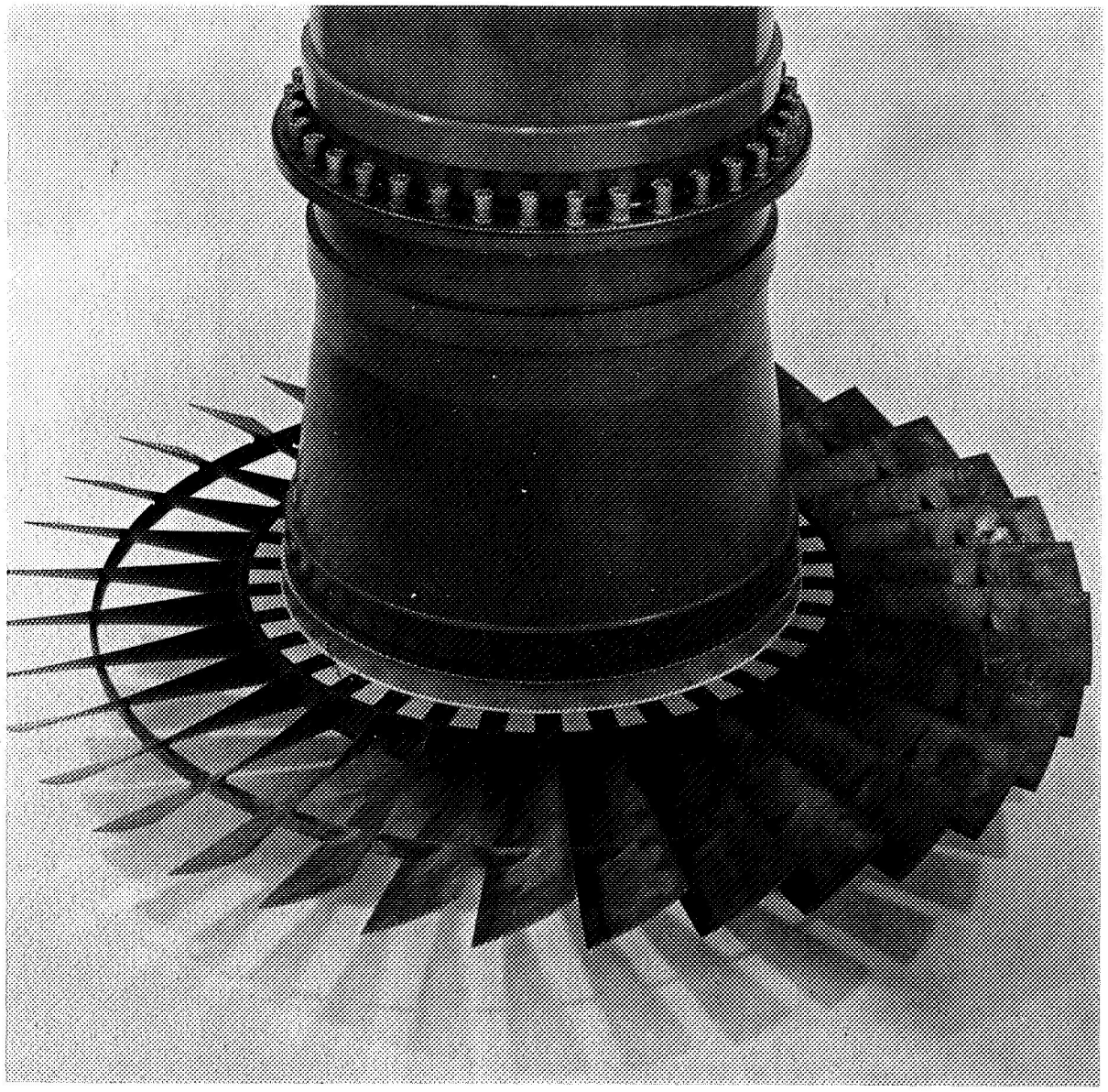

FE 68448

Figure 3. Rotor Assembly

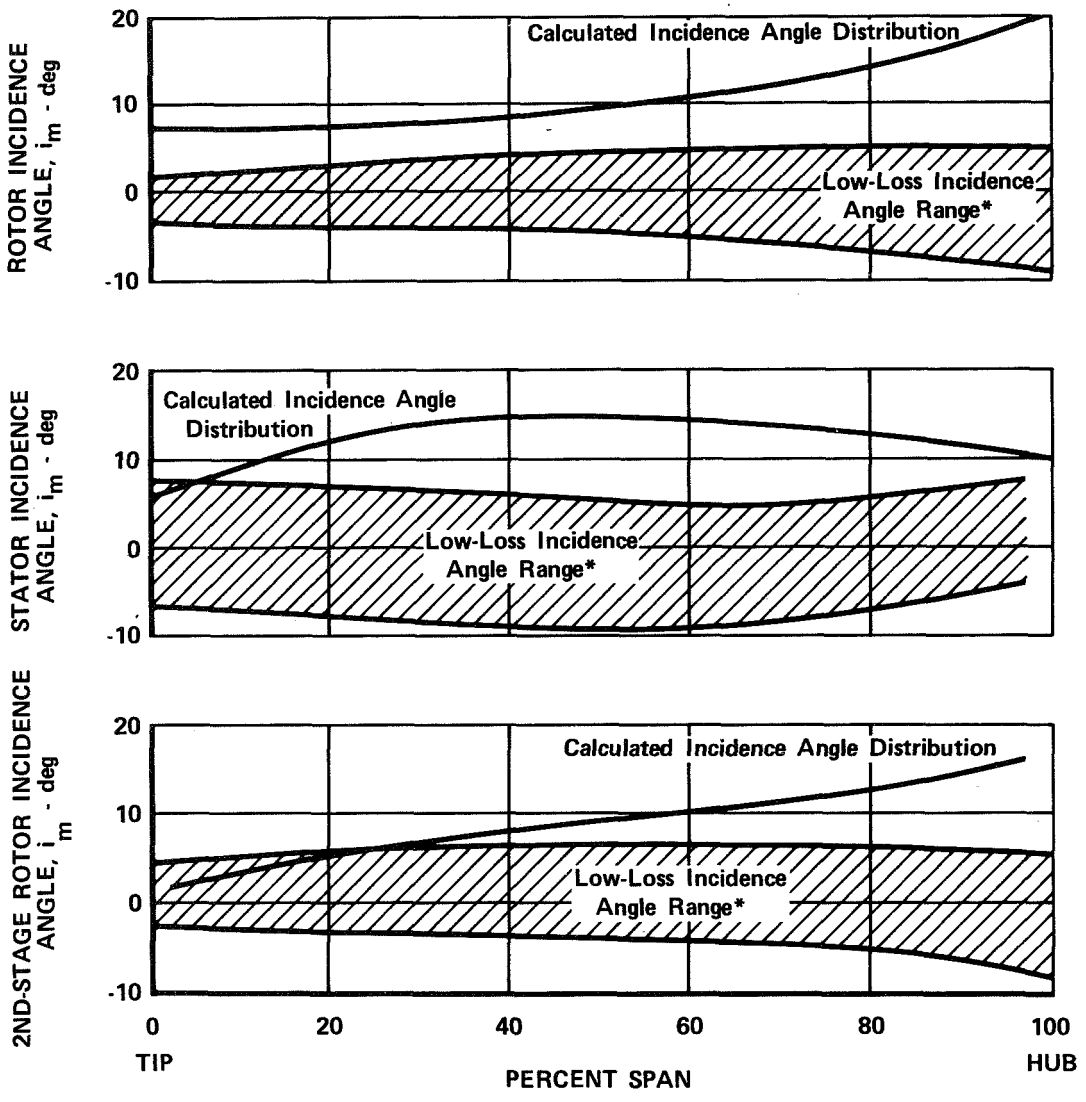

Figure 4. Comparison of Calculated Cruise Design Point Incidence Angles for Fixed Geometry Blade Rows With Low-Loss Incidence Range for Rematched Blade Rows

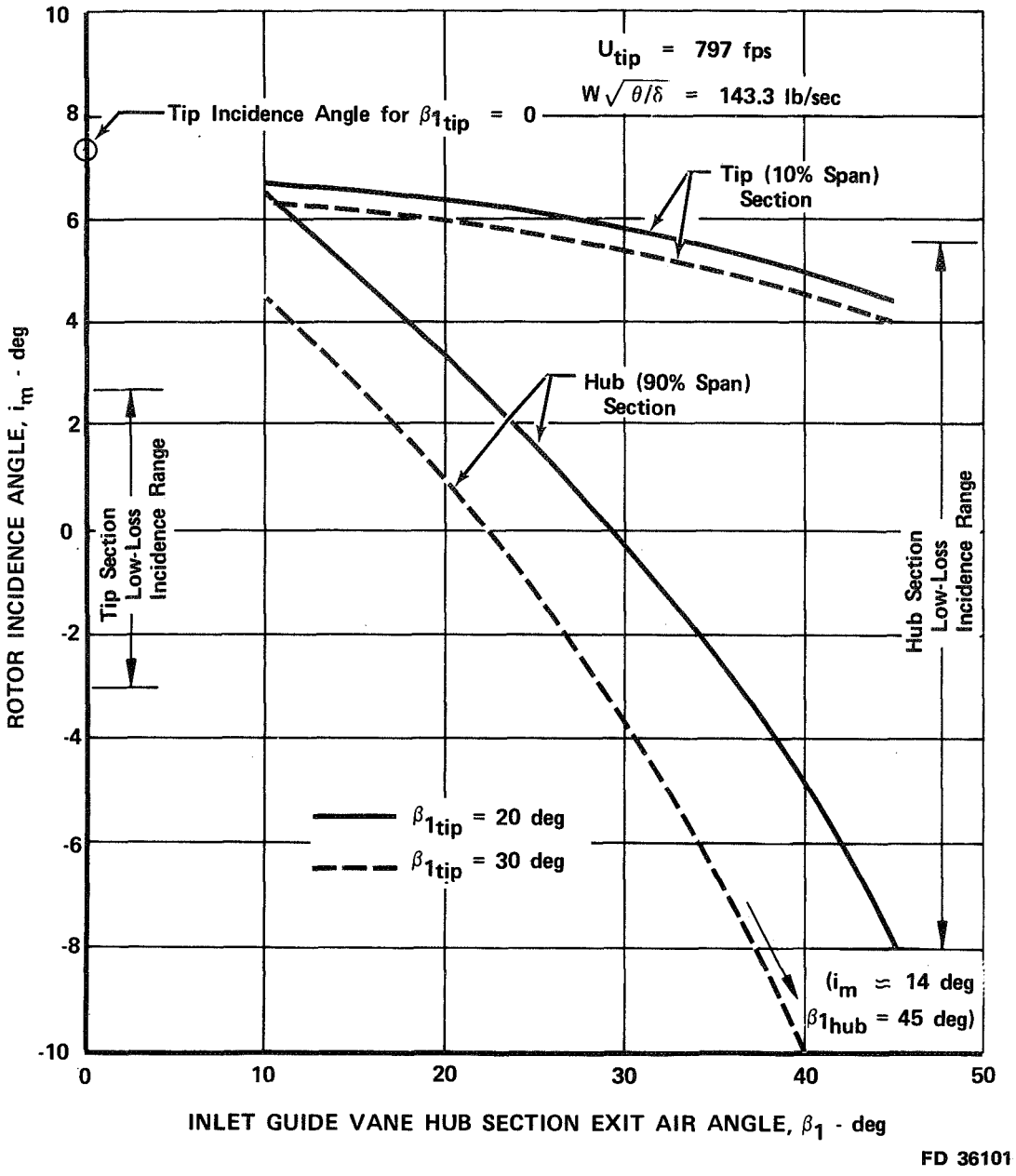

Figure 5. Effect of Inlet Guide Vane Swirl Distribution on Rotor Incidence (Reference 2)

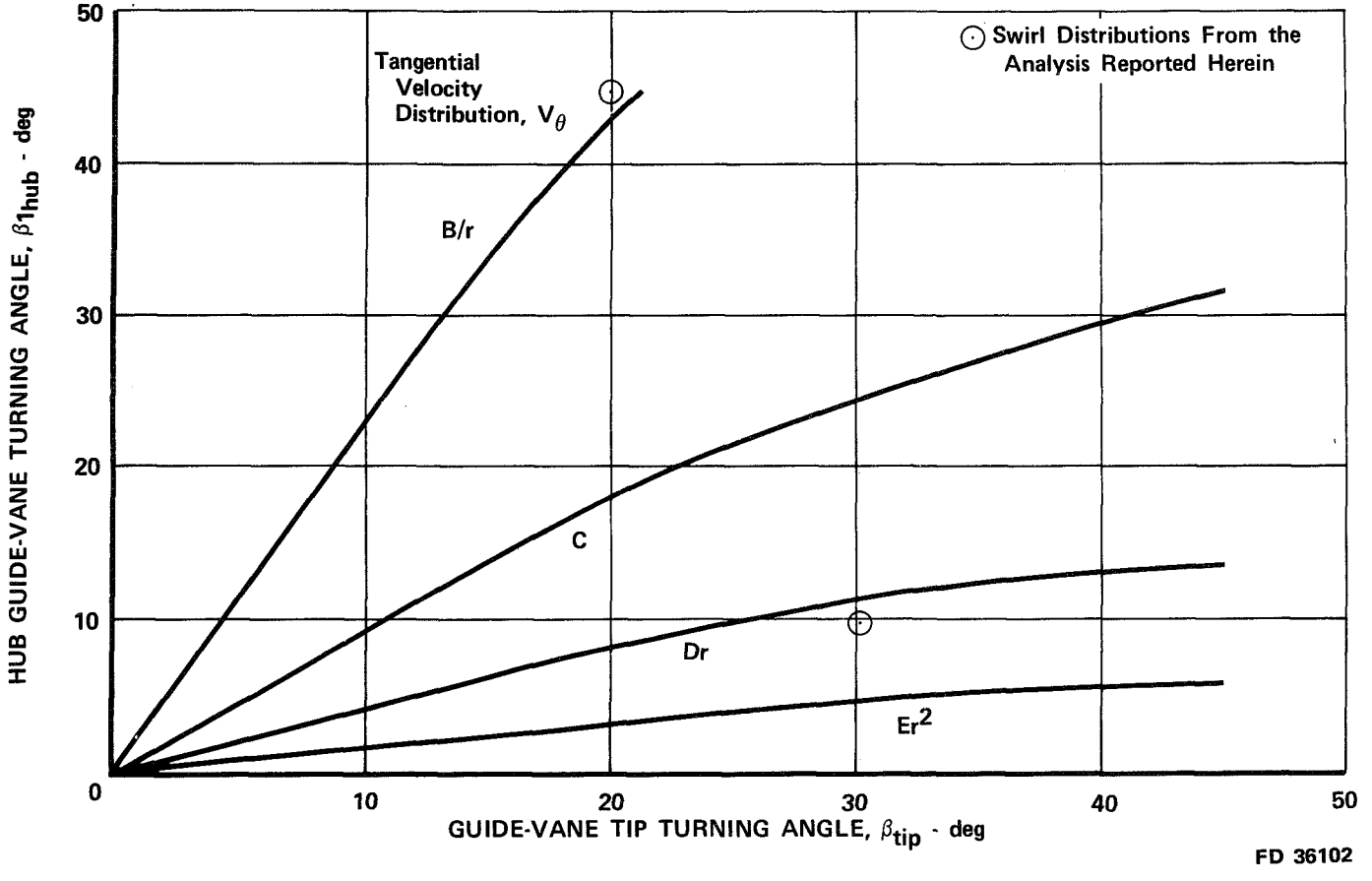

Figure 6. Hub Guide-Vane Turning Angle as Function of Guide-Vane-Tip Turning Angle with Rotor-Tip Incidence Angle Held Constant (Reference 1)

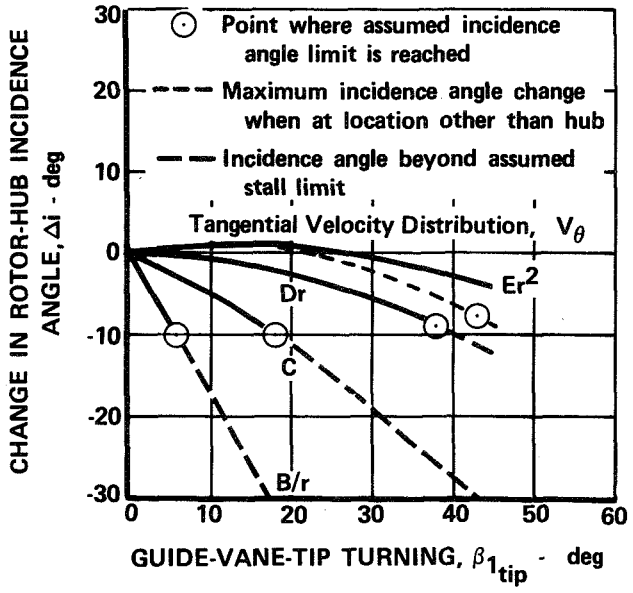

a. Change in rotor hub incidence angle as function of guide-vane-tip turning angle with rotor-tip incidence angle held constant. (Reference 1)

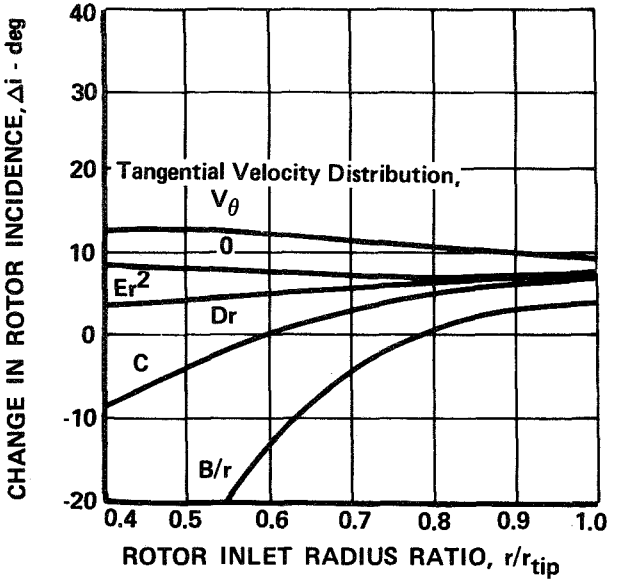

b. Effectiveness of guide vanes with 30-deg tip turning in reducing change of rotor incidence angle for mass-flow reduction from 100 to 67.6 percent of design. (Reference 1)

FD 36103

Figure 7. Rotor Incidence Angle Change Trends

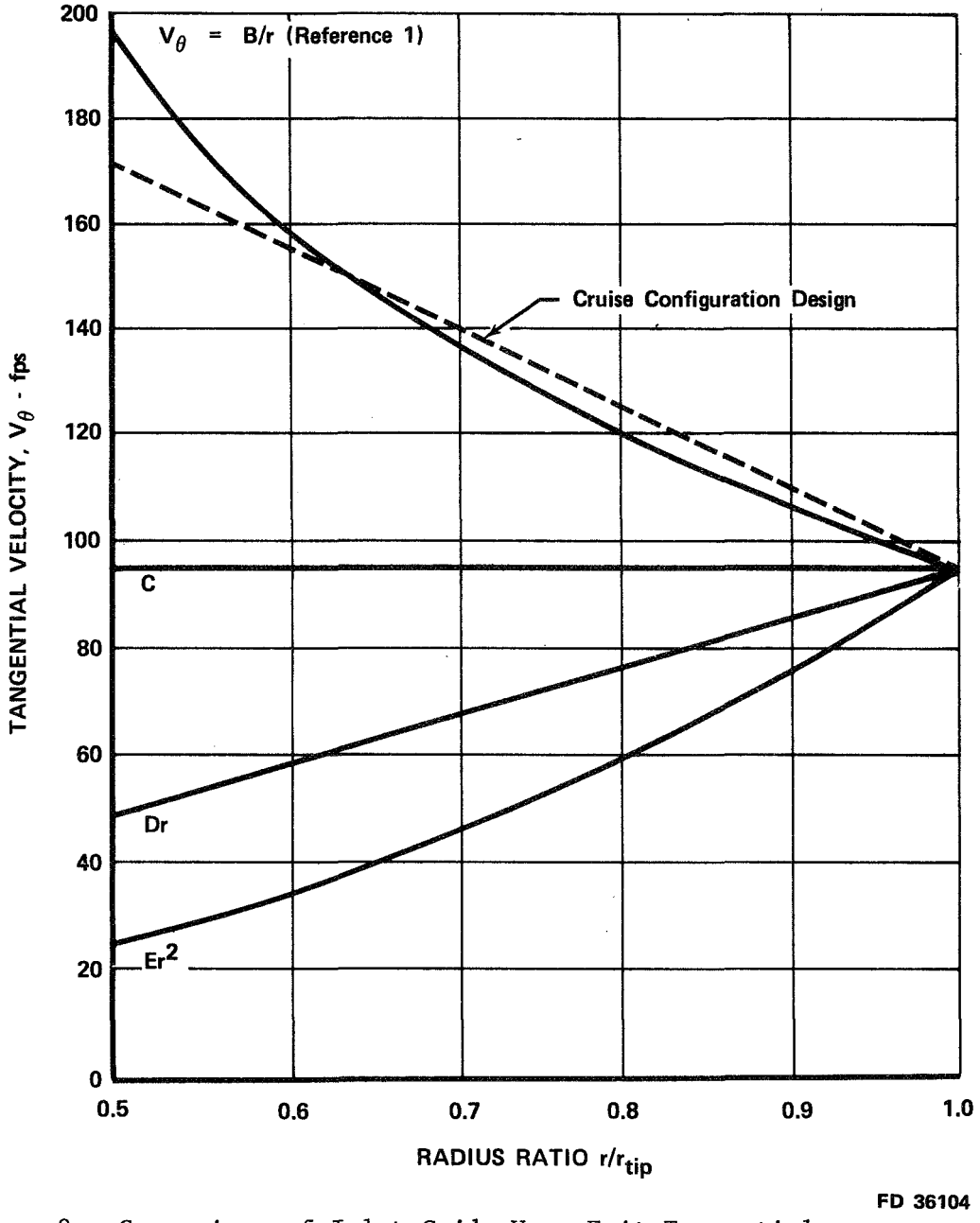

Figure 8. Comparison of Inlet Guide Vane Exit Tangential Velocity Distributions

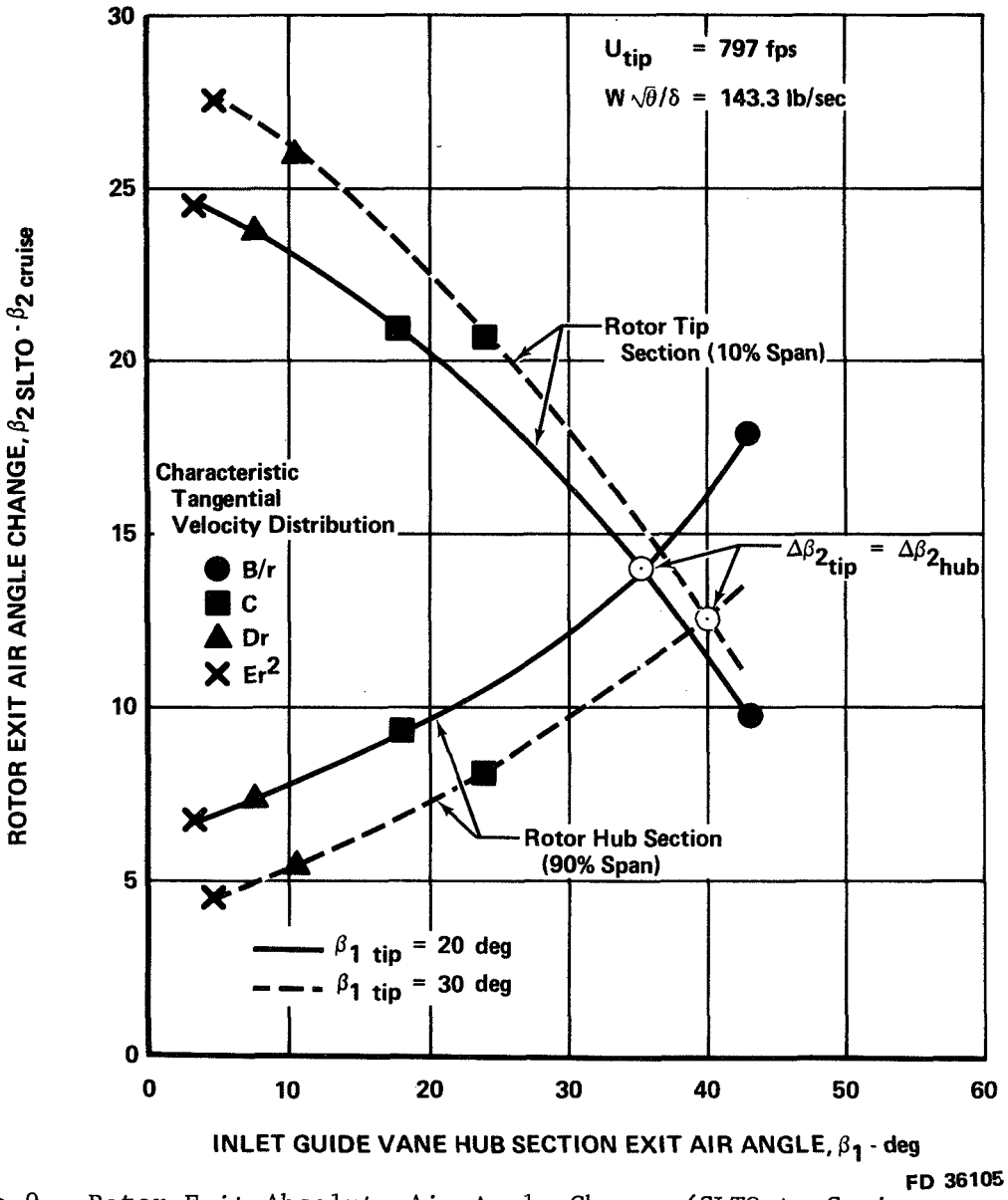

Figure 9. Rotor Exit Absolute Air Angle Change (SLTO to Cruise Conditions) vs Inlet Guide Vane Hub Section Exit Air Angle

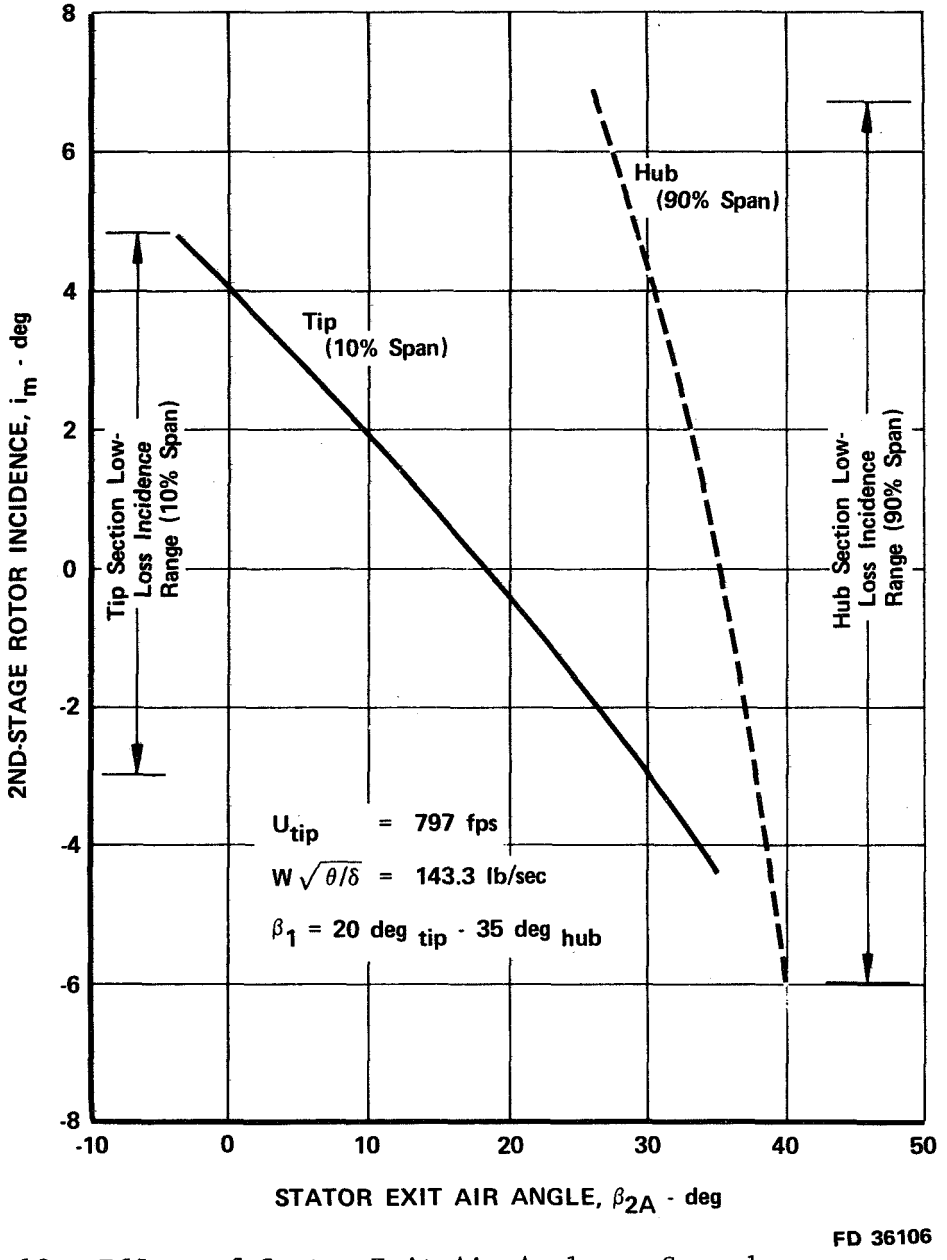

Figure 10. Effect of Stator Exit Air Angle on Second-Stage Rotor Incidence Angle

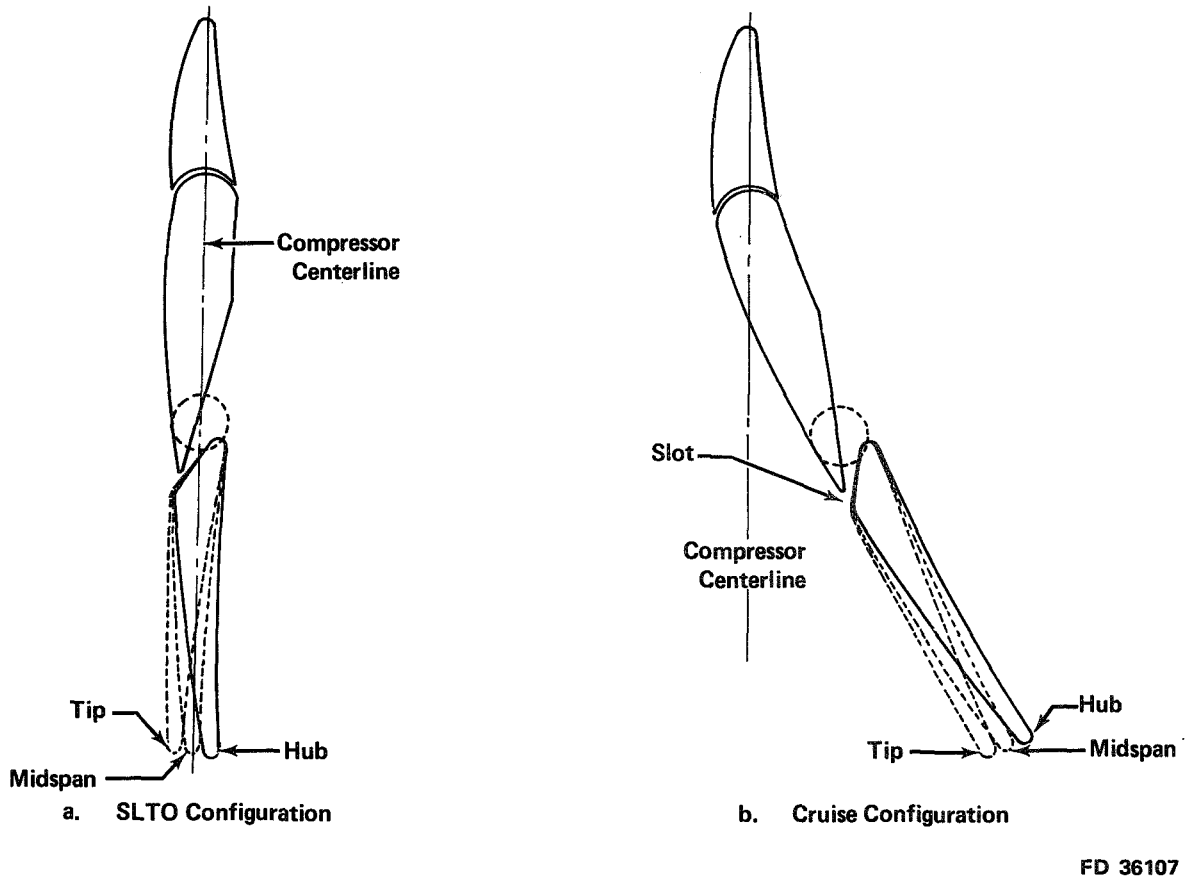

Figure 11. Variable Camber Inlet Guide Vane Sections

GS 5428

Figure 12. Variable Camber Inlet Guide Vane Assembly in SLTO Configuration

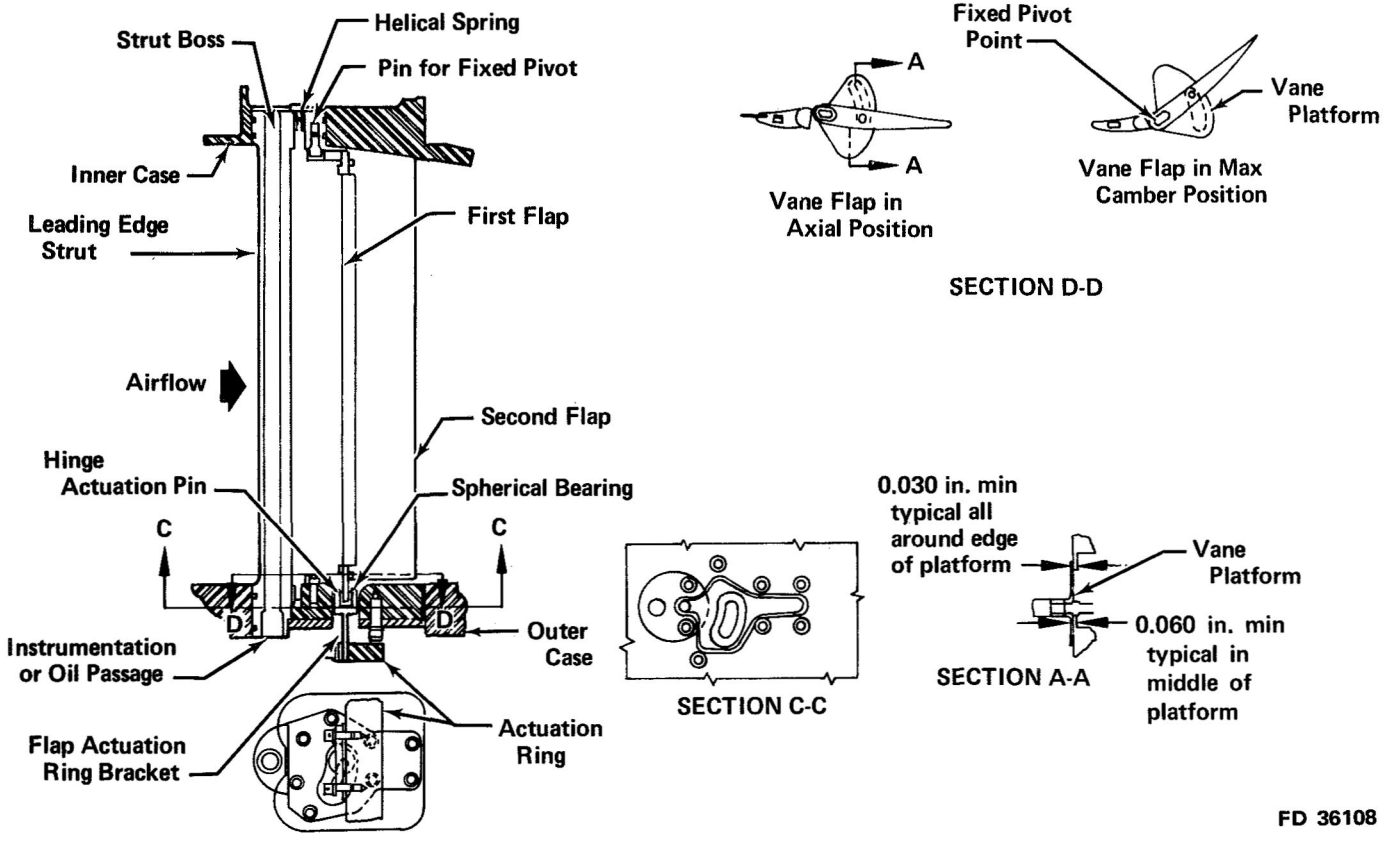

Figure 13. Variable Geometry Inlet Guide Vane Linkage

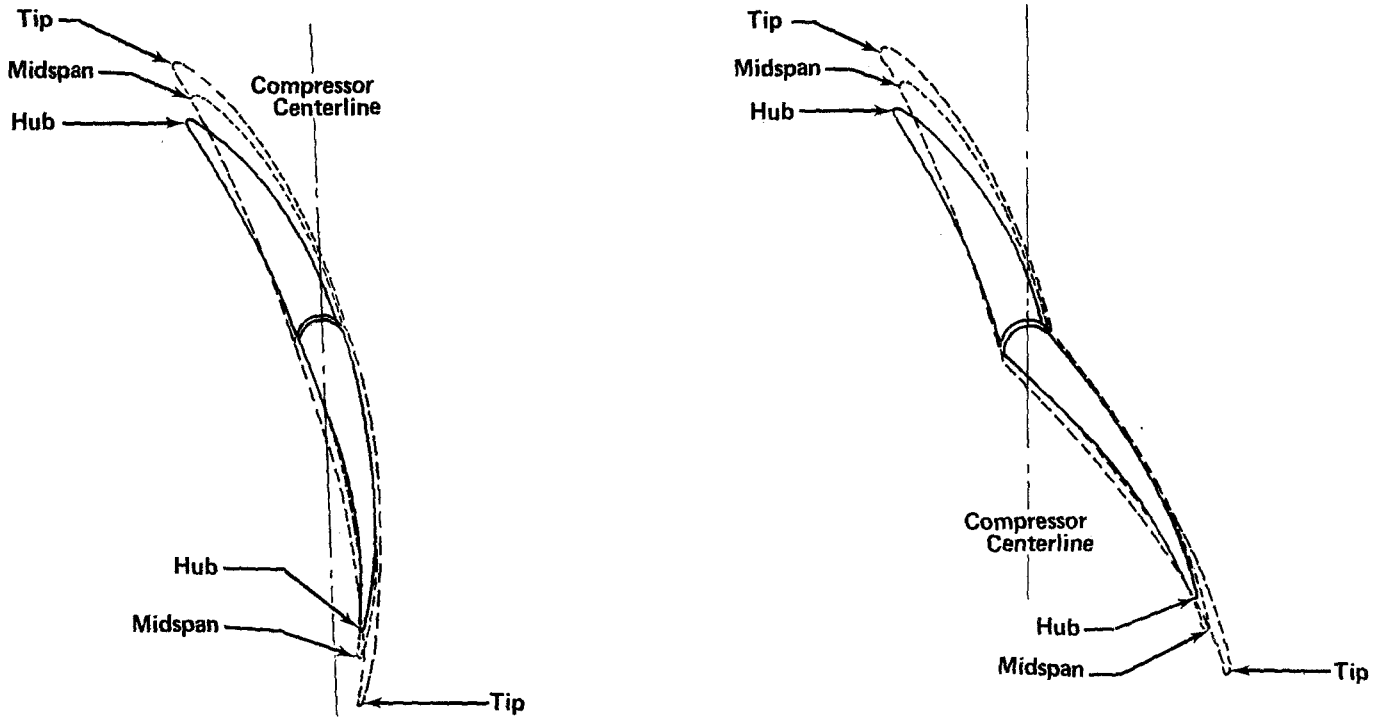

a. SLTO Configuration

b. Cruise Configuration

Figure 14. Variable Geometry Stator A Sections

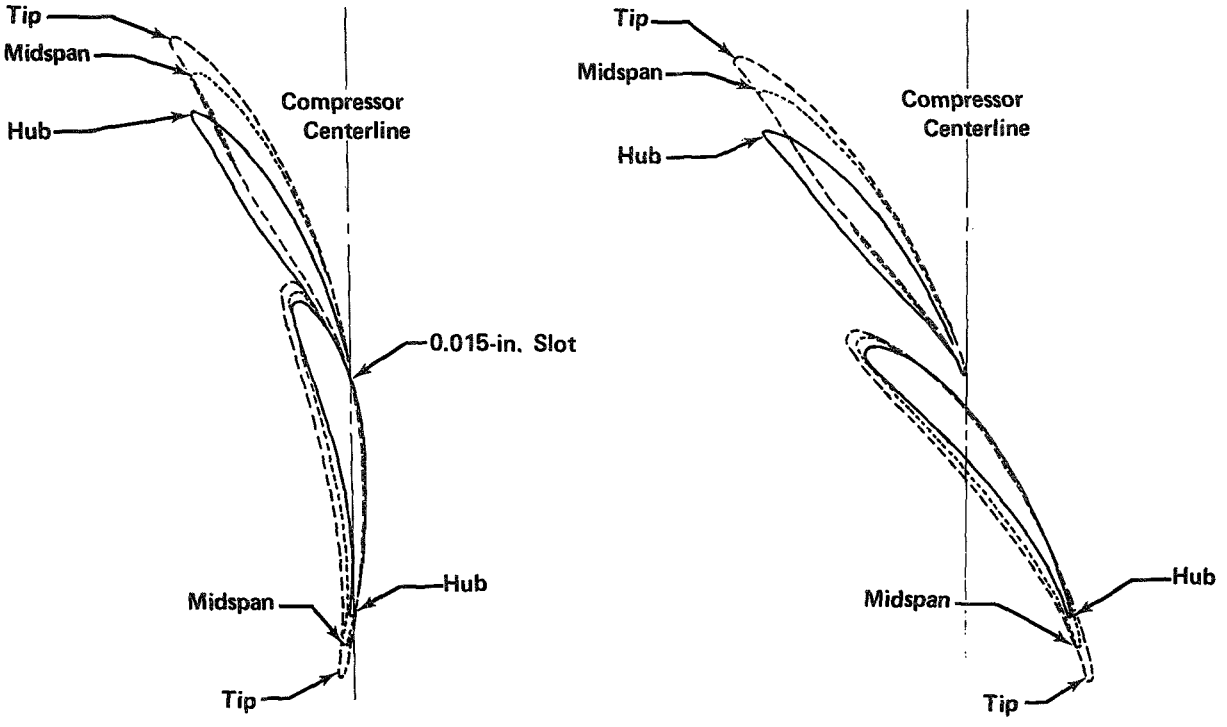

Figure 15. Variable Geometry Stator B Sections

FE 67684

Figure 16. Variable Geometry Stator A Assembly

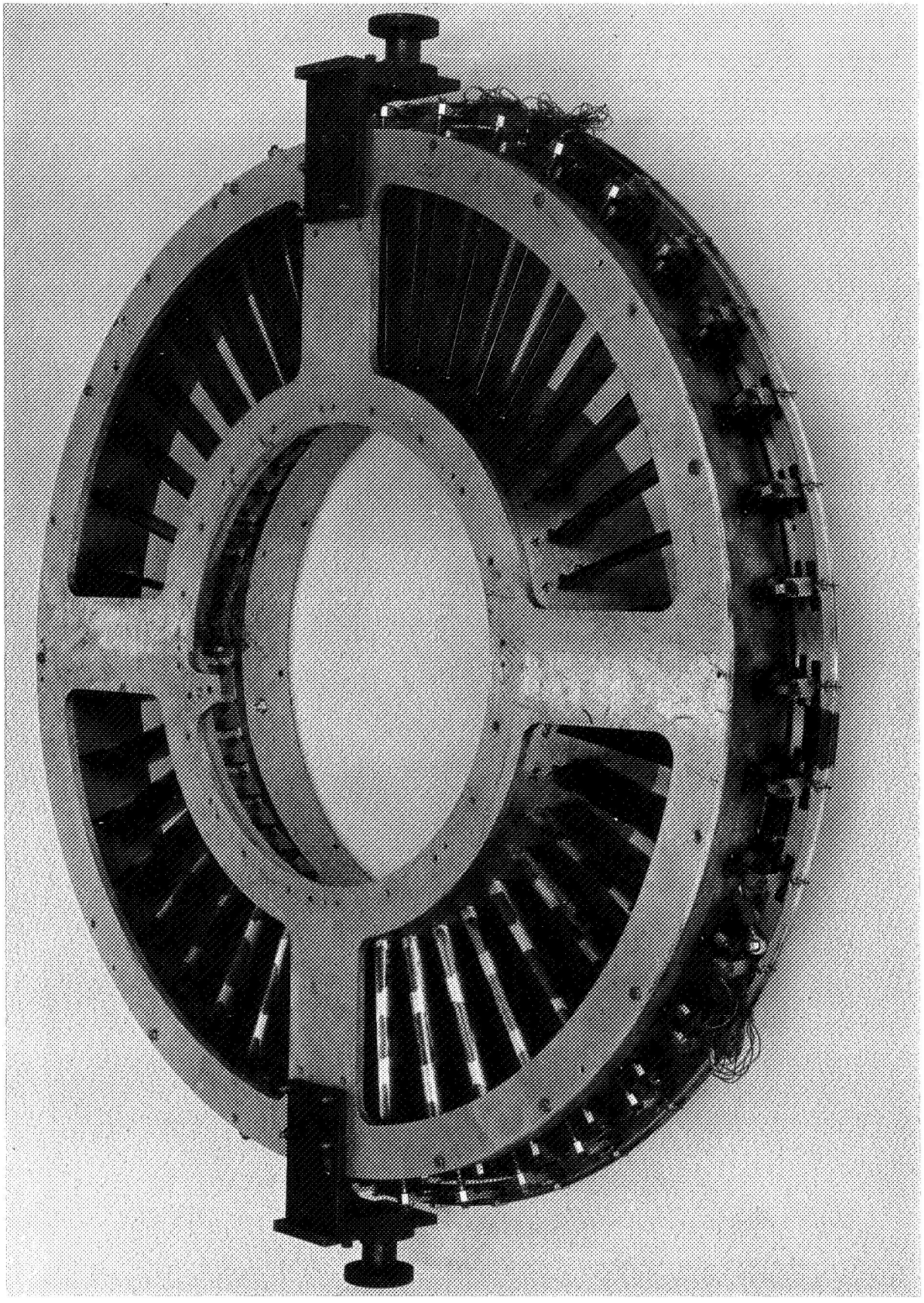

FE 70134

Figure 17. Variable Geometry Stator B Assembly

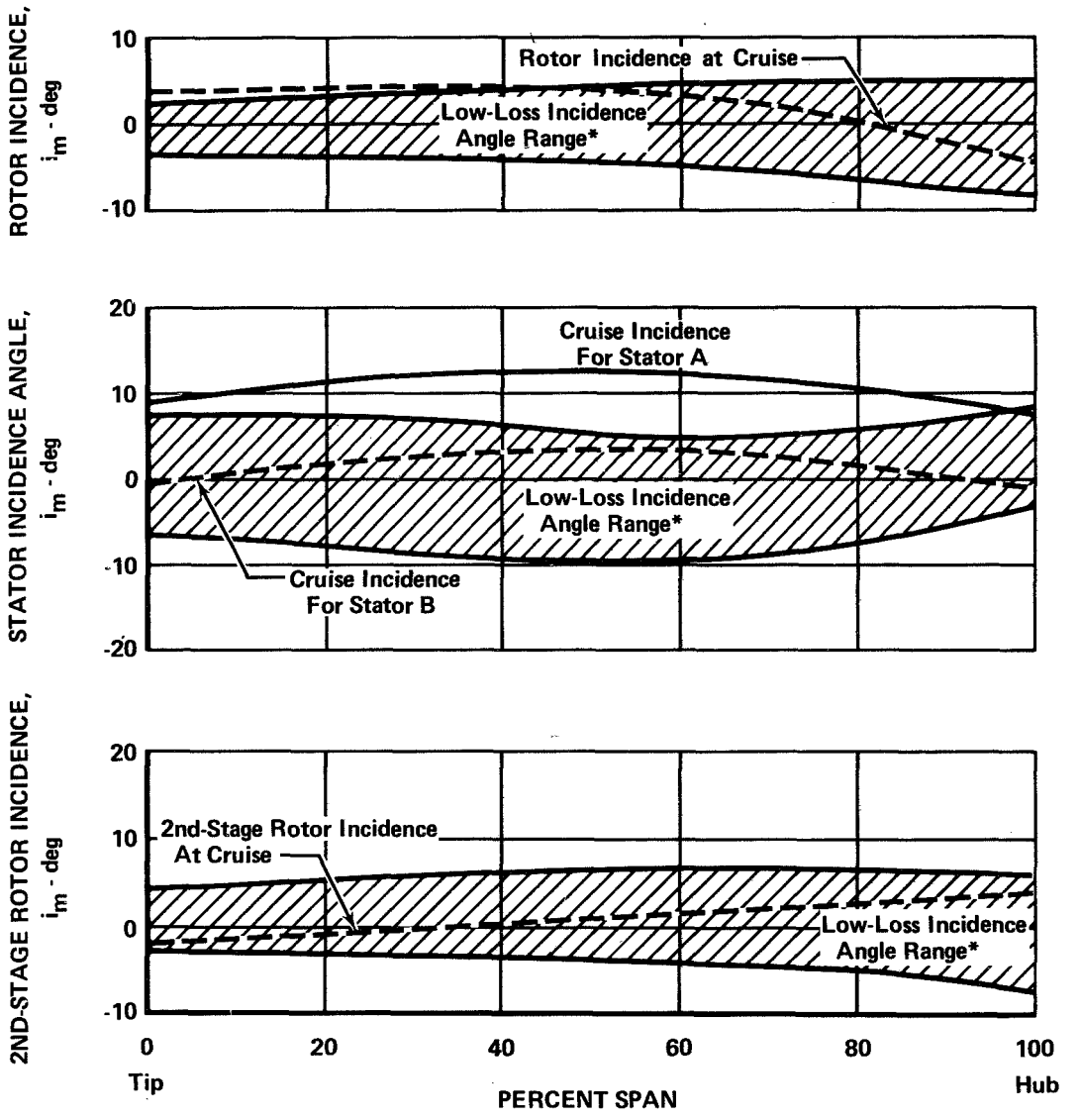

Figure 18. Comparison of Calculated Cruise Design Point Incidence Angles with Predicted Low-Loss Incidence Range for Rematched (Variable Geometry) Blade Rows

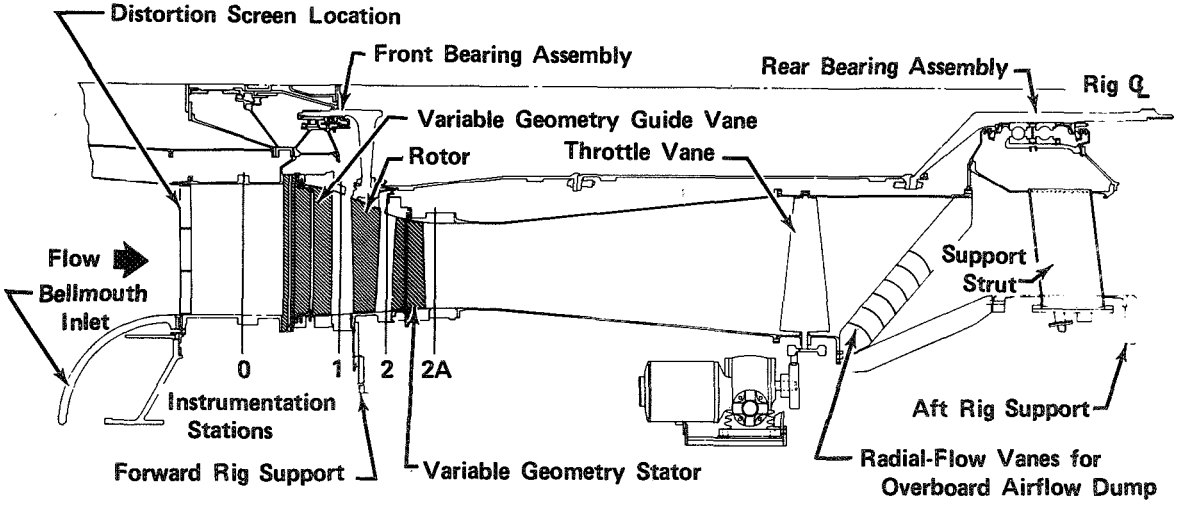

Figure 19. Compressor Test Rig

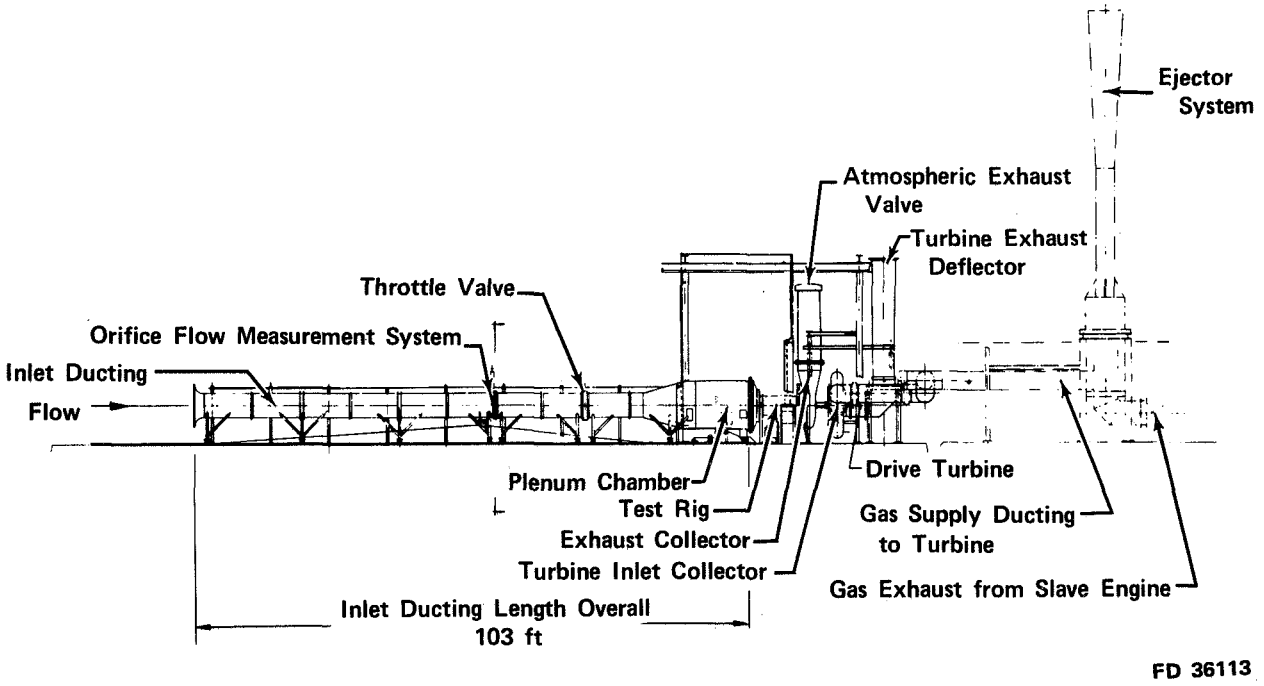

Figure 20. Compressor Test Facility

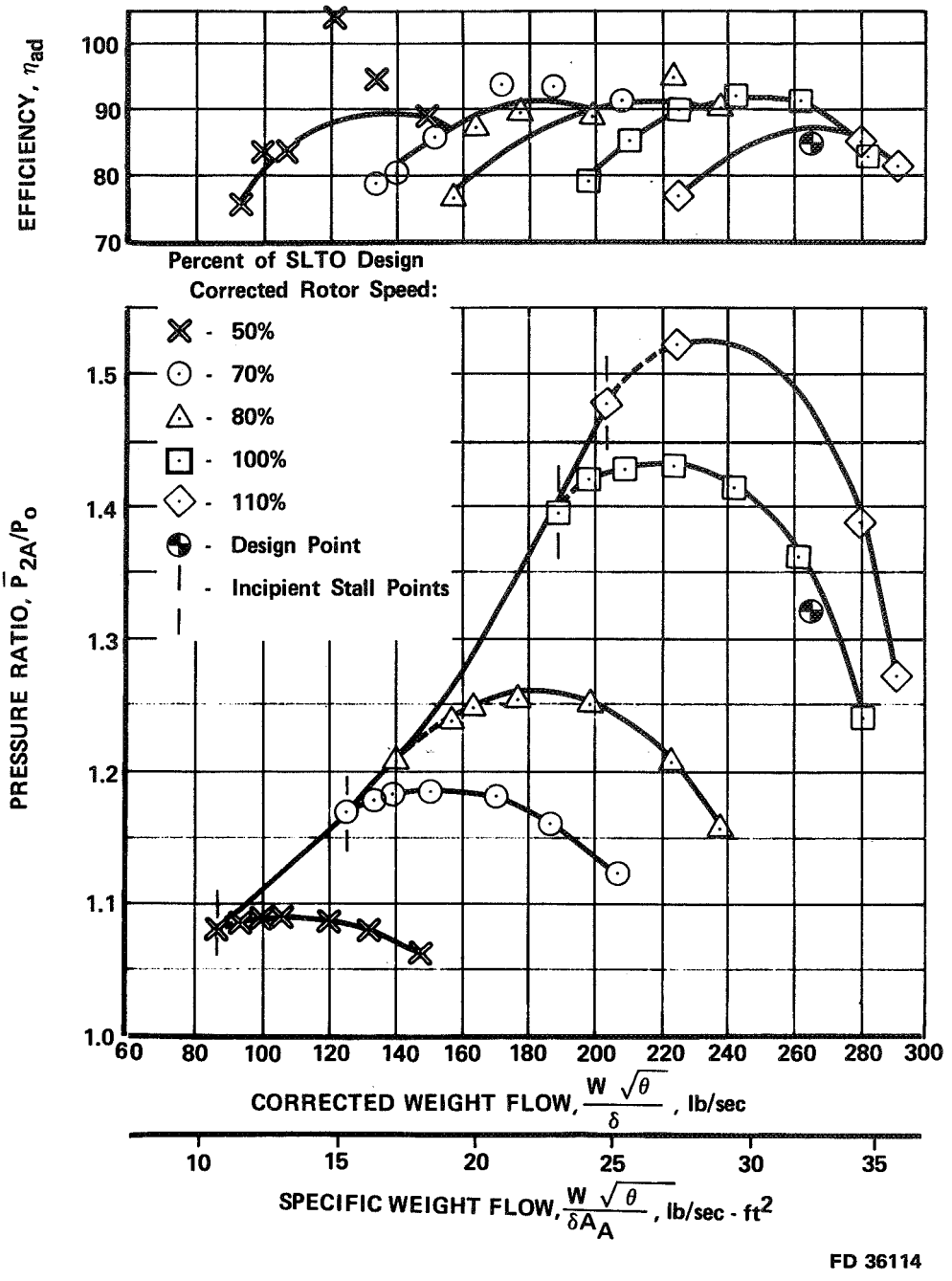

Figure 21. Overall Performance of Stator B Stage in the SLTO Configuration

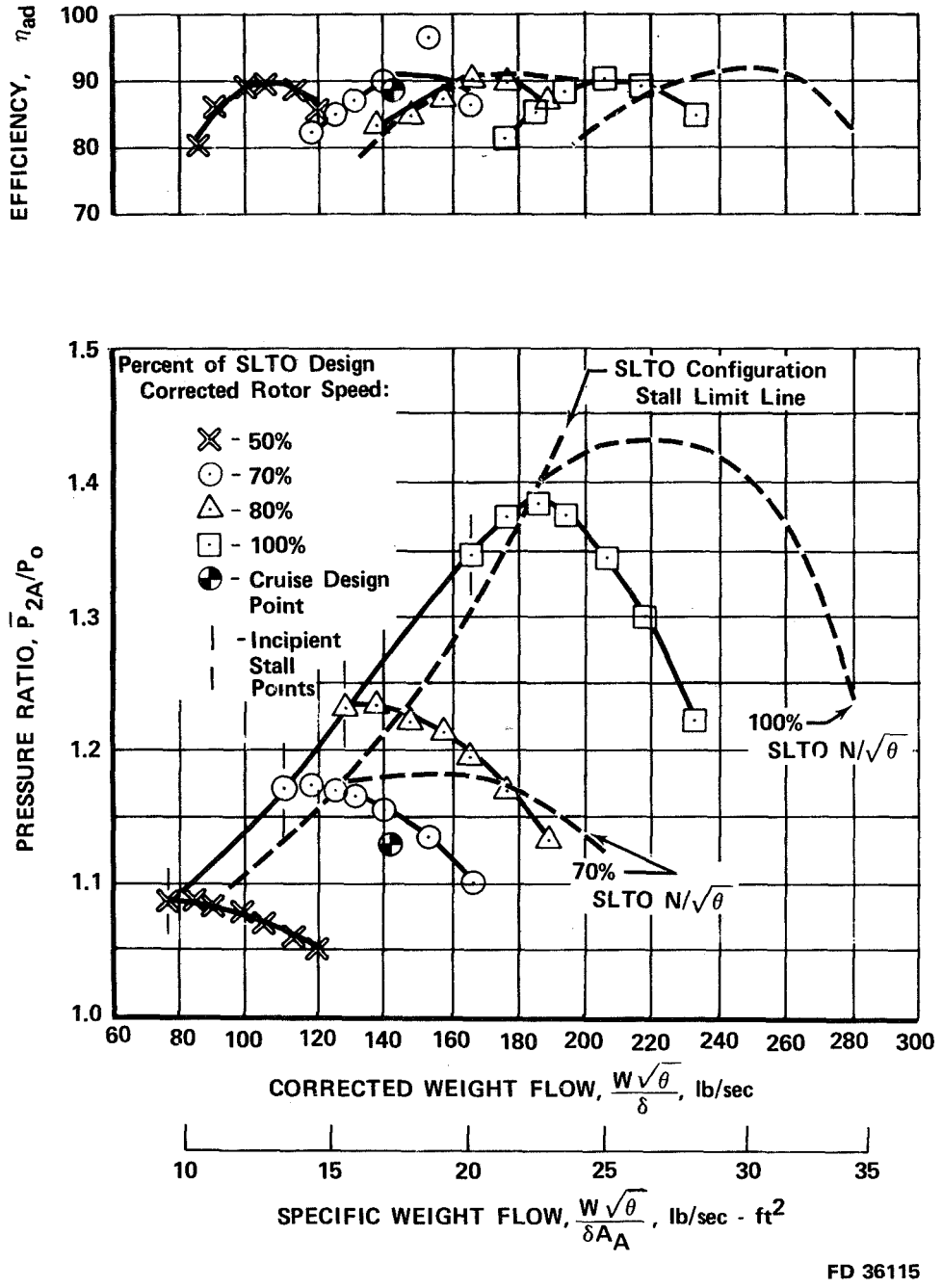

Figure 22. Overall Performance of Stator B Stage in the Cruise Configuration

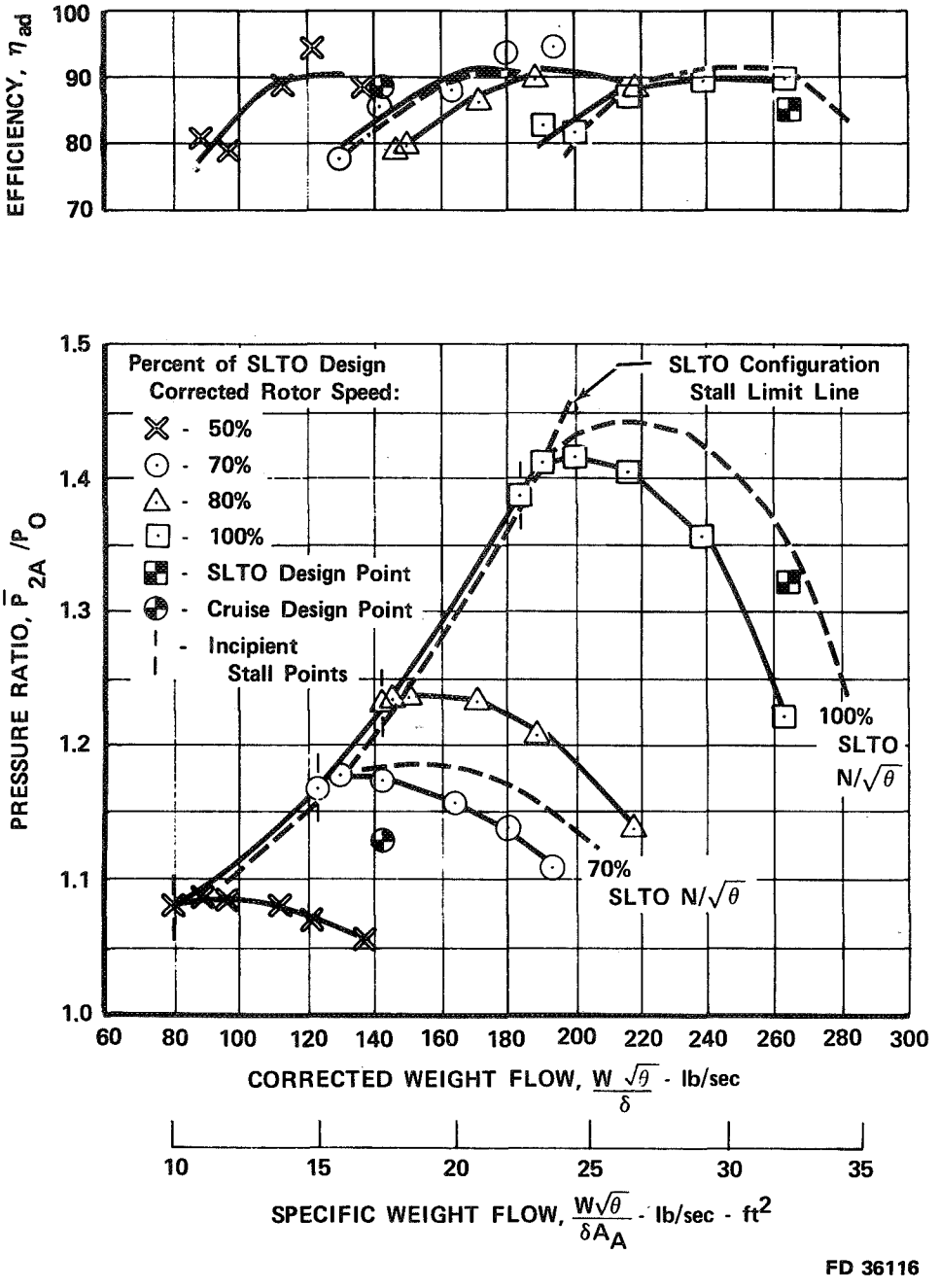

Figure 23. Overall Performance of Stator B Stage in the Intermediate Configuration

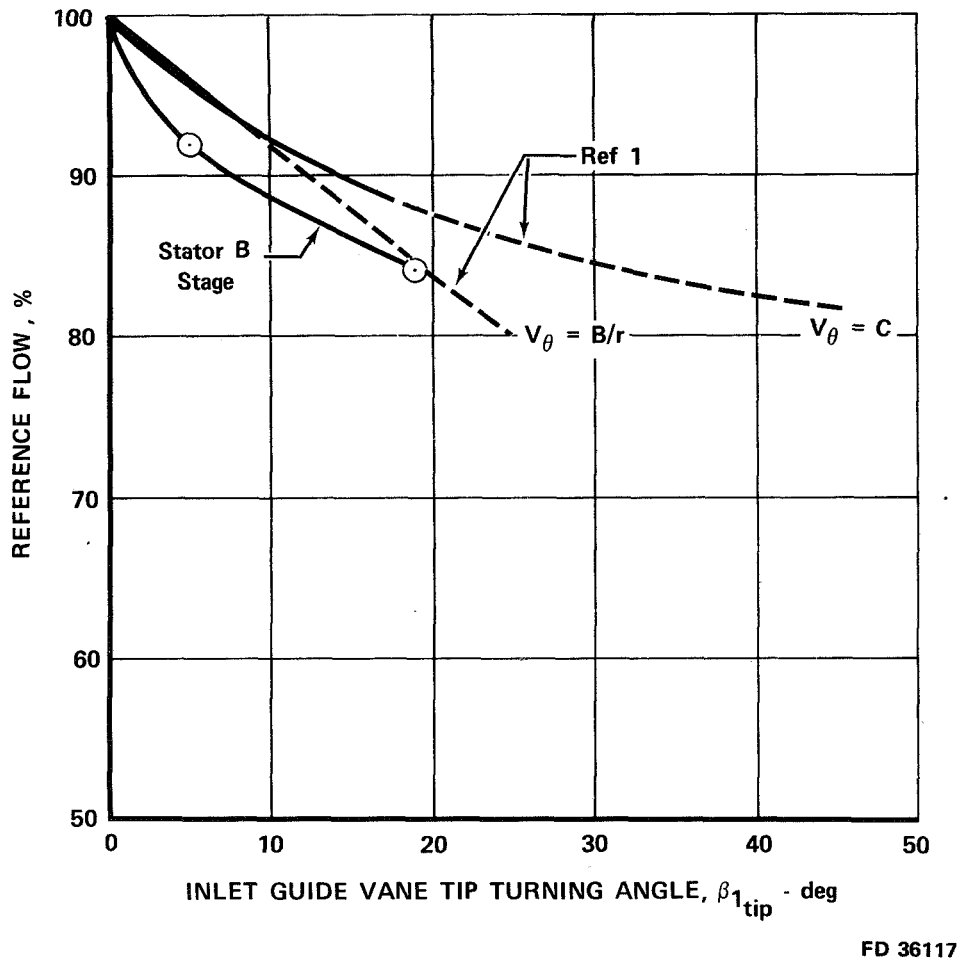

Figure 24. Mass Flow Reduction as a Function of Inlet Guide Vane Tip Turning Angle

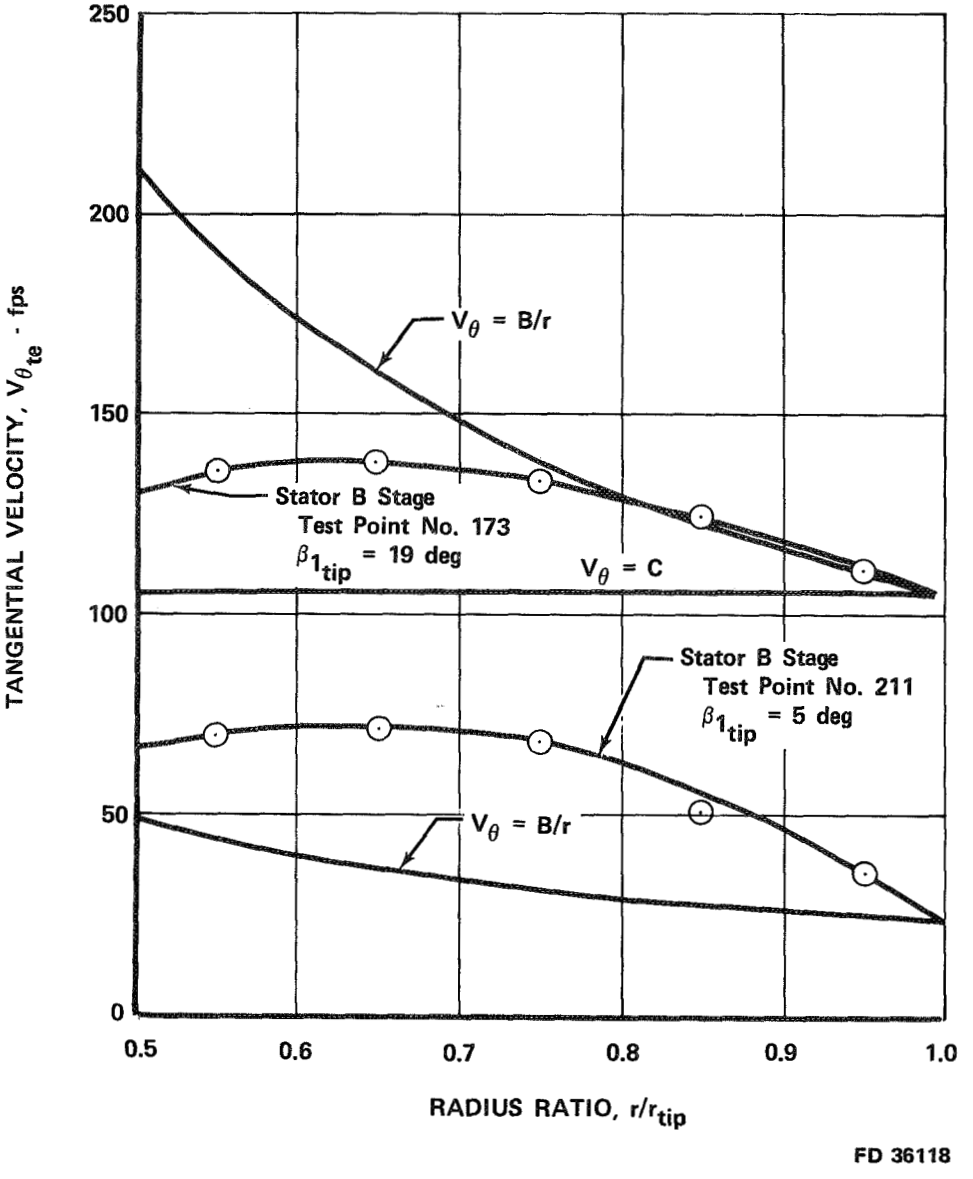

Figure 25. Experimental Inlet Guide Vane Exit Tangential Velocity Distributions

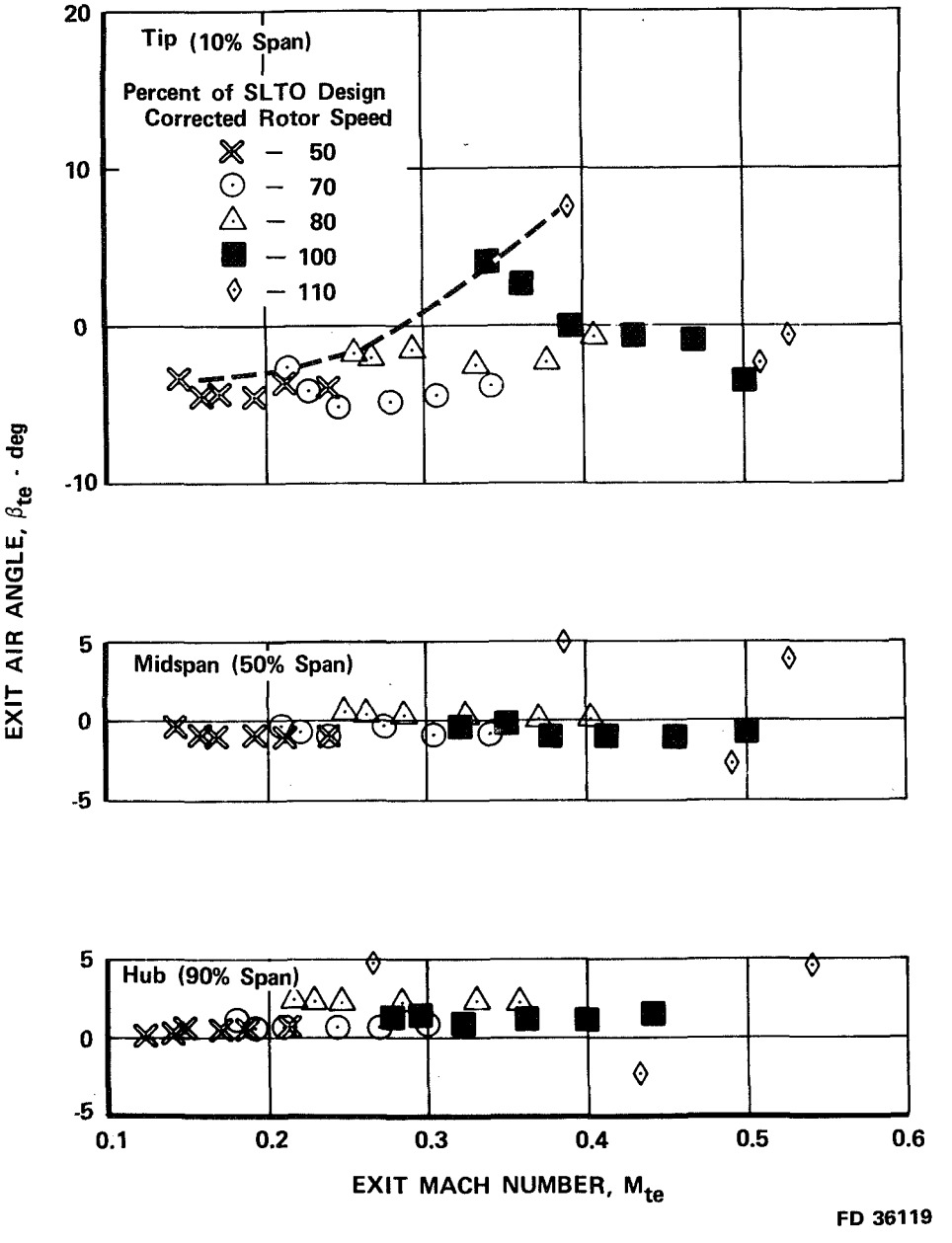

Figure 26. Inlet Guide Vane Exit Air Angle as a Function of Guide Vane Exit Mach Number; SLTO Configuration

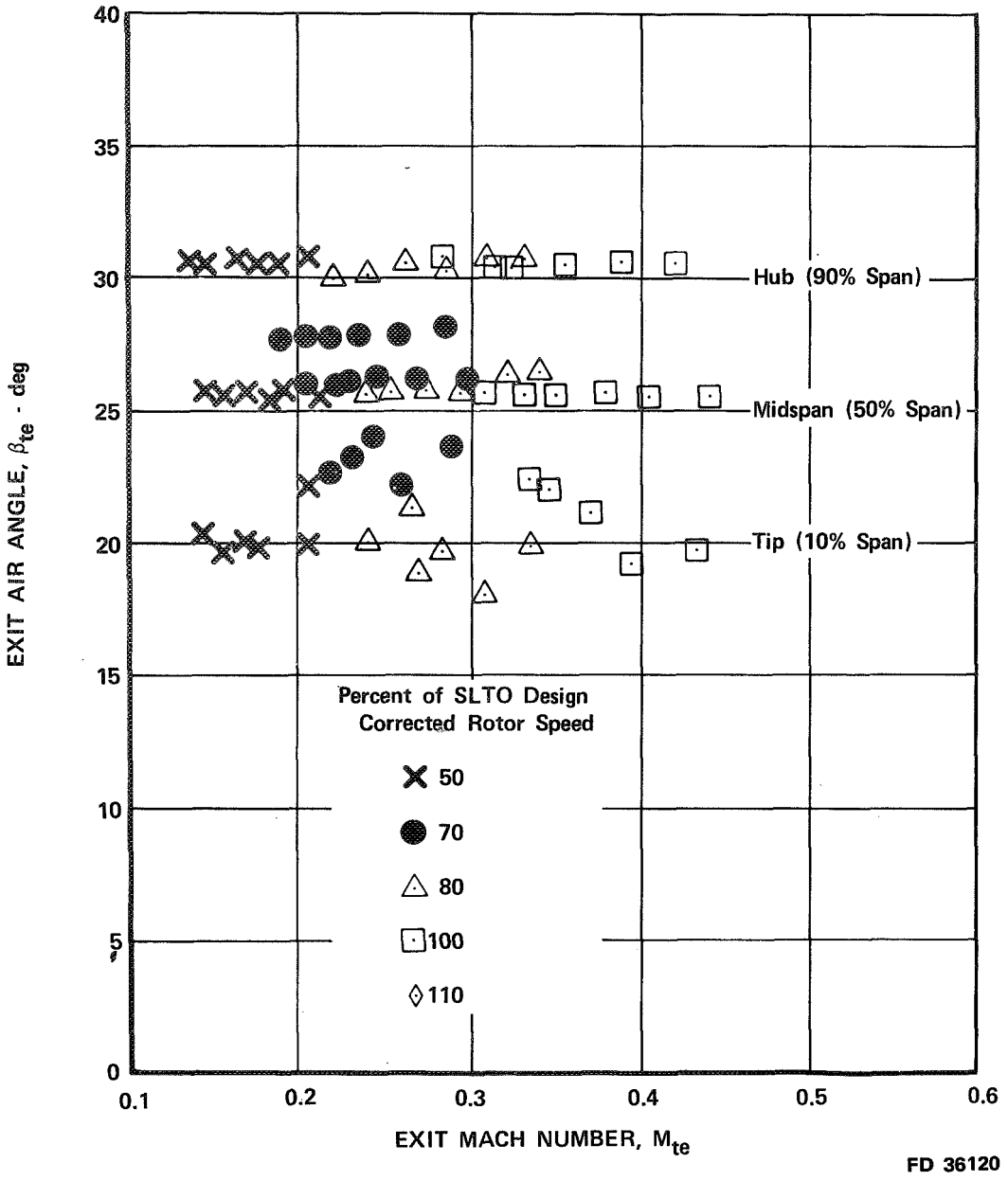

Figure 27. Inlet Guide Vane Exit Air Angle as a Function of Guide Vane Exit Mach Number; Cruise Configuration

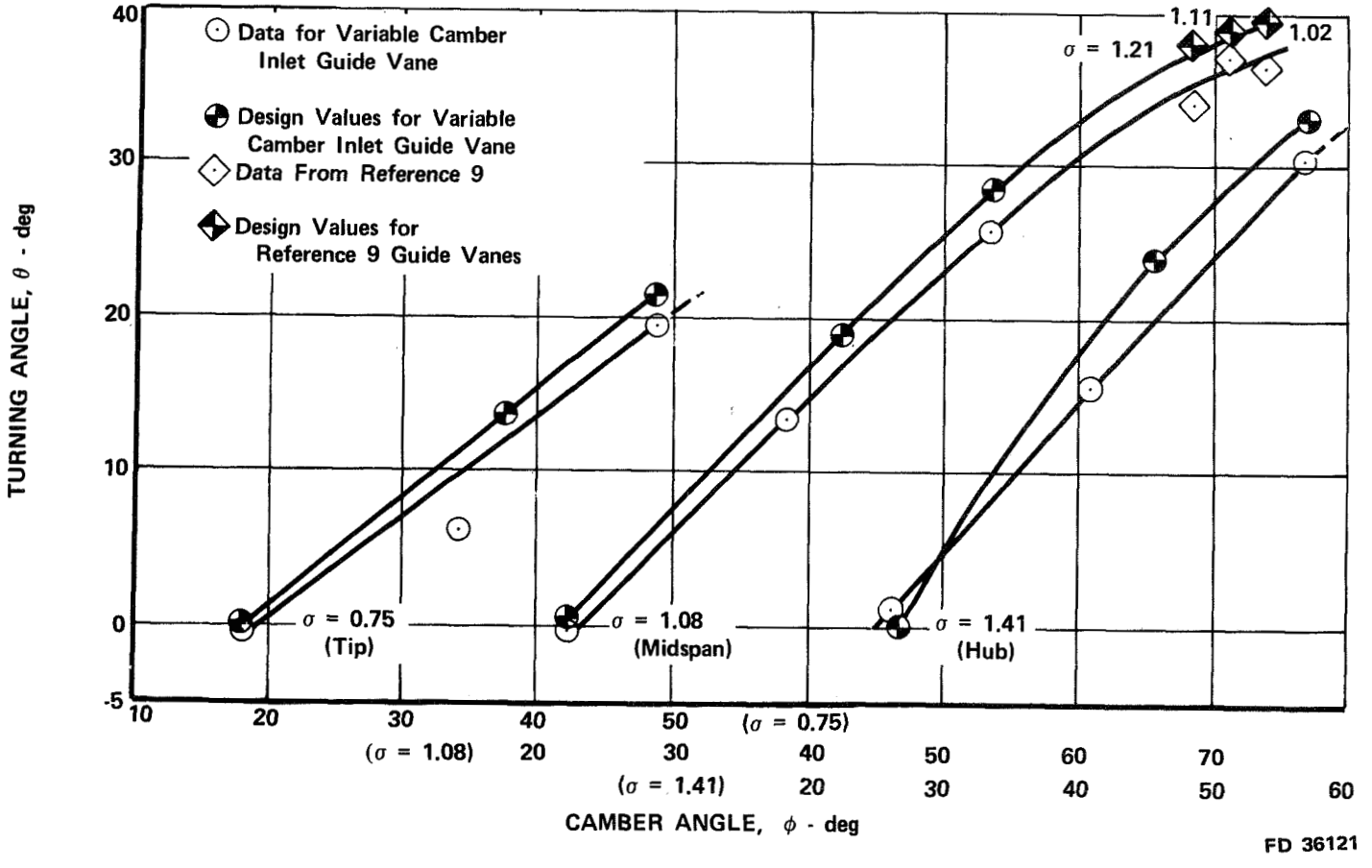

Figure 28. Inlet Guide Vane Turning Angle as a Function of Camber Angle

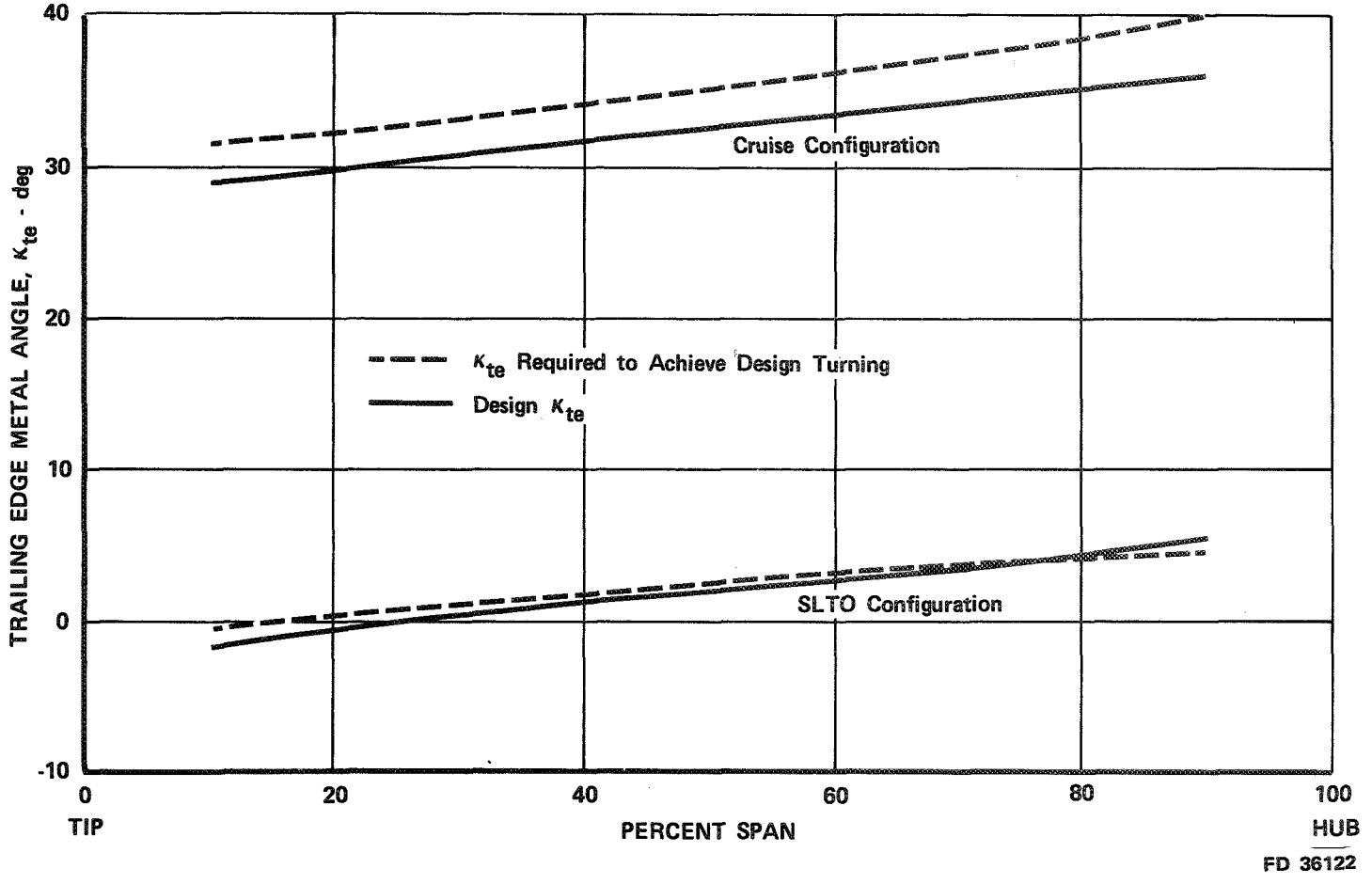

Figure 29. Adjustment of Variable Geometry Inlet Guide Vane Camber to Achieve Design Turning

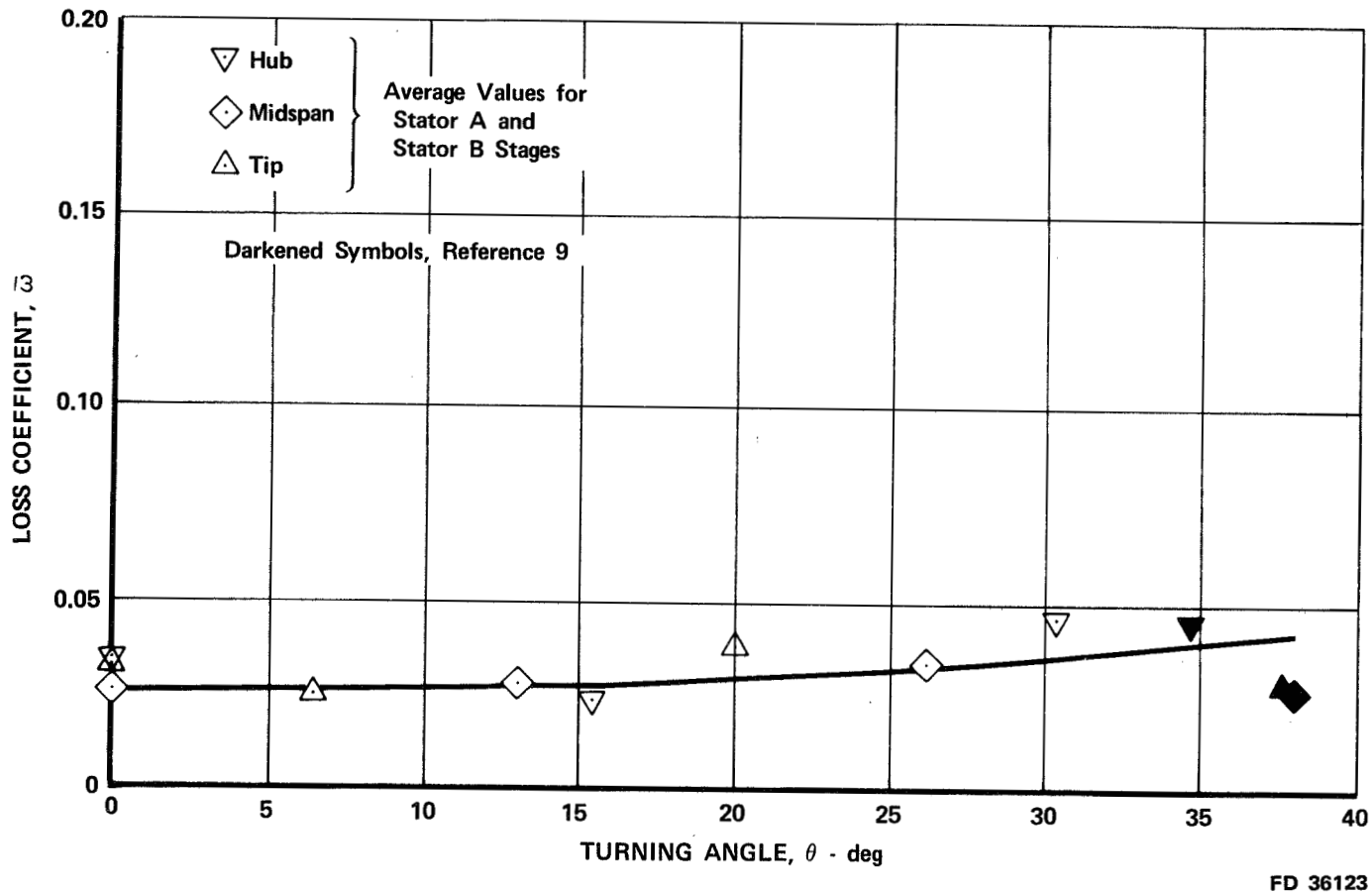

Figure 30. Inlet Guide Vane Loss Coefficient as a Function of Guide Vane Turning Angle

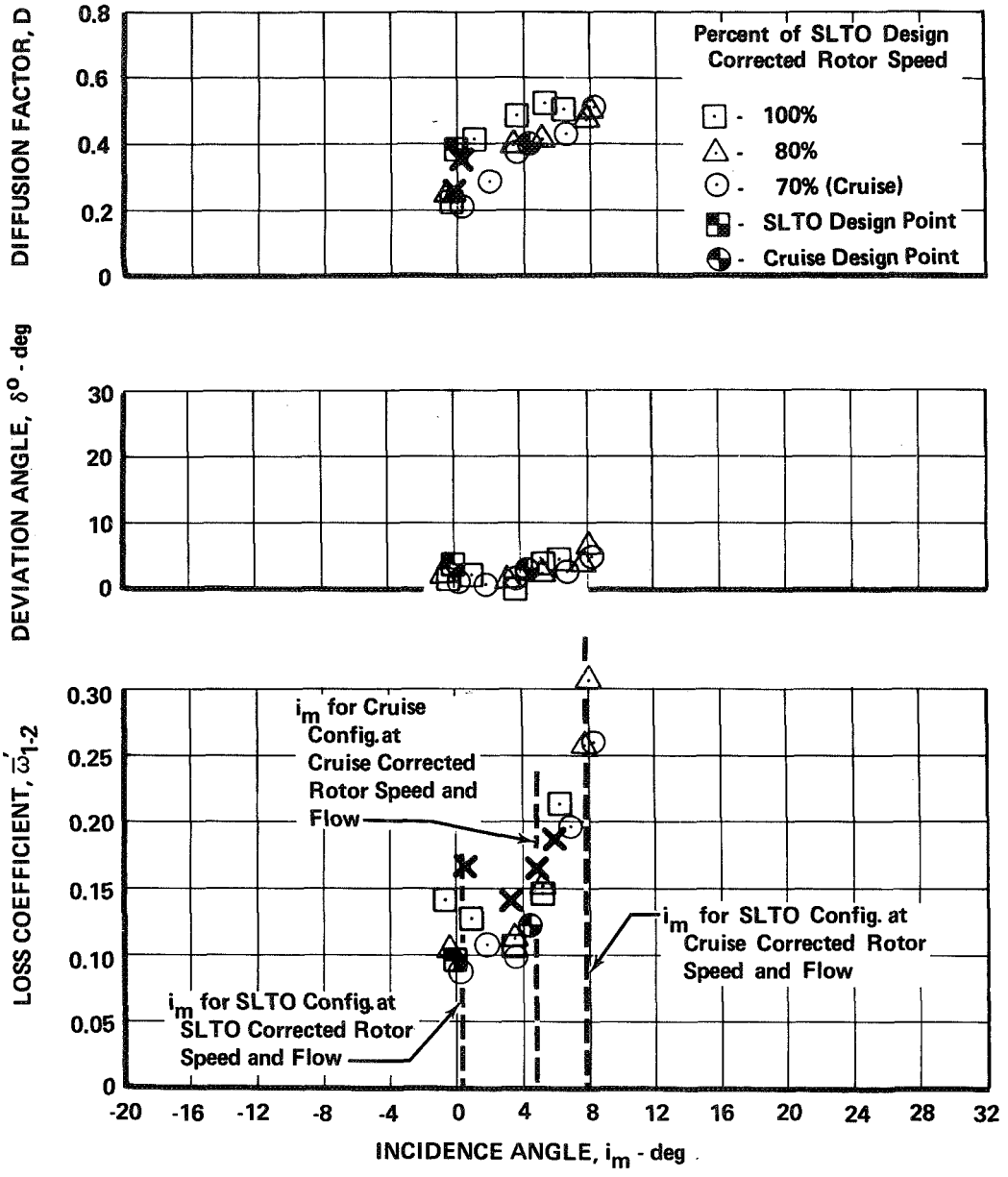

Figure 31a. Rotor Blade Element Performance: Stator B Stage, Intermediate Configuration, 10% Span From Tip

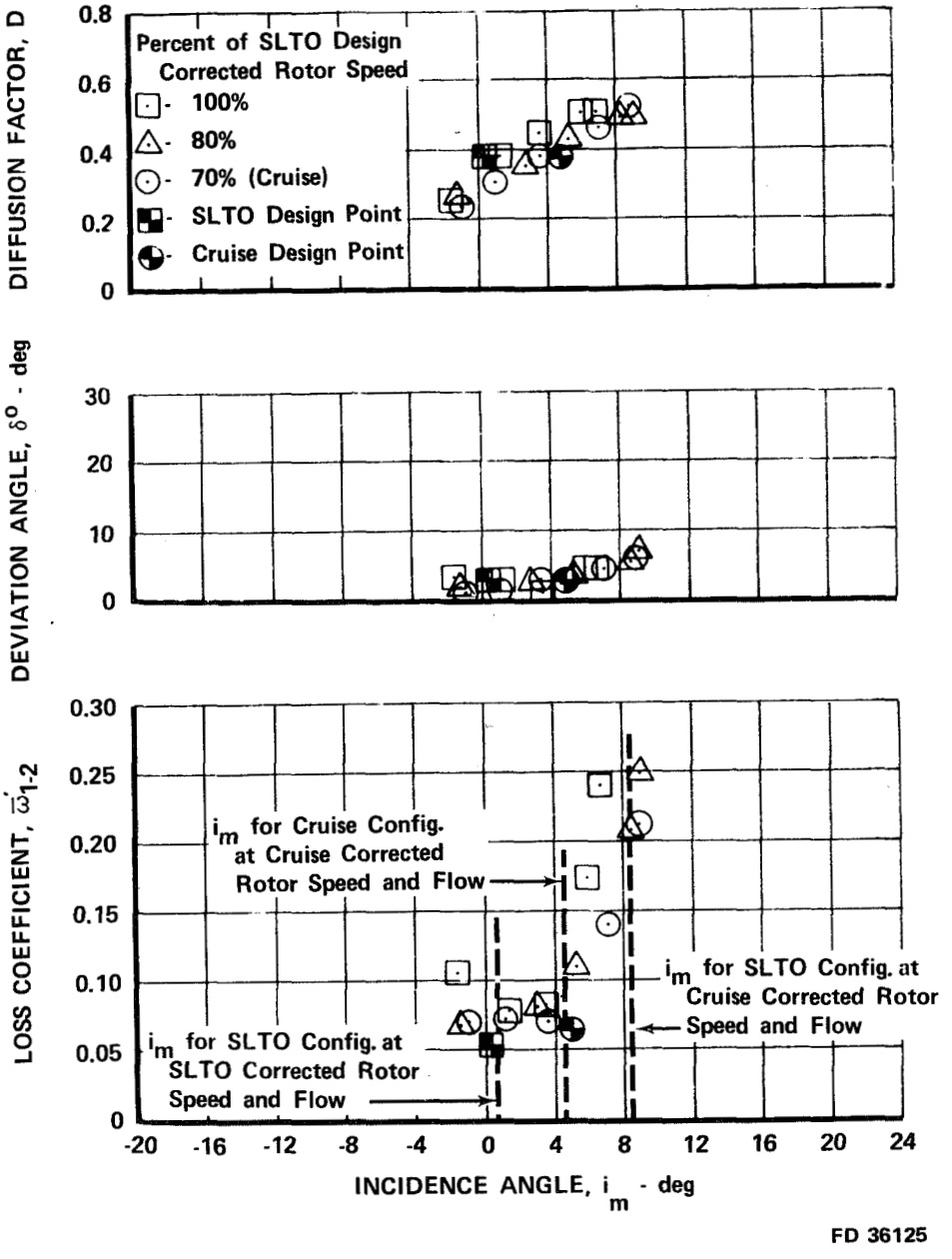

Figure 31b. Rotor Blade Element Performance: Stator B Stage, Intermediate Configuration, 30% Span From Tip

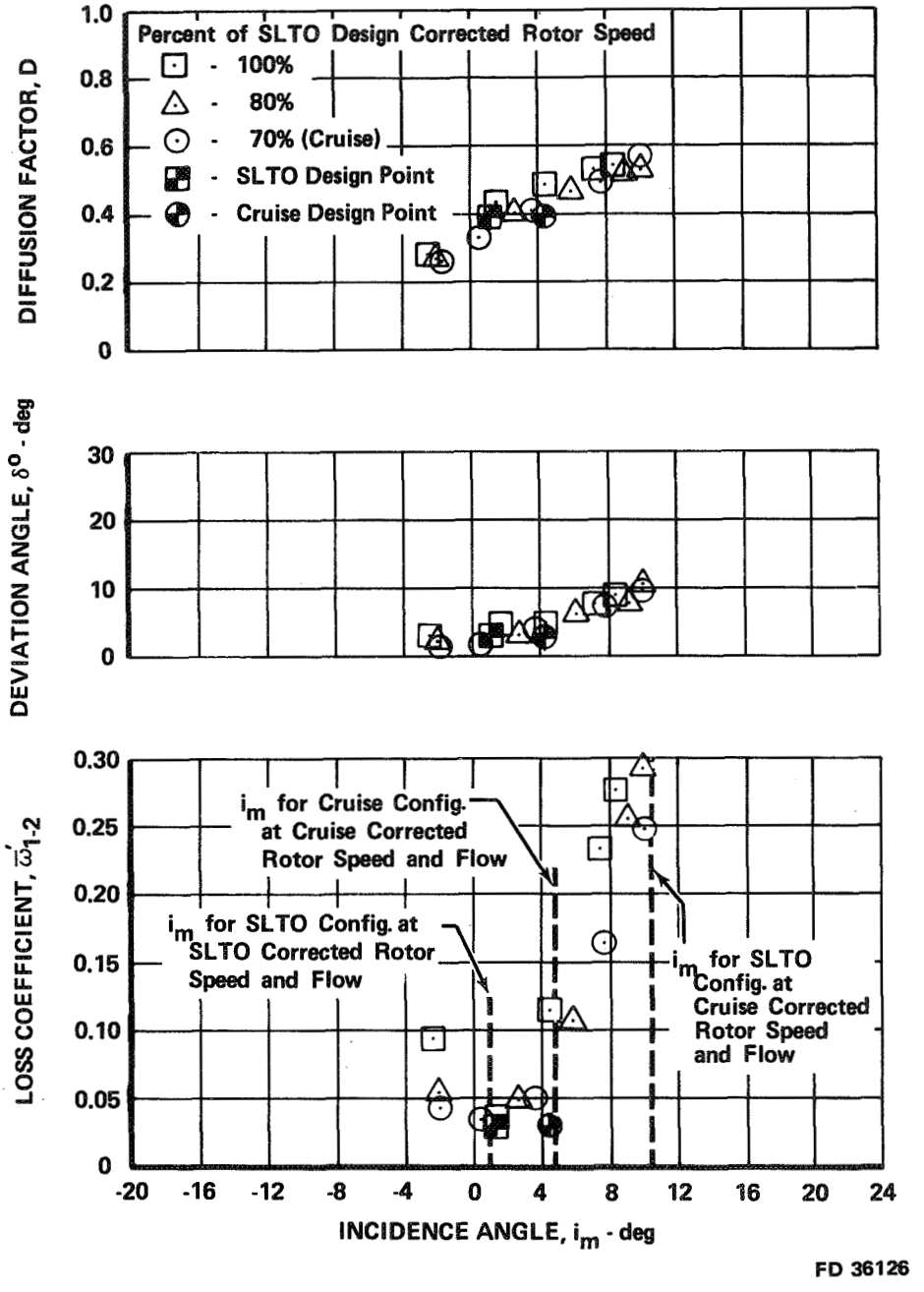

Figure 31c. Rotor Blade Element Performance: Stator B Stage, Intermediate Configuration, 50% Span From Tip

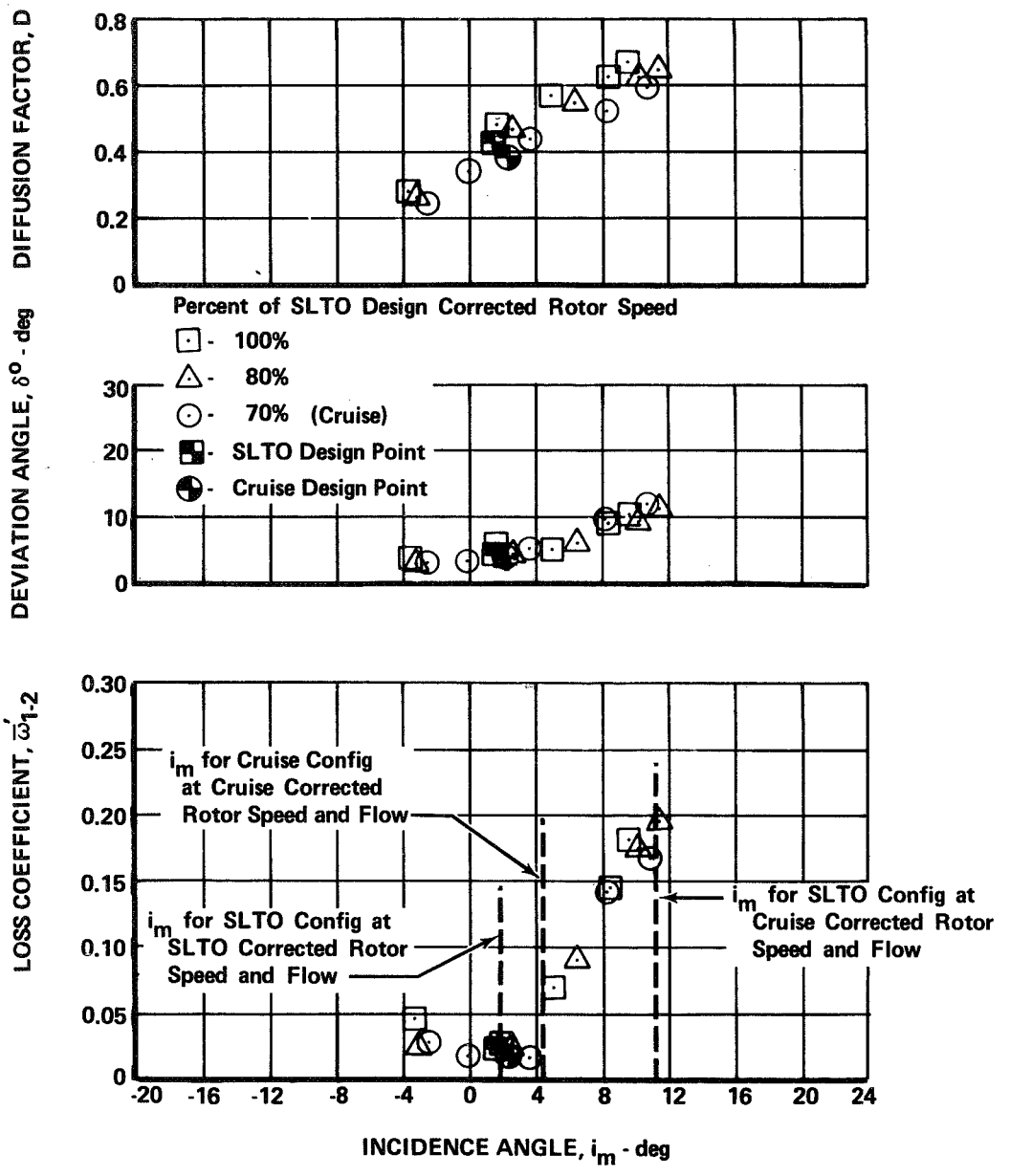

Figure 31d. Rotor Blade Element Performance: Stator B Stage, Intermediate Configuration, 70% Span From Tip

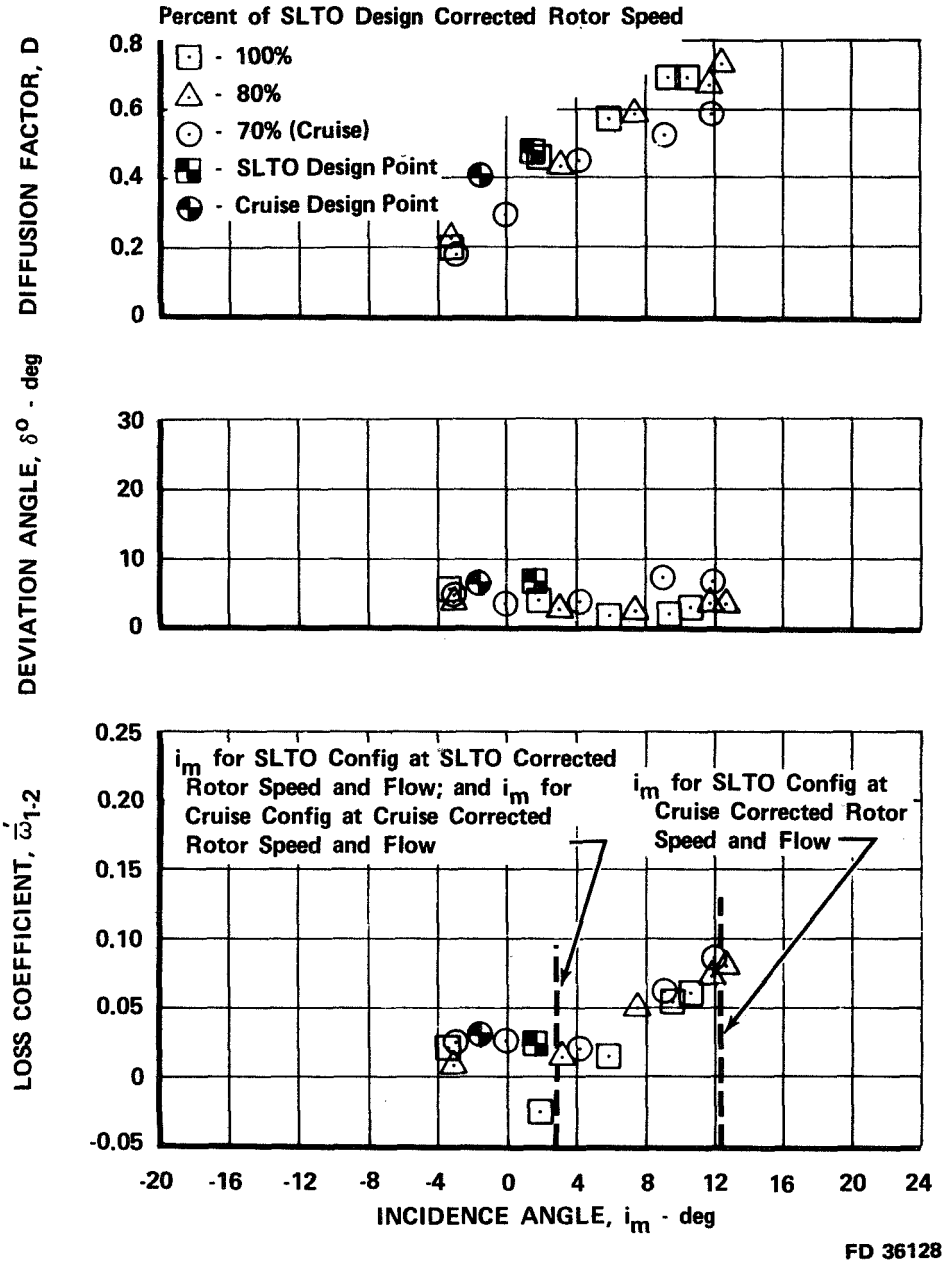

Figure 31e. Rotor Blade Element Performance: Stator B Stage, Intermediate Configuration, 90% Span From Tip

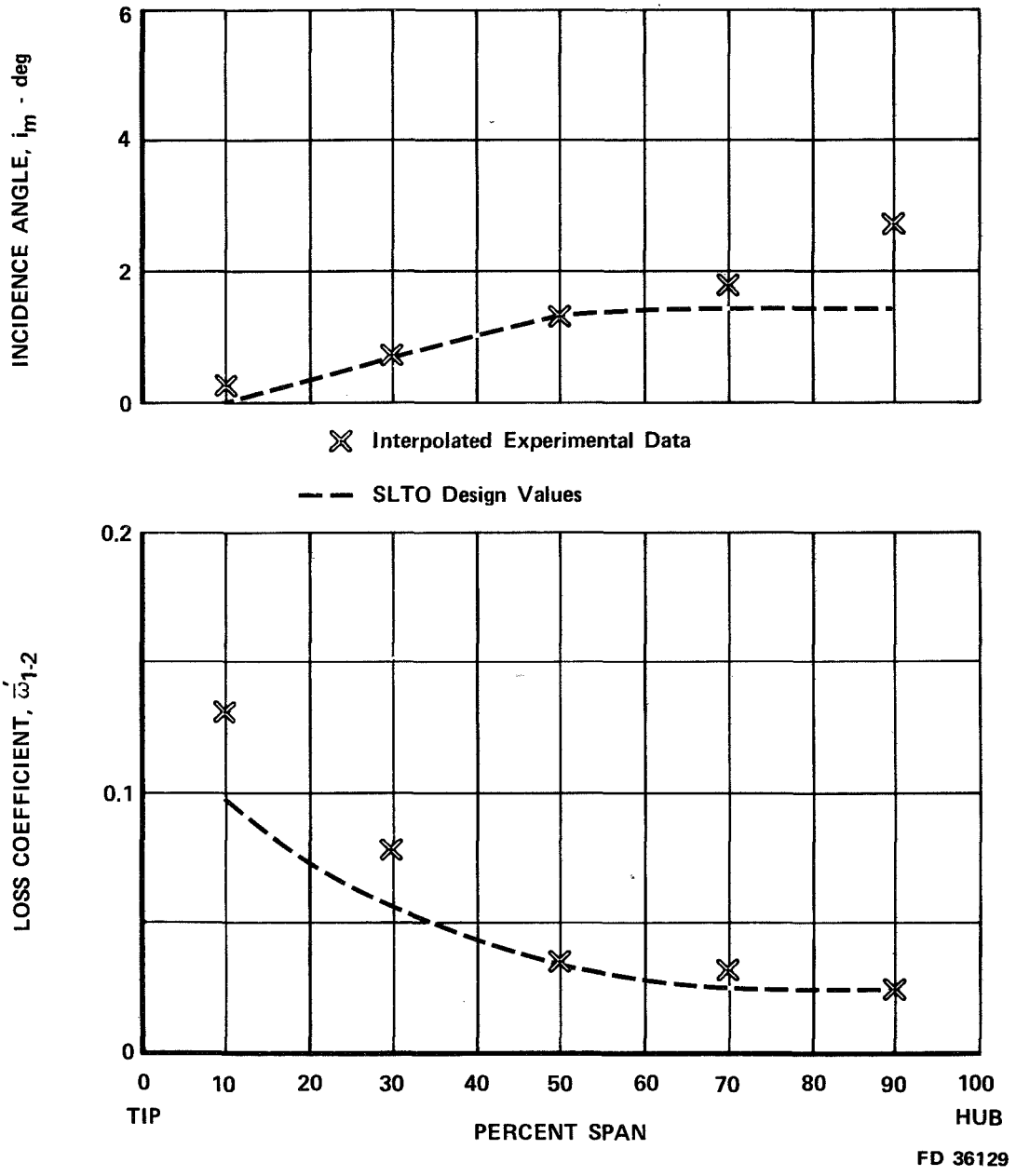

Figure 32. Rotor Incidence Angle and Loss Coefficient Distribution for SLTO Configuration Operating at SLTO Corrected Rotor Speed and Flow

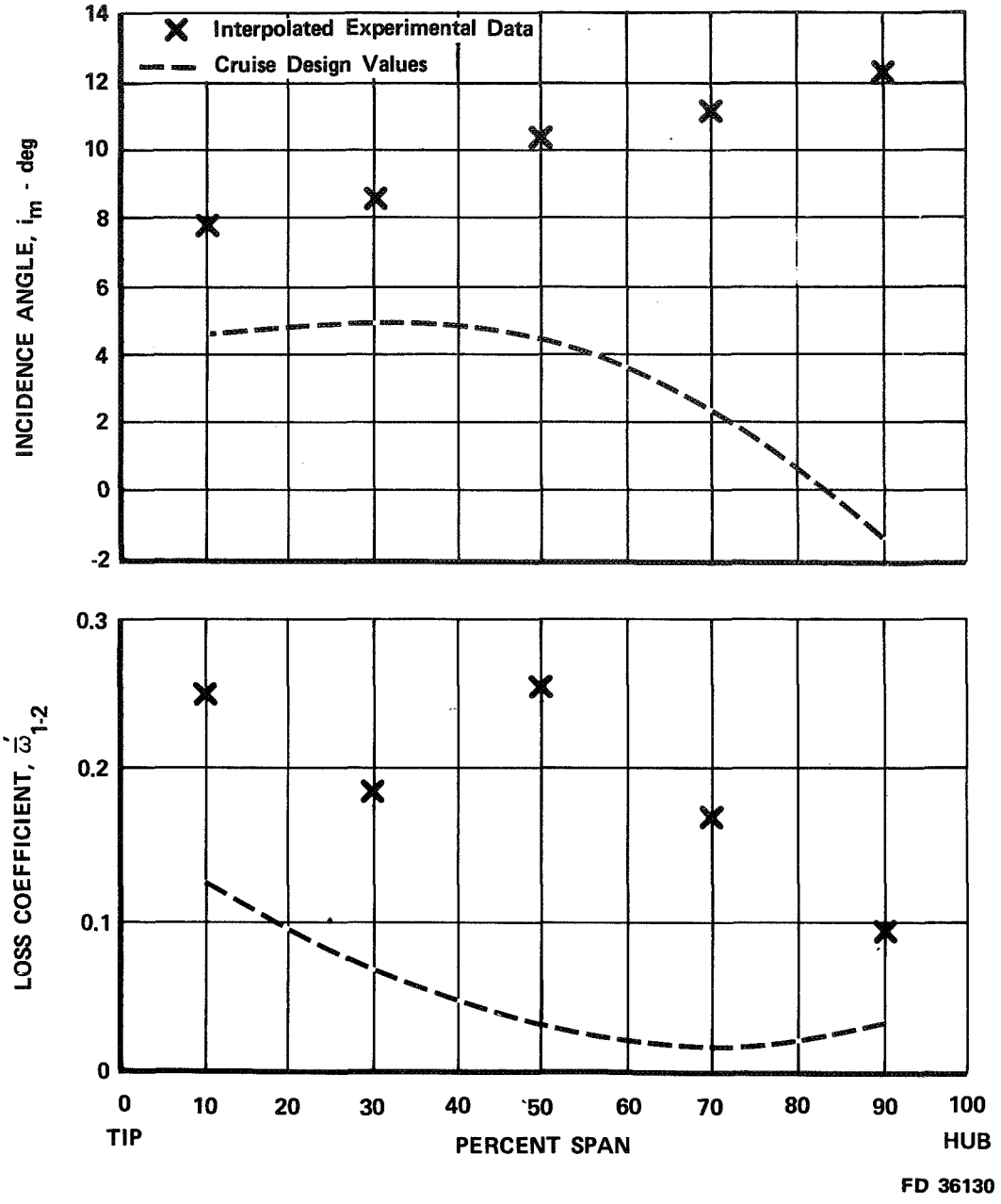

Figure 33. Rotor Incidence Angle and Loss Coefficient Distributions for SLTO Configuration Operating at Cruise Corrected Rotor Speed and Flow

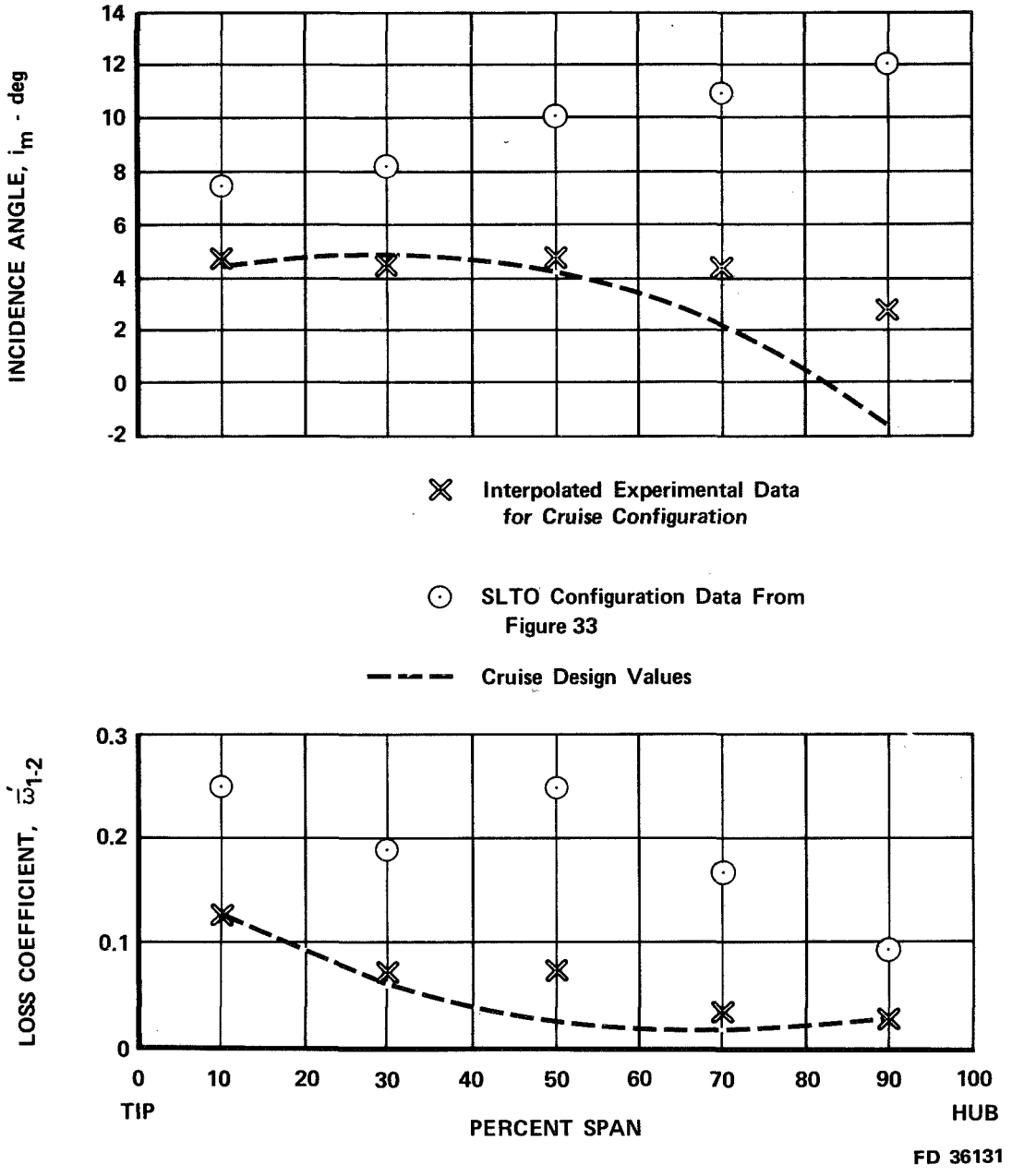

Figure 34. Rotor Incidence Angle and Loss Coefficient Distributions for Cruise Configuration Operating at Cruise Corrected Rotor Speed and Flow

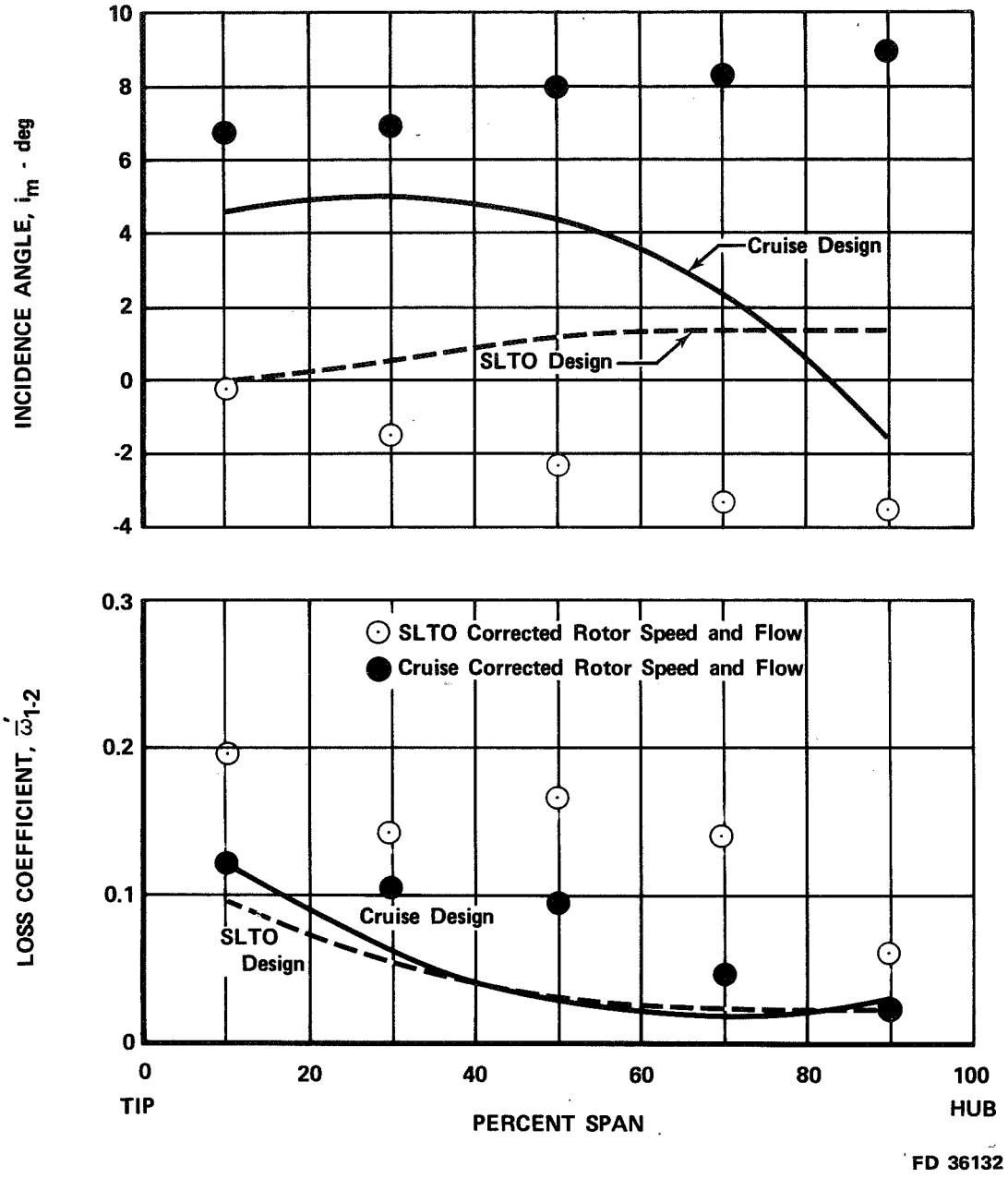

Figure 35. Rotor Incidence Angle and Loss Coefficient Distributions for Intermediate Configuration at SLTO and Cruise Corrected Rotor Speed and Flow

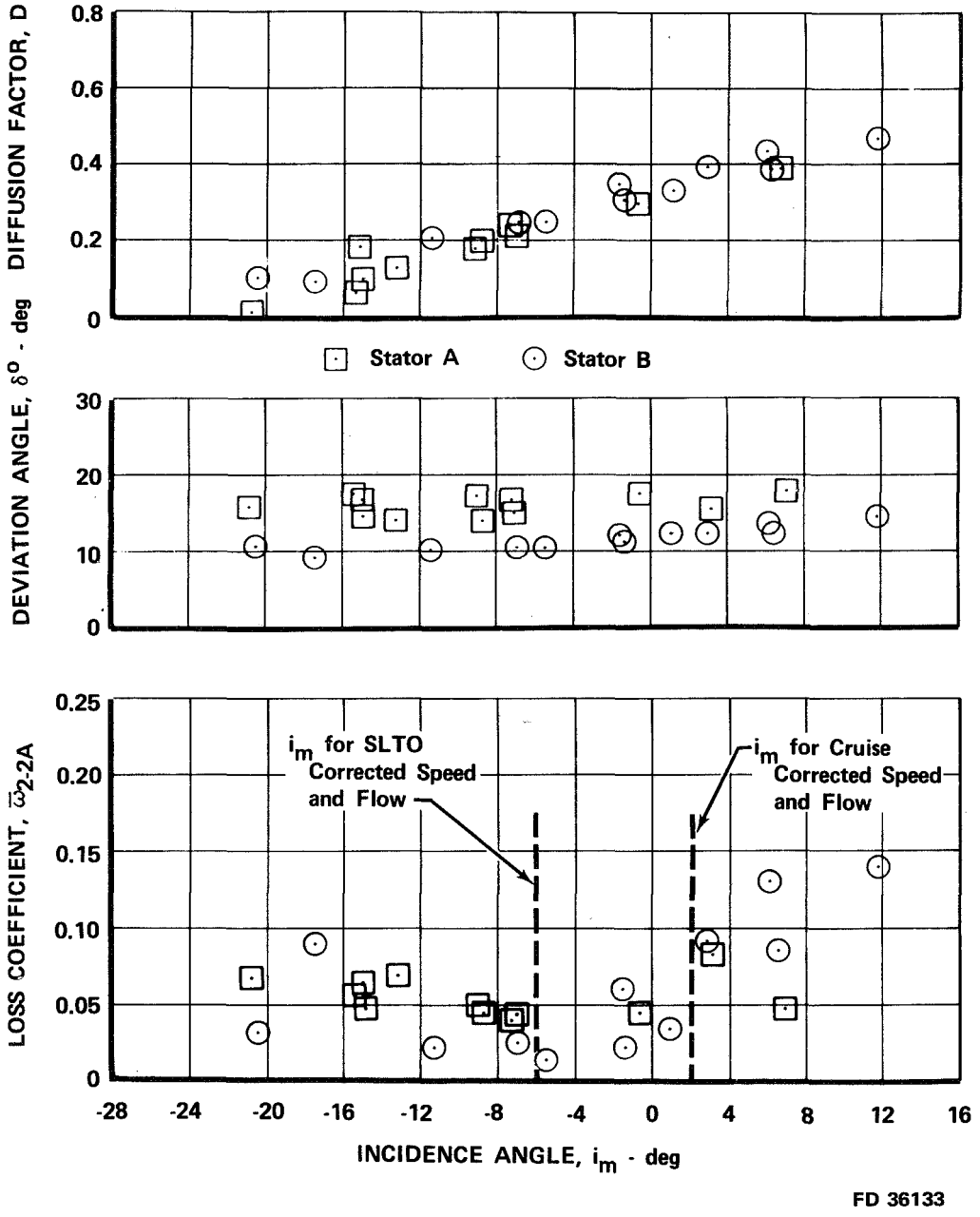

Figure 36a. Stator Blade Element Performance: SLTO Configuration; 70 and 100% SLTO Corrected Rotor Speed; 10% Span From Tip

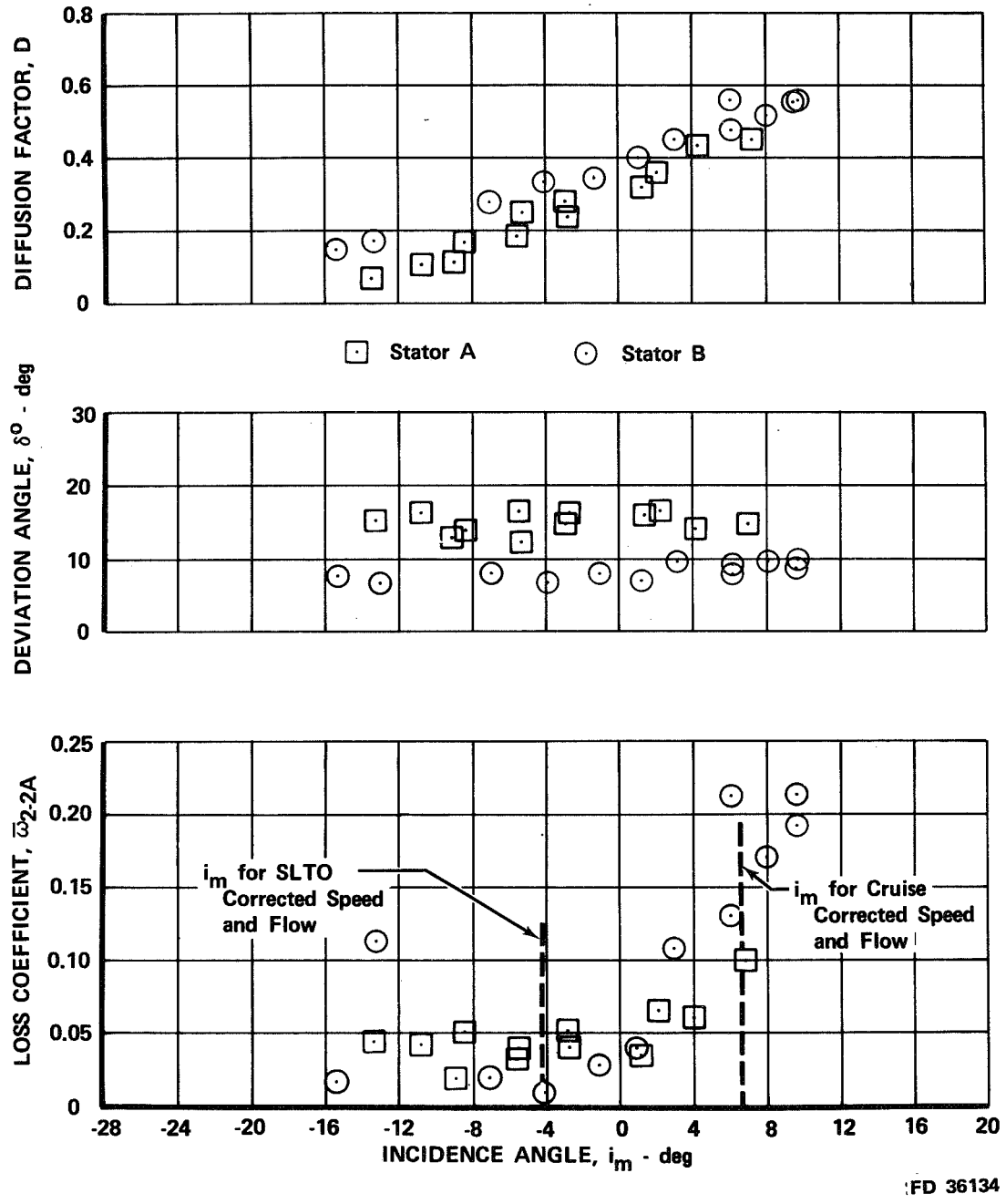

Figure 36b. Stator Blade Element Performance: SLTO Configuration; 70 and 100% SLTO Corrected Rotor Speed; 30% Span From Tip

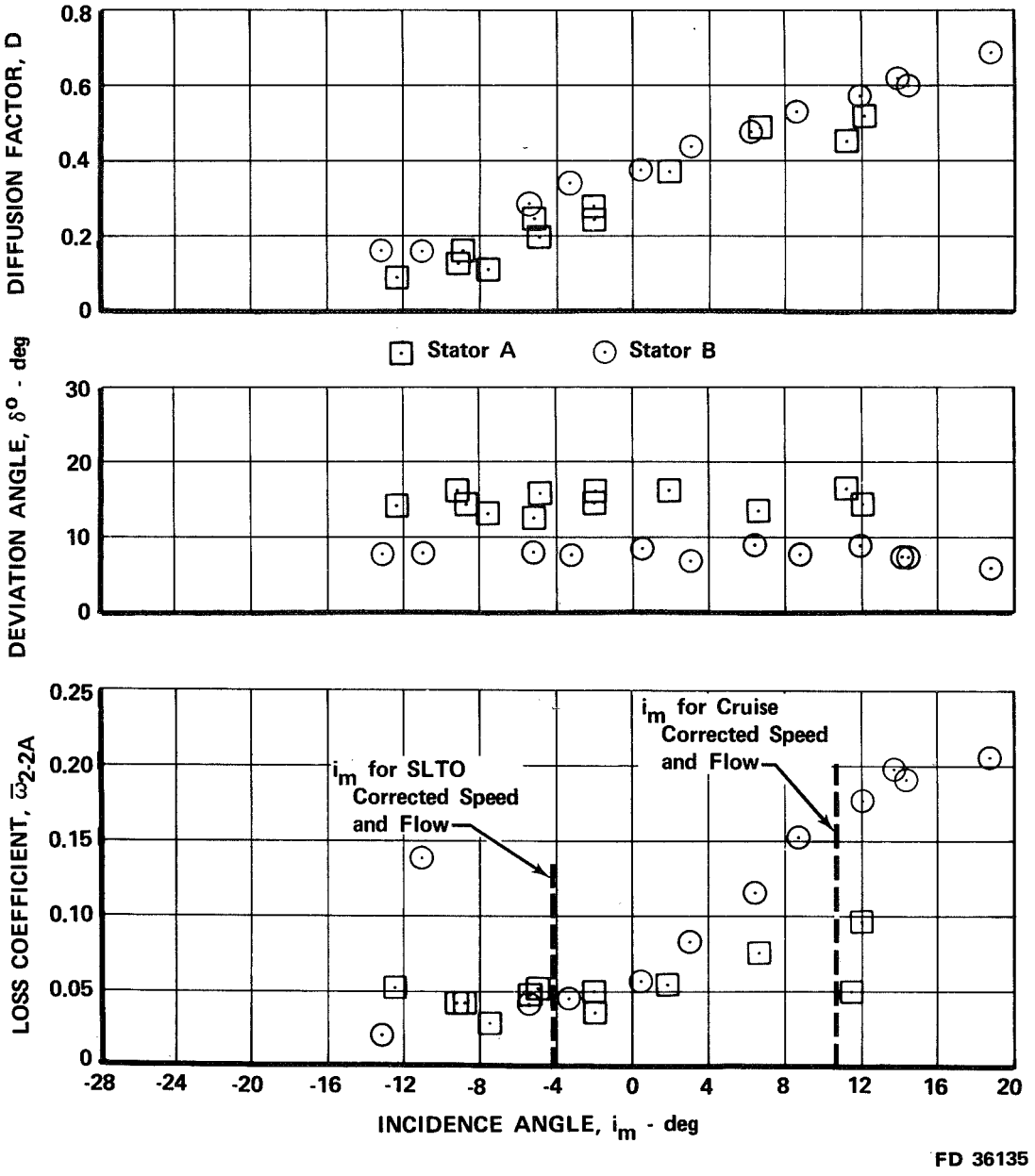

Figure 36c. Stator Blade Element Performance: SLTO Configuration; 70 and 100% SLTO Corrected Rotor Speed; 50% Span From Tip

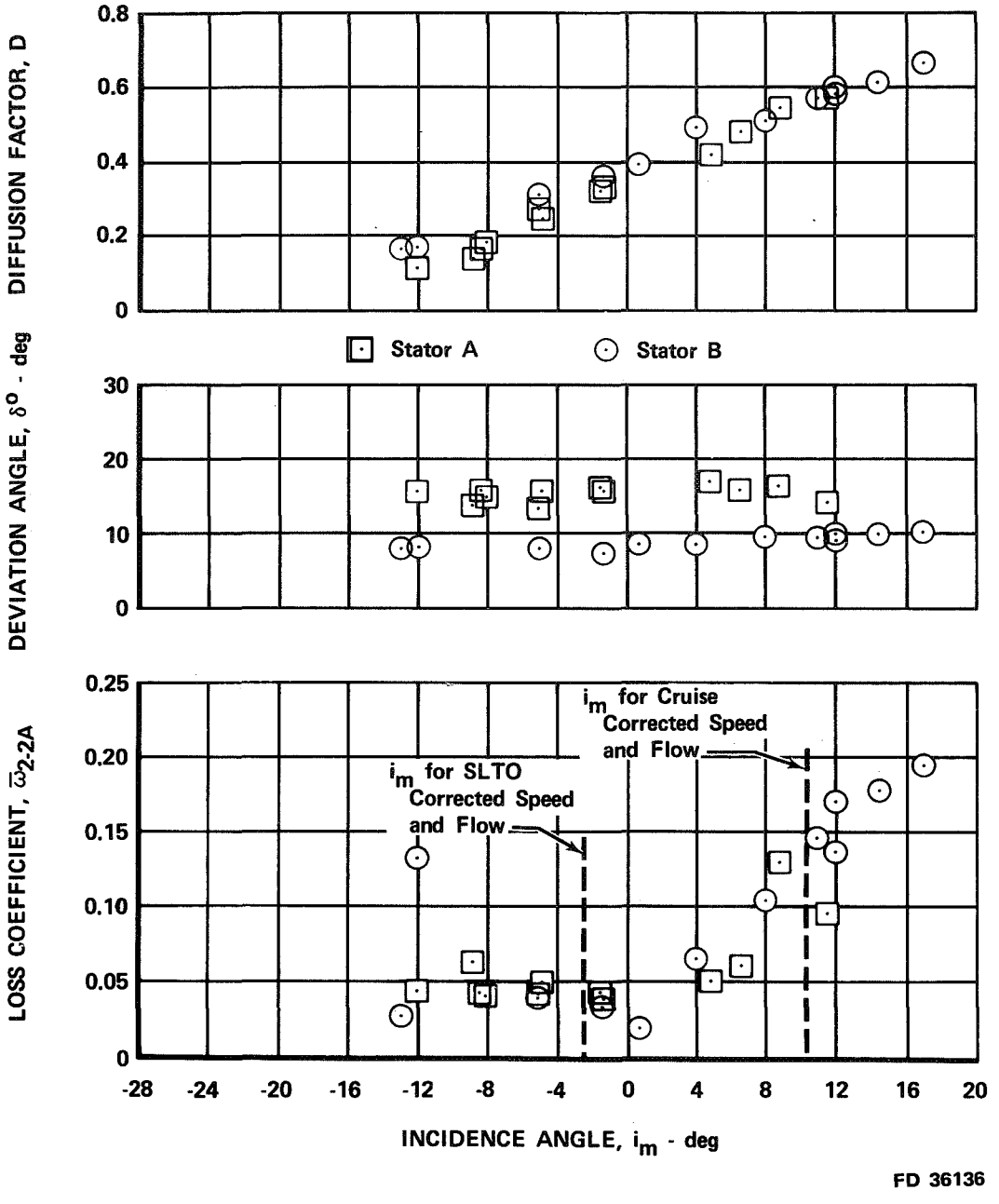

Figure 36d. Stator Blade Element Performance: SLTO Configuration; 70 and 100% SLTO Corrected Rotor Speed; 70% Span From Tip

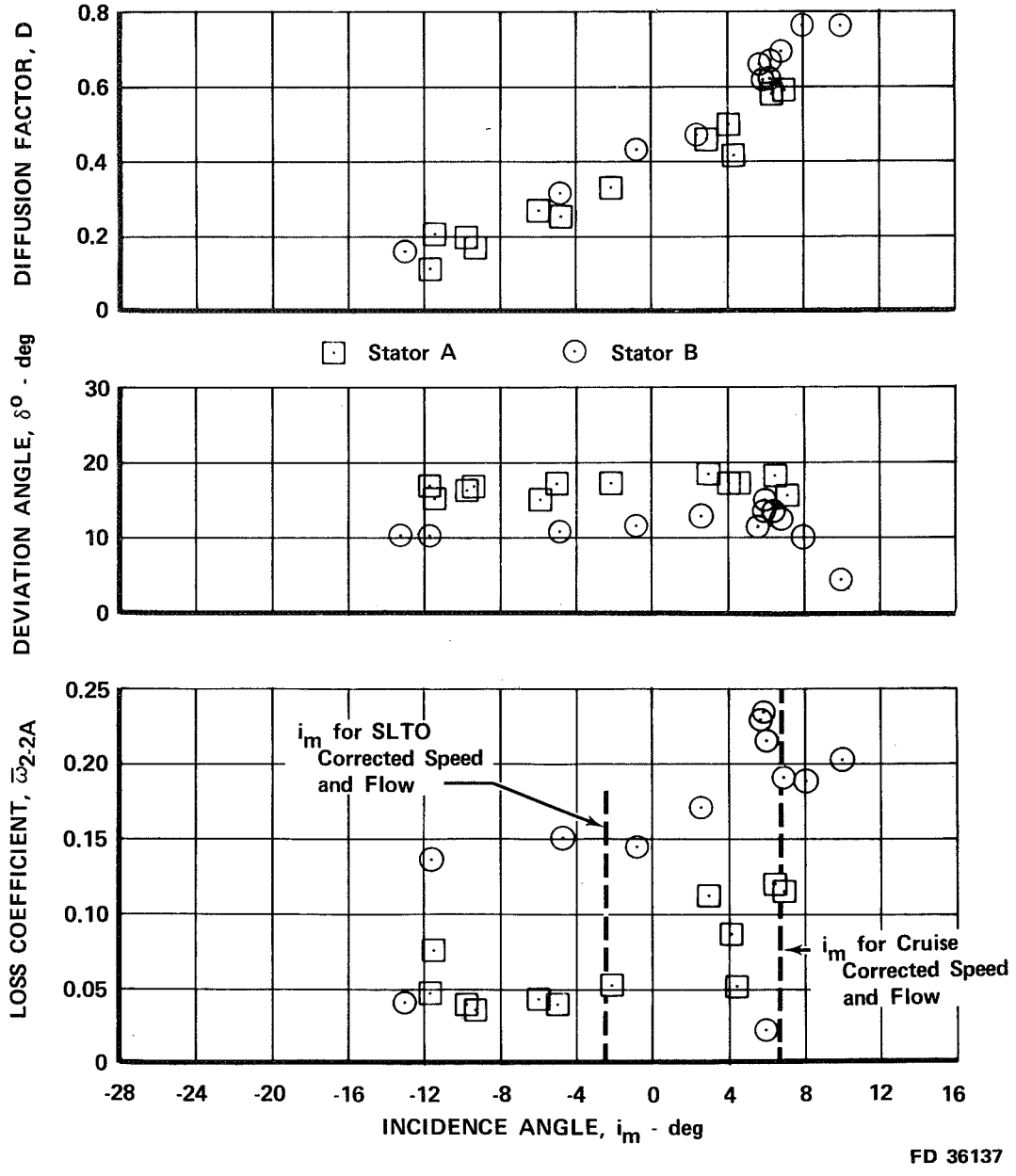

Figure 36e. Stator Blade Element Performance: SLTO Configuration; 70 and 100% SLTO Corrected Rotor Speed; 90% Span From Tip

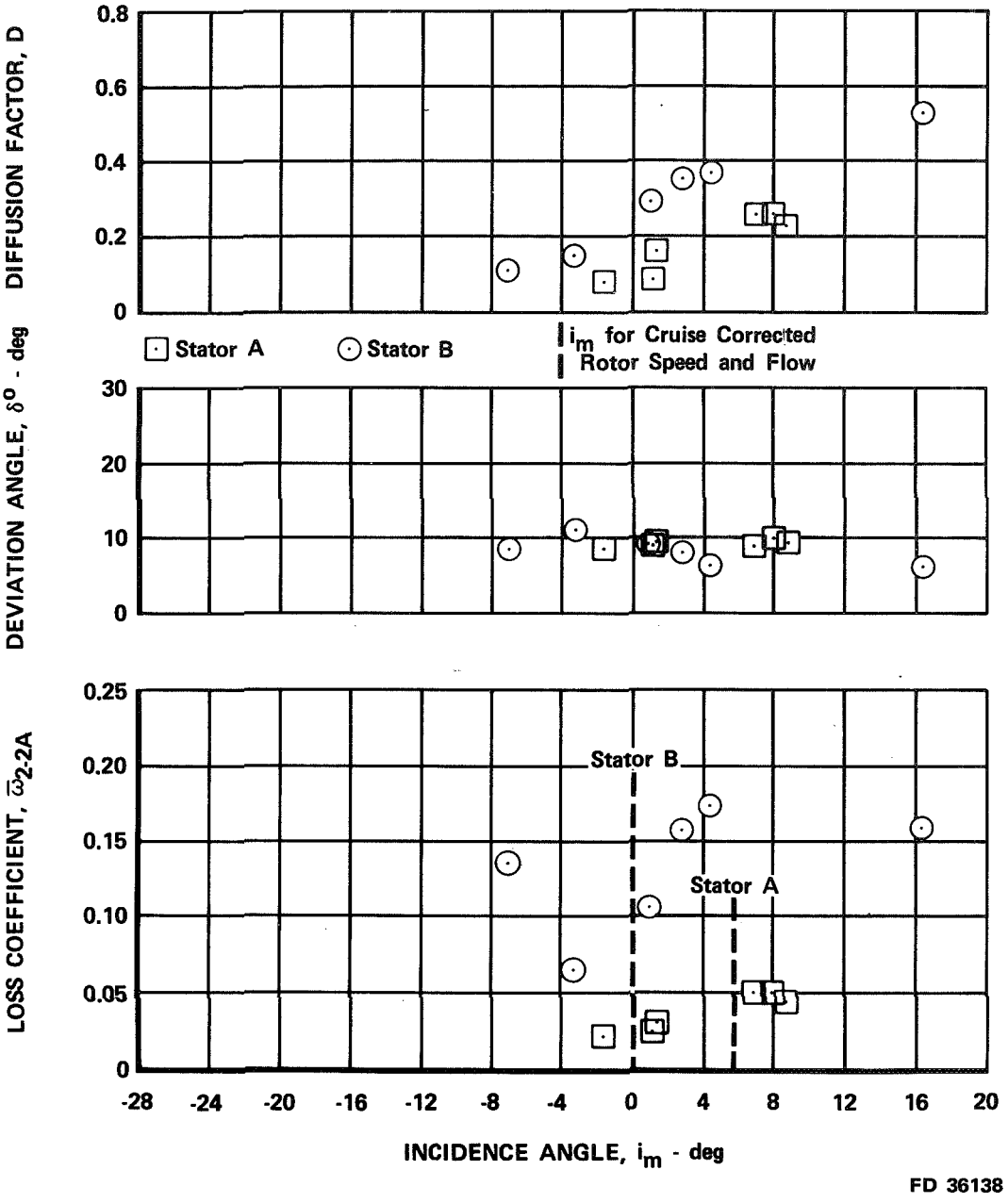

Figure 37a. Stator Blade Element Performance: Cruise Configuration; Cruise Corrected Rotor Speed; 10% Span From Tip

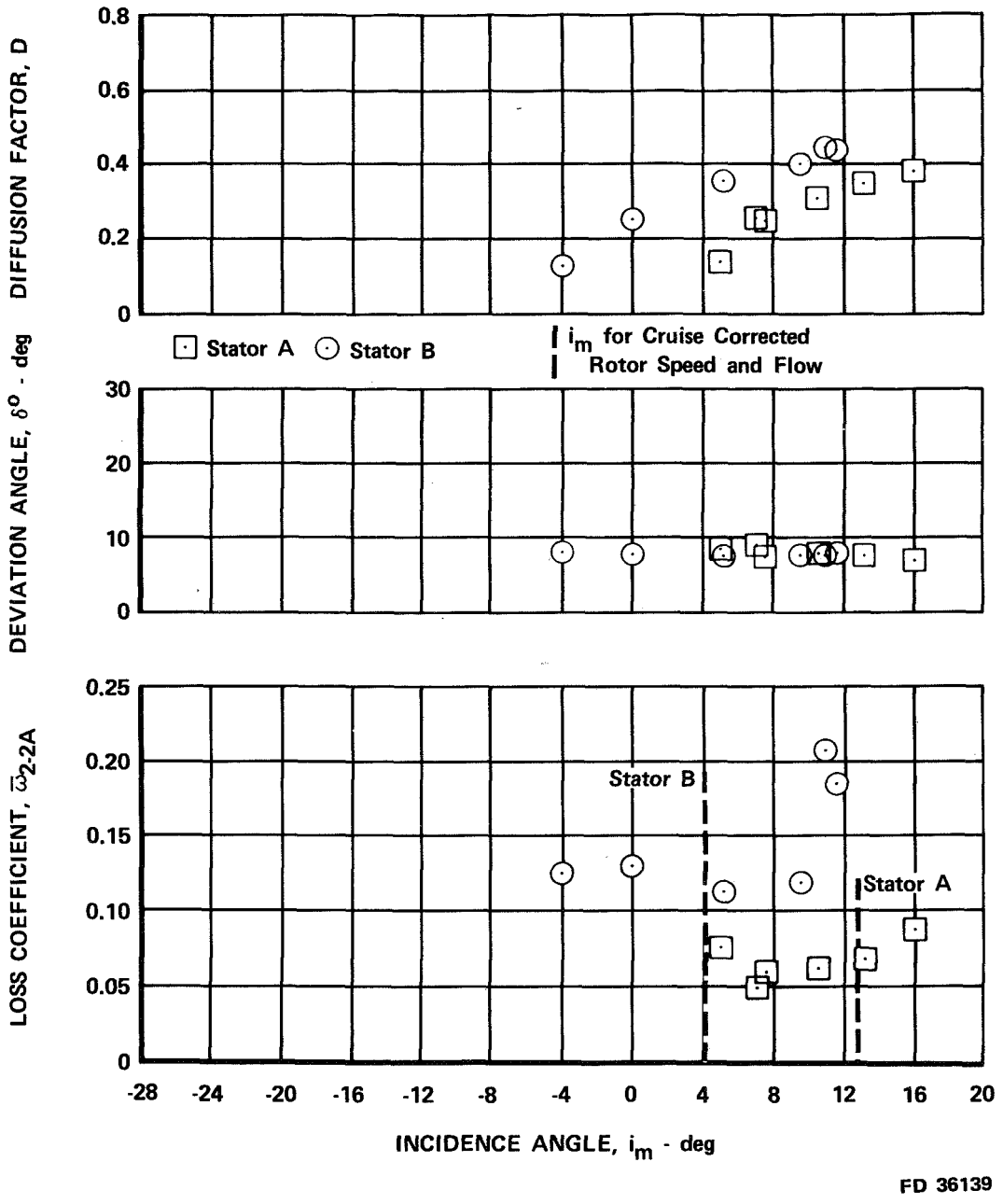

Figure 37b. Stator Blade Element Performance: Cruise Configuration; Cruise Corrected Rotor Speed; 30% Span From Tip

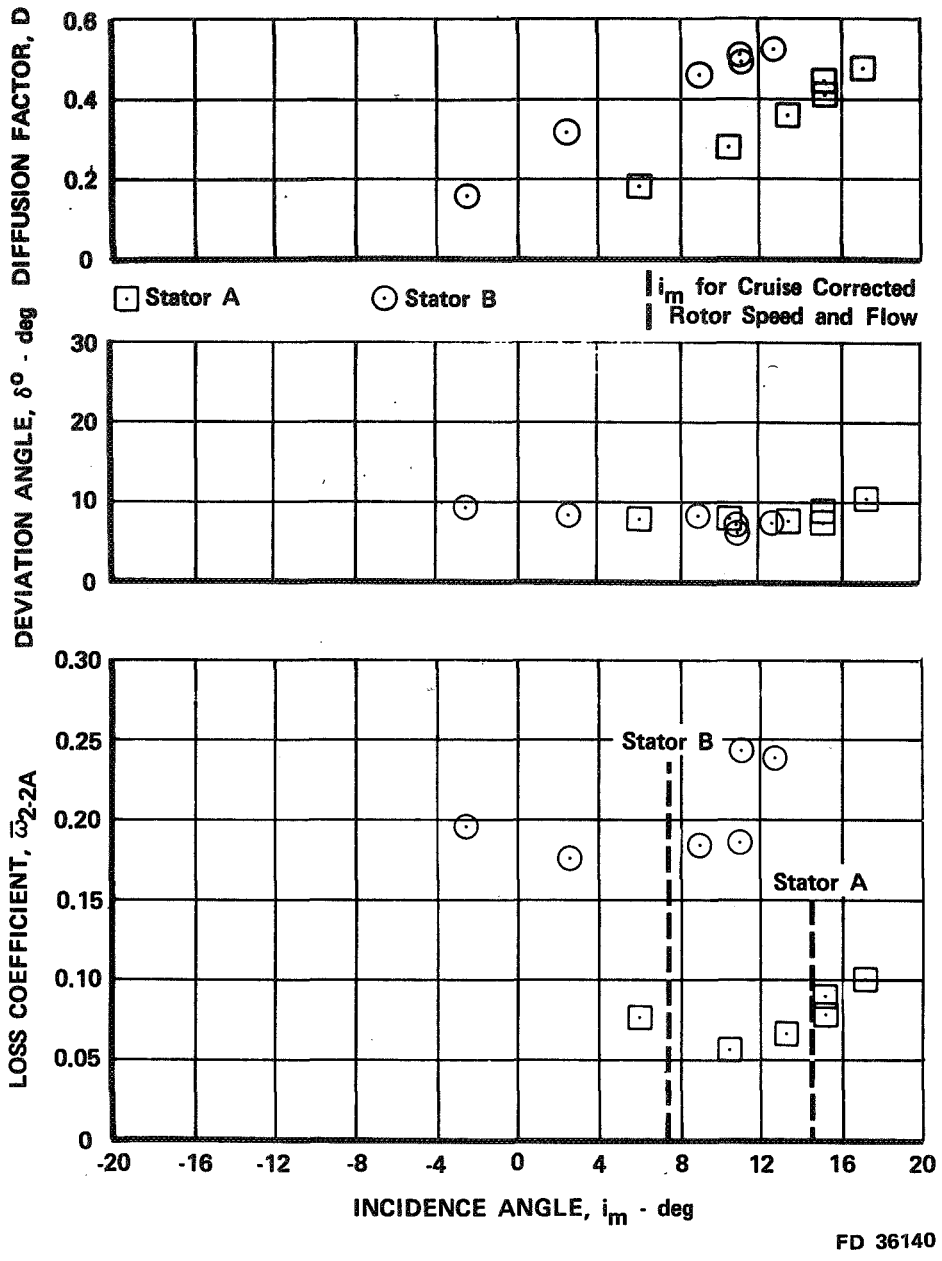

Figure 37c. Stator Blade Element Performance: Cruise Configuration; Cruise Corrected Rotor Speed; 50% Span From Tip

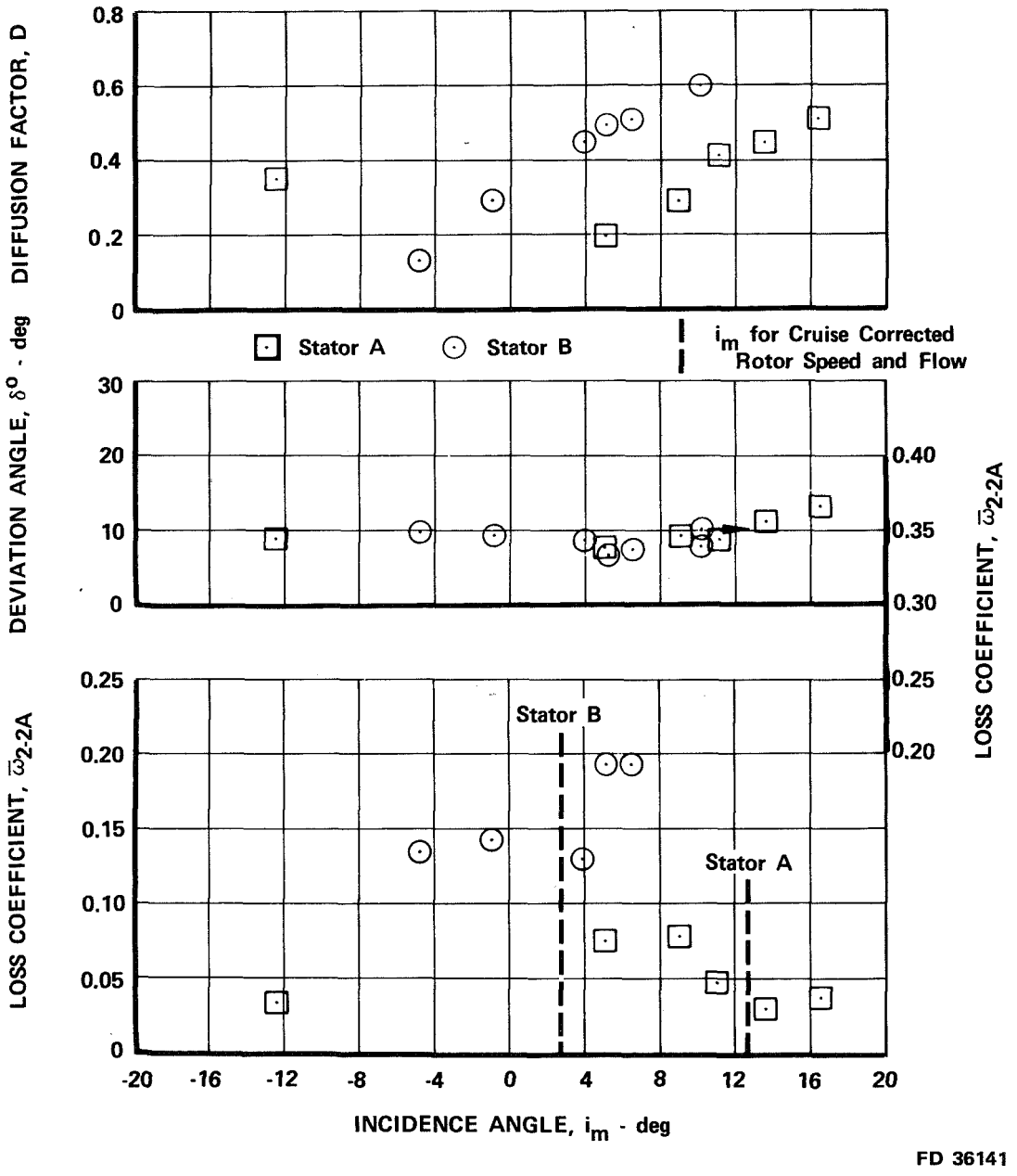

Figure 37d. Stator Blade Element Performance: Cruise Configuration; Cruise Corrected Rotor Speed; 70% Span From Tip

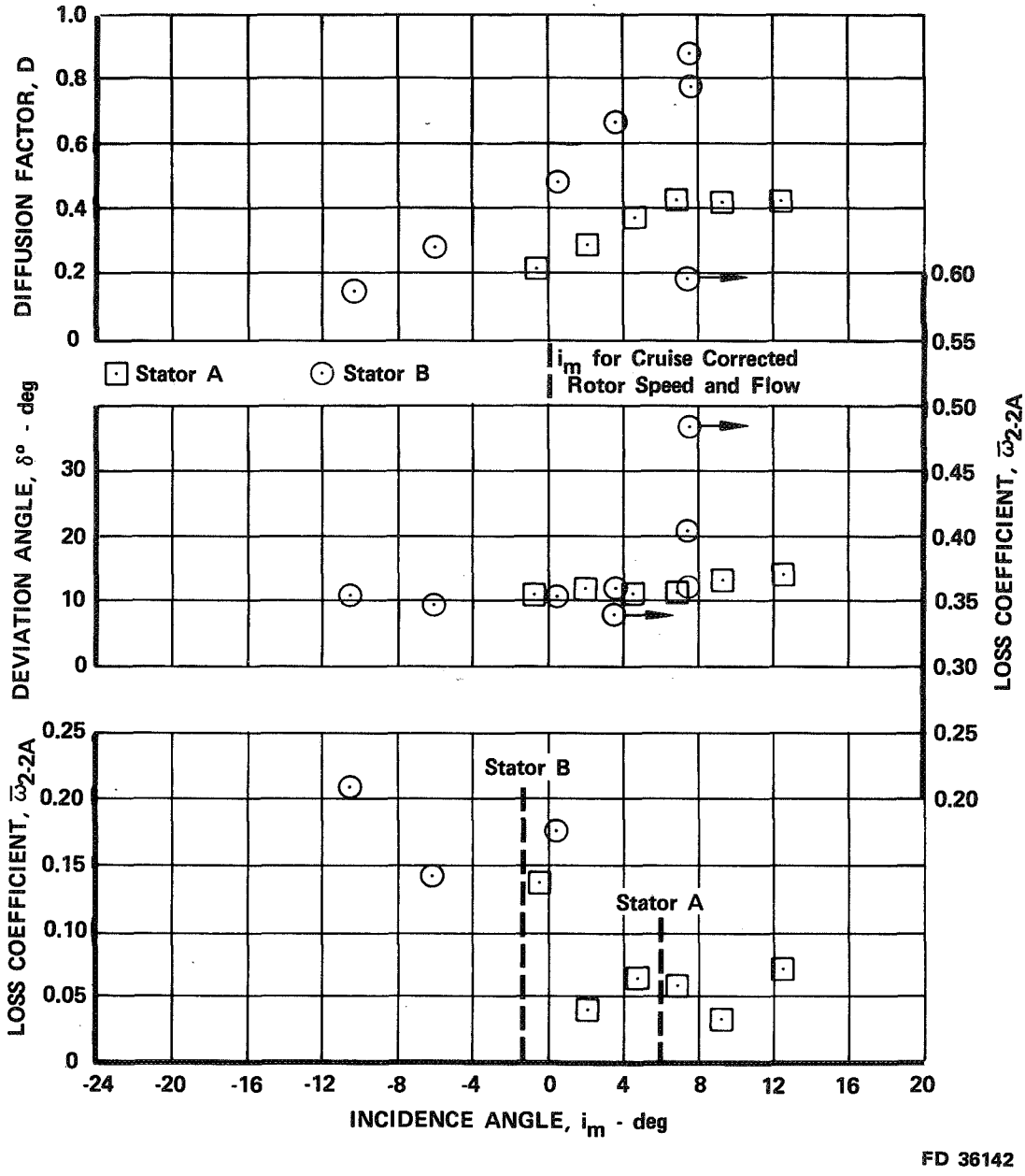

Figure 37e. Stator Blade Element Performance: Cruise Configuration; Cruise Corrected Rotor Speed; 90% Span From Tip

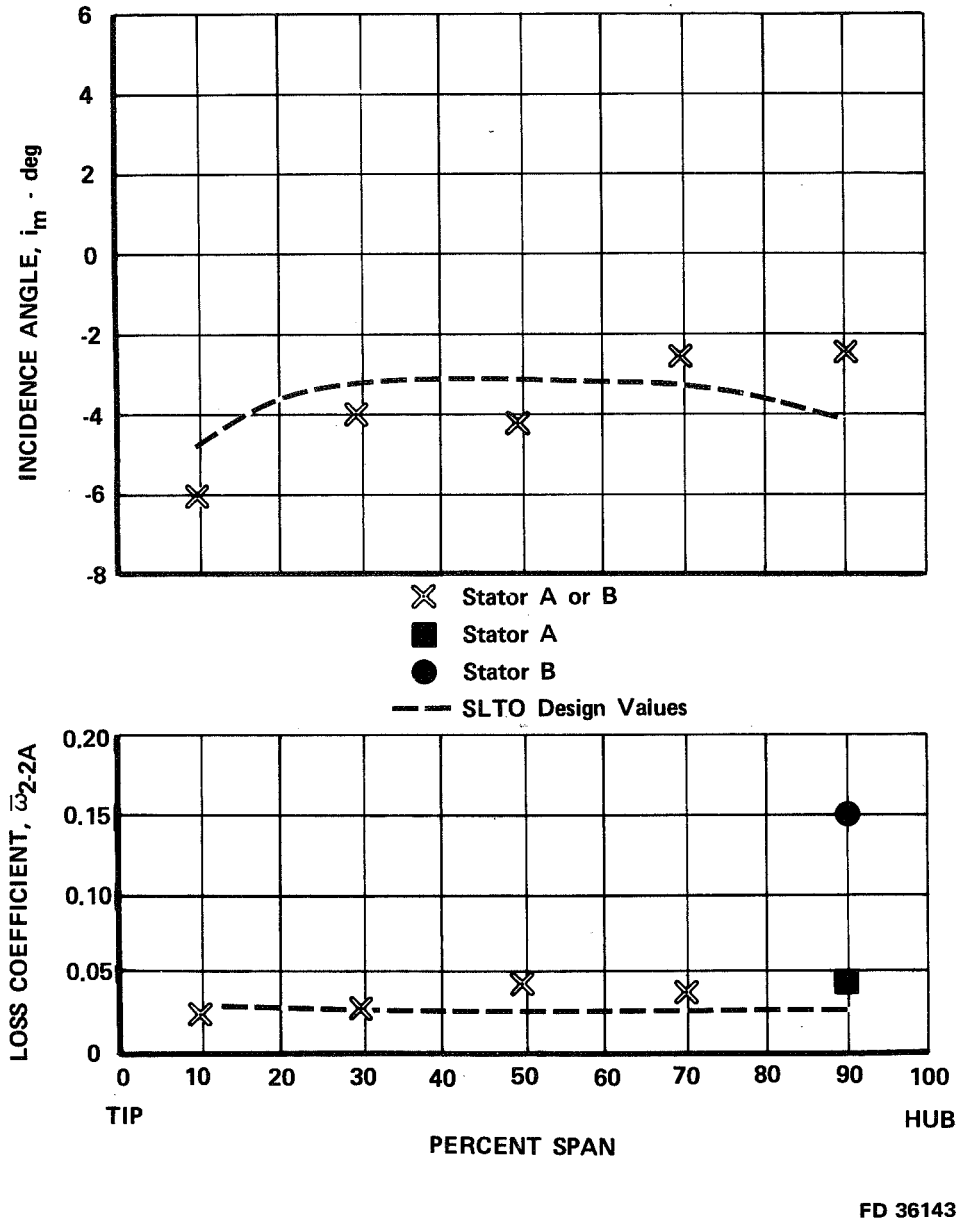

Figure 38. Stator A and B Incidence Angle and Loss Coefficient Distributions for SLTO Configuration Operating at SLTO Corrected Rotor Speed and Flow

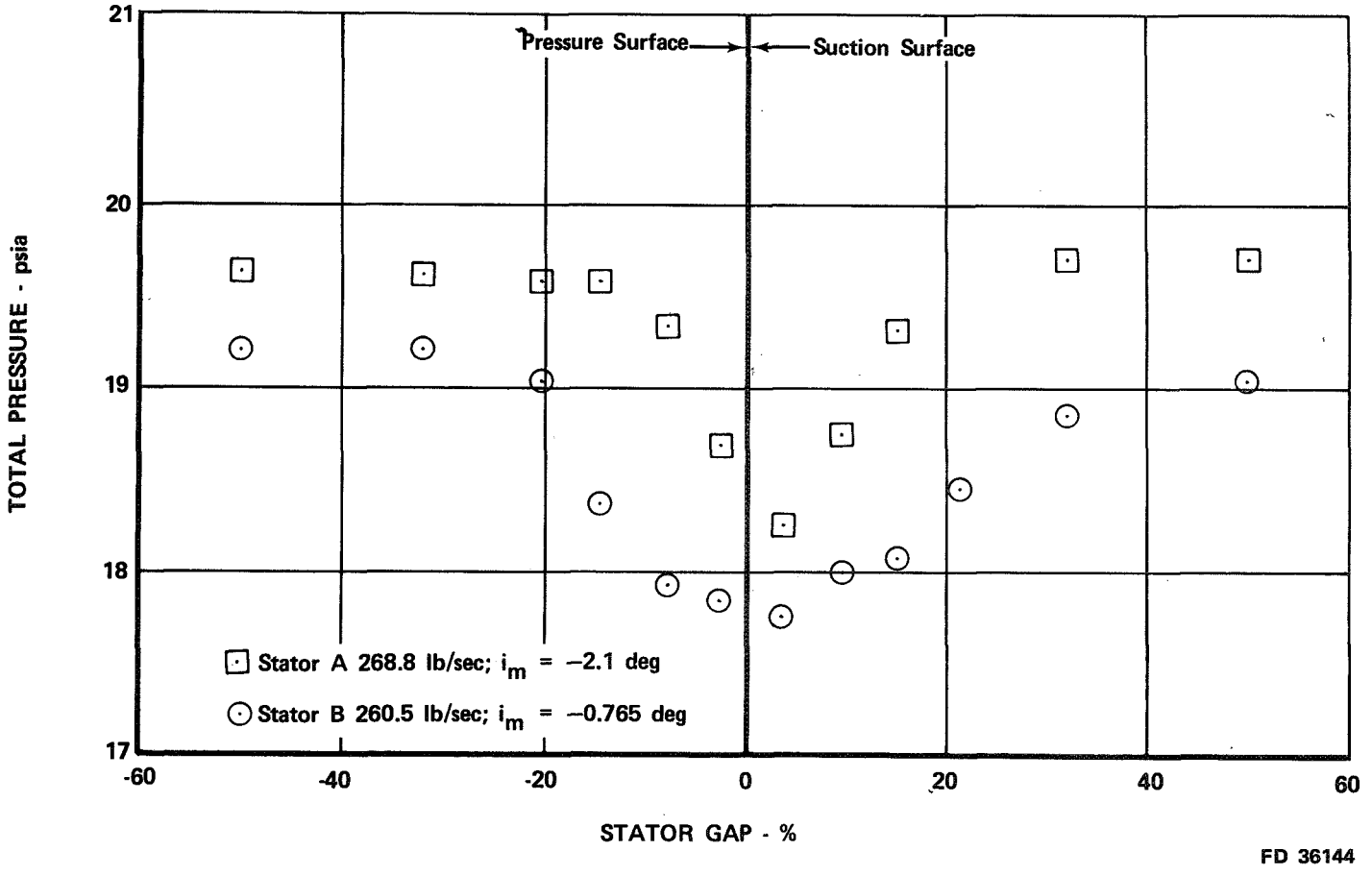

Figure 39. Comparison of Stator A and Stator B Hub (90% Span) Wakes at SLTO Corrected Rotor Speed and Flow

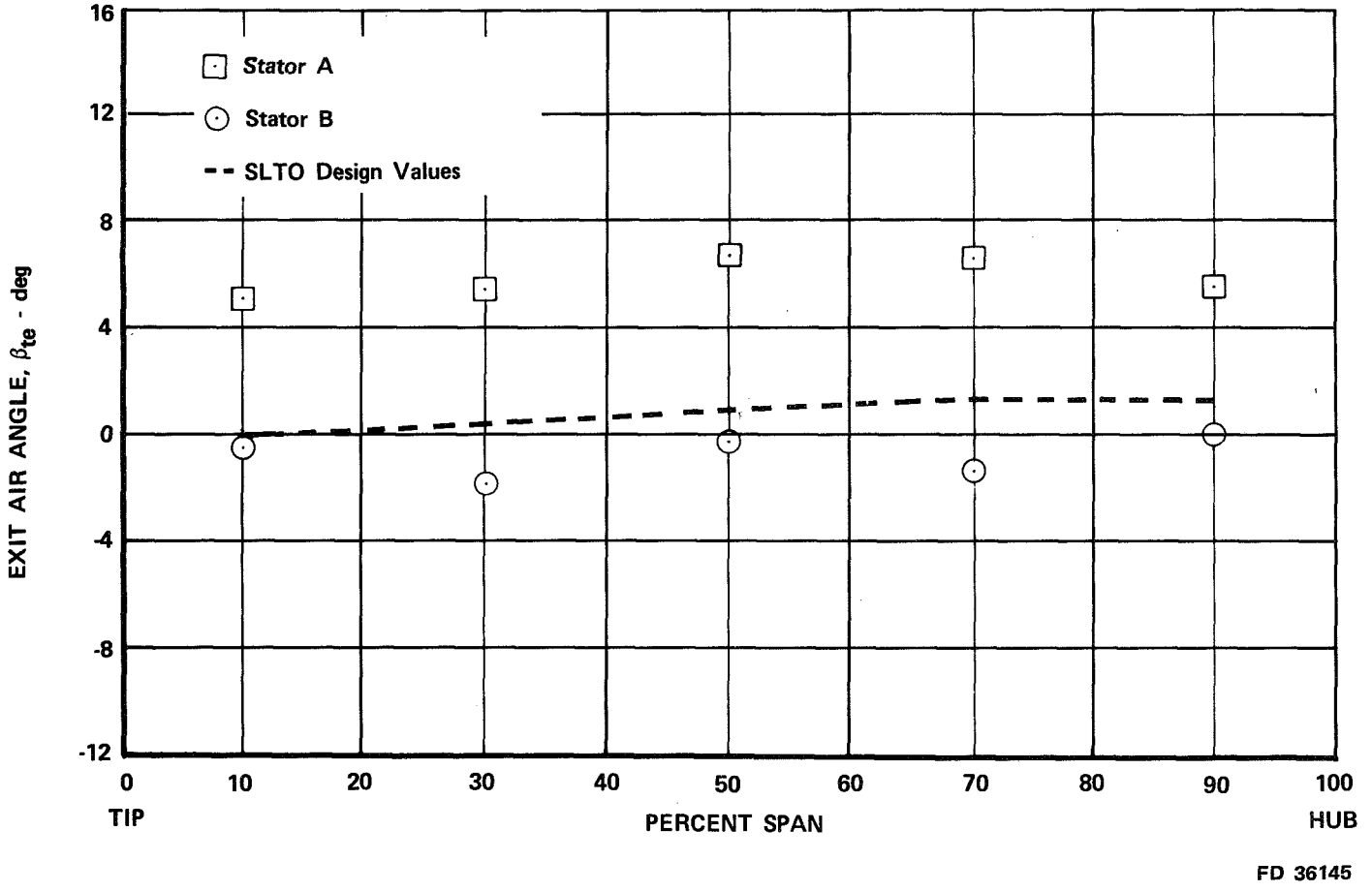

Figure 40. Stator Exit Air Angles; SLTO Configuration at SLTO Corrected Rotor Speed and Flow

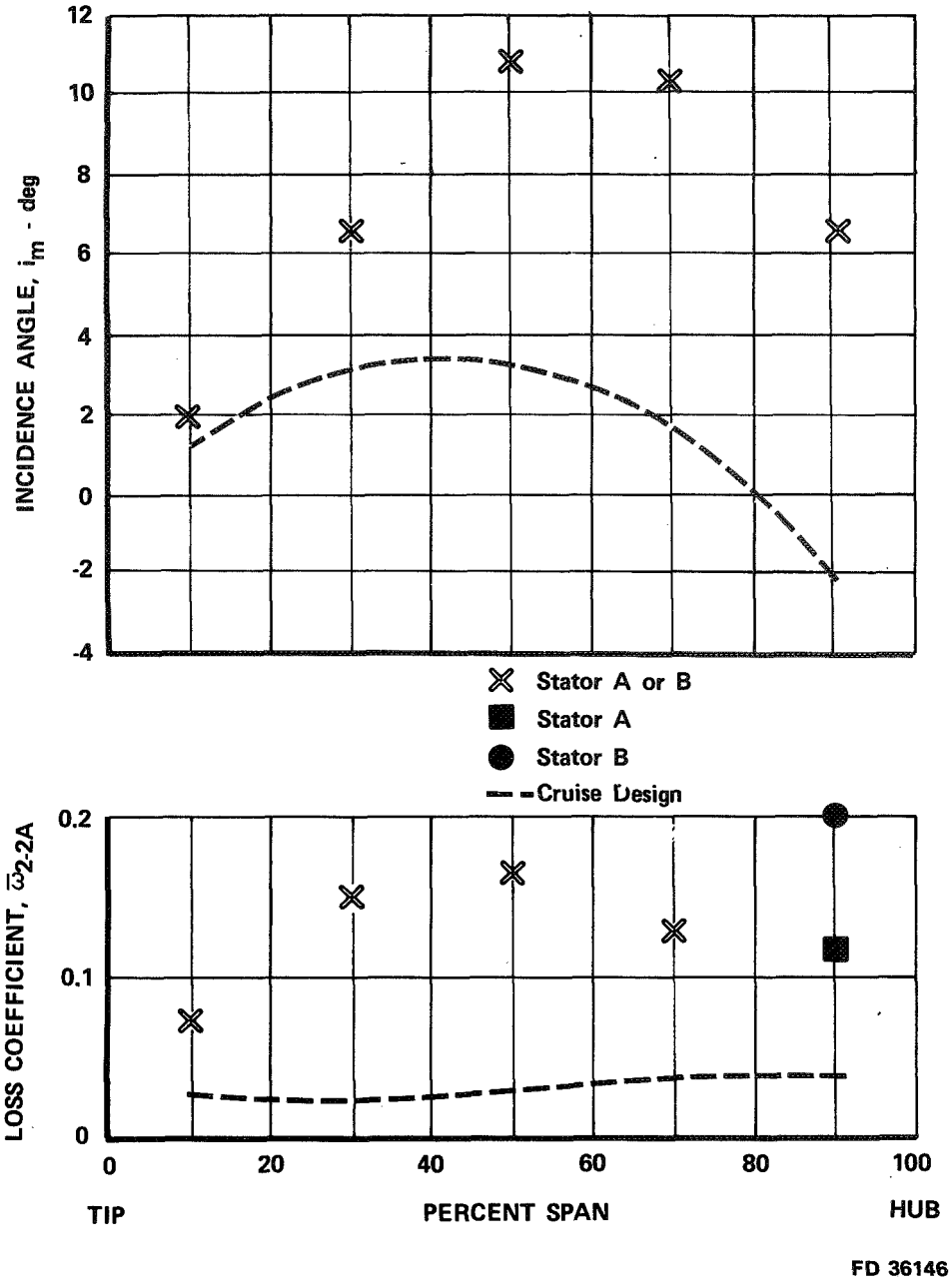

Figure 41. Stator Incidence Angle and Loss Coefficient Distributions for SLTO Configuration Operating at Cruise Corrected Rotor Speed and Flow

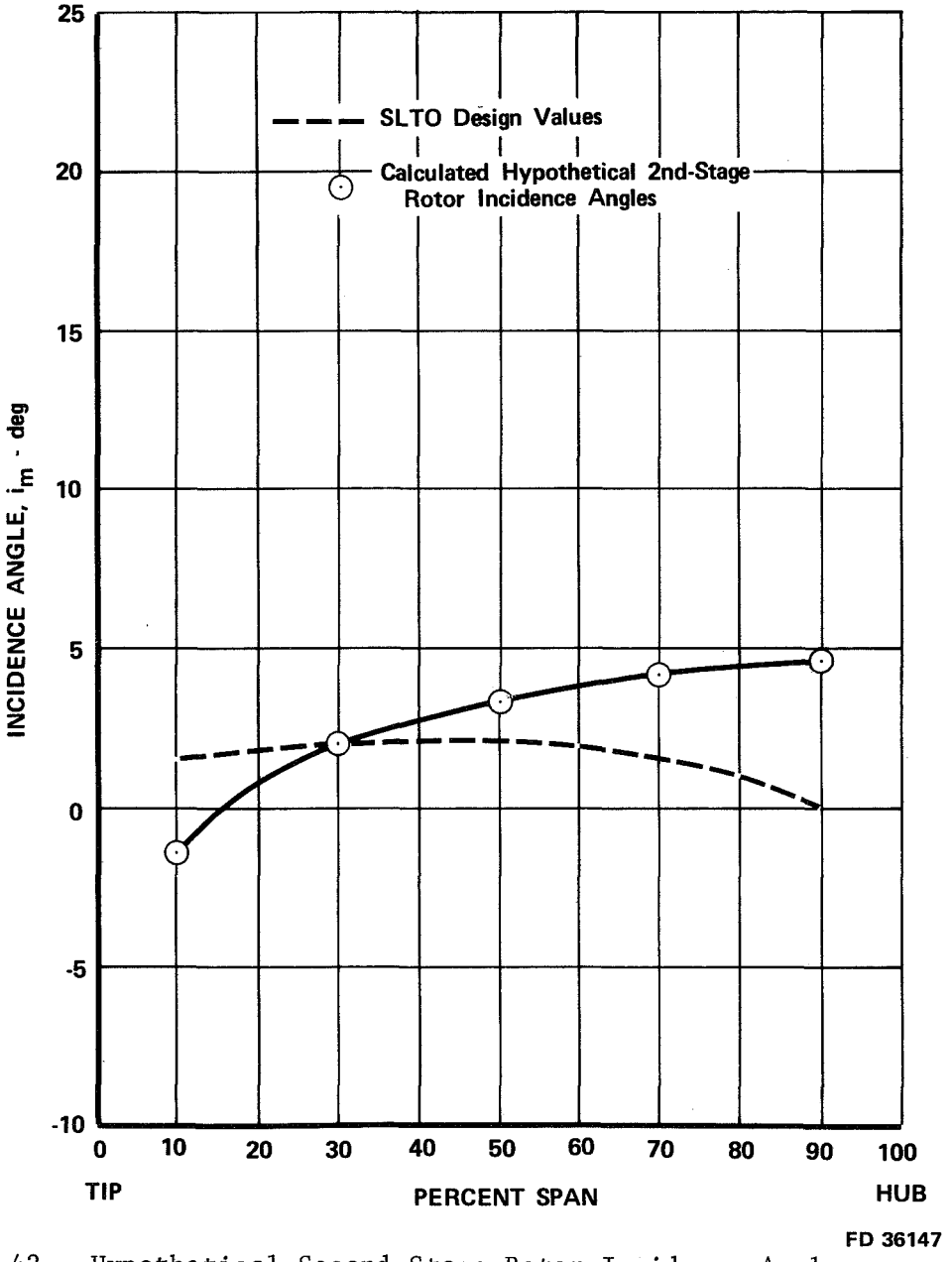

Figure 42. Hypothetical Second-Stage Rotor Incidence Angle Distribution for SLTO Configuration at SLTO Corrected Rotor Speed and Flow

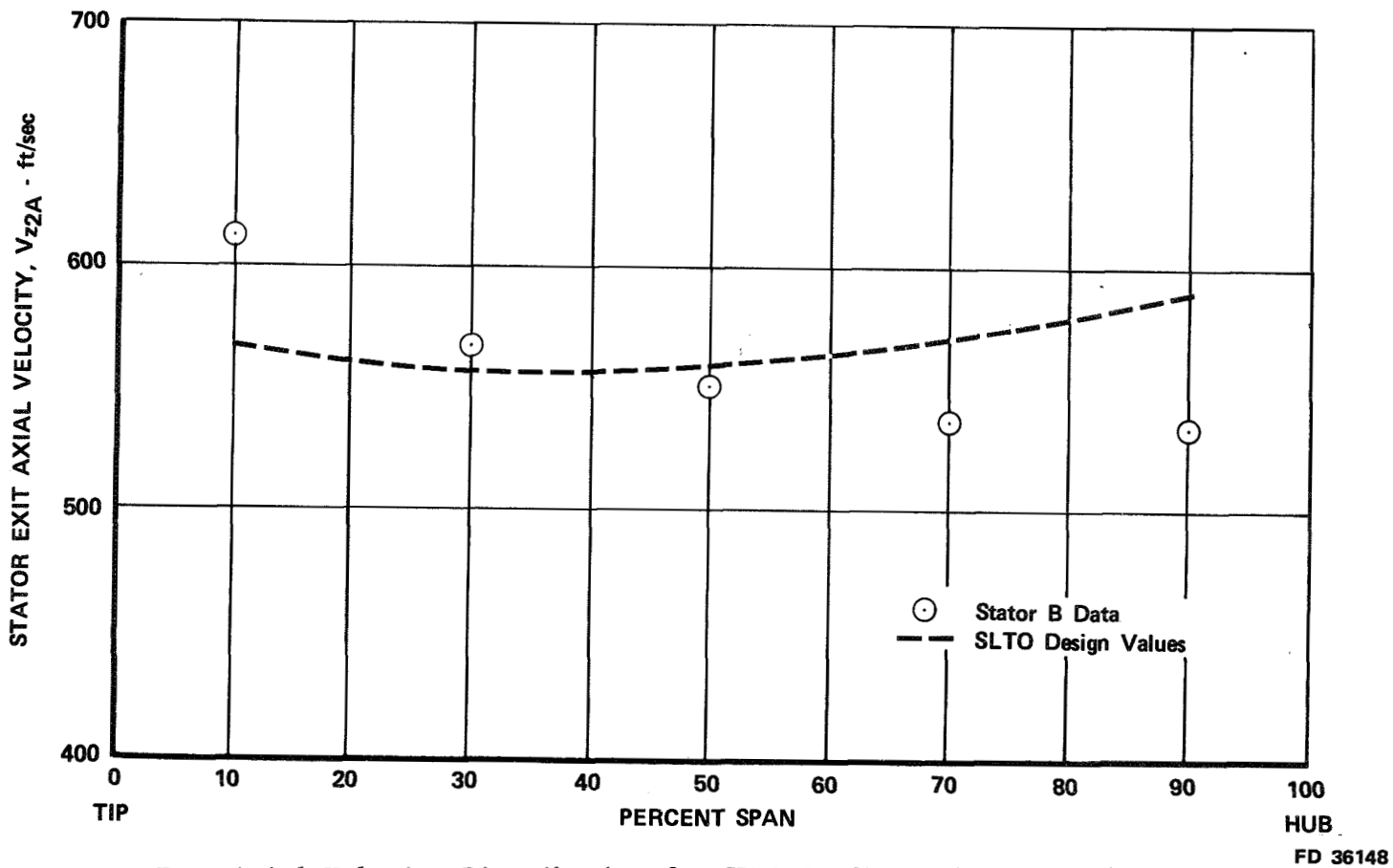

Figure 43. Stator B Exit Axial Velocity Distribution for SLTO Configuration Operating at SLTO Corrected Rotor Speed and Flow

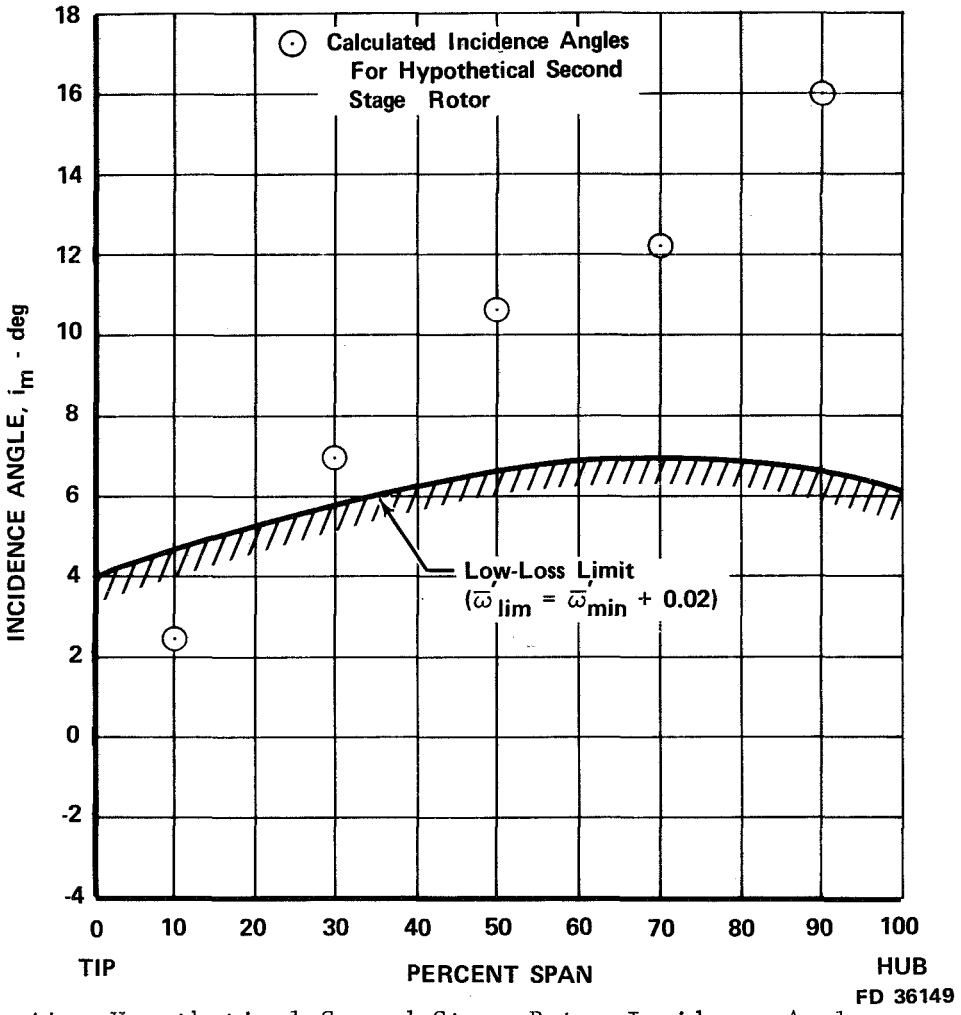

Figure 44. Hypothetical Second-Stage Rotor Incidence Angle for SLTO Configuration Operating at Cruise Corrected Rotor Speed and Flow

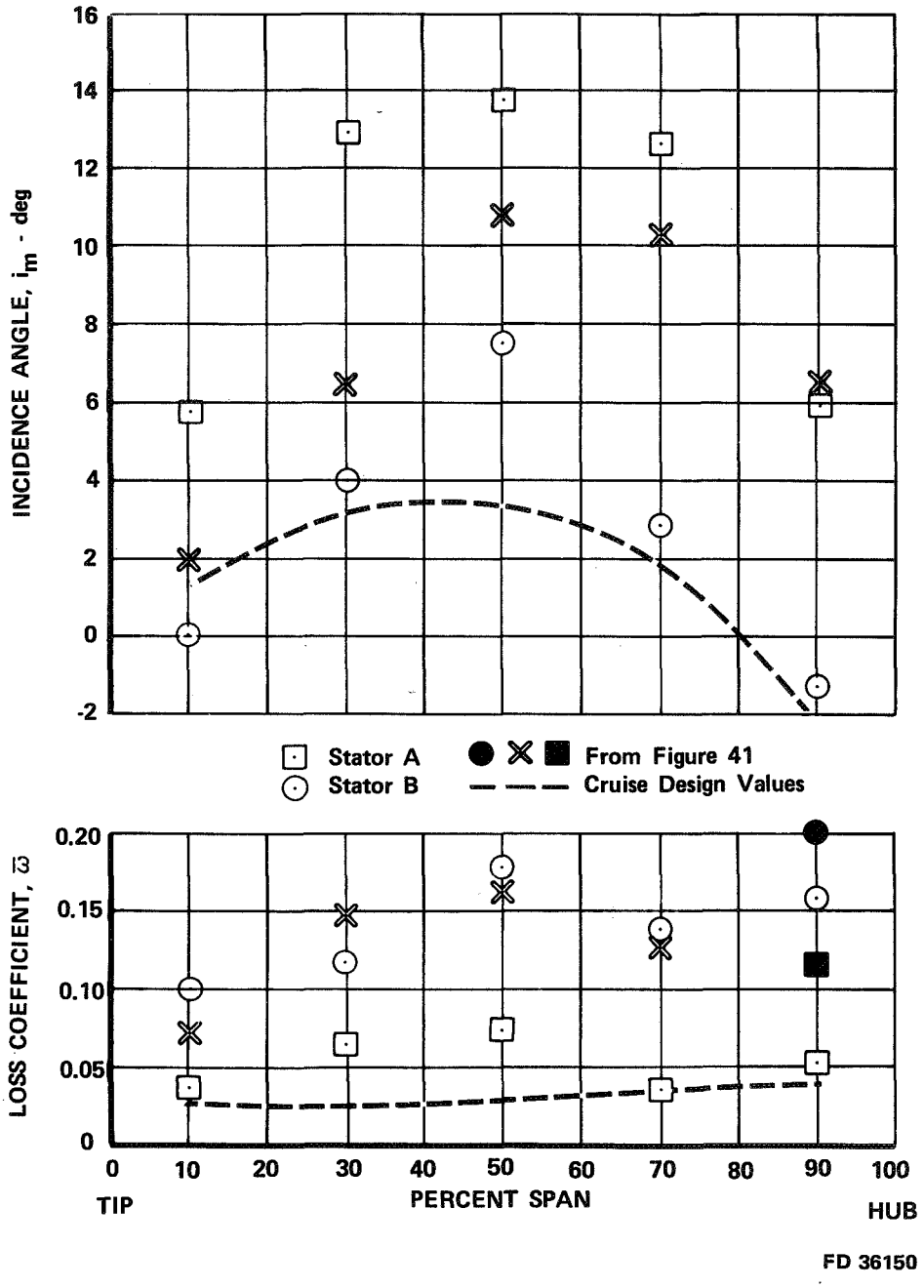

Figure 45. Stator Incidence Angle and Loss Coefficient Distributions for Cruise Configurations Operating at Cruise Corrected Rotor Speed and Flow

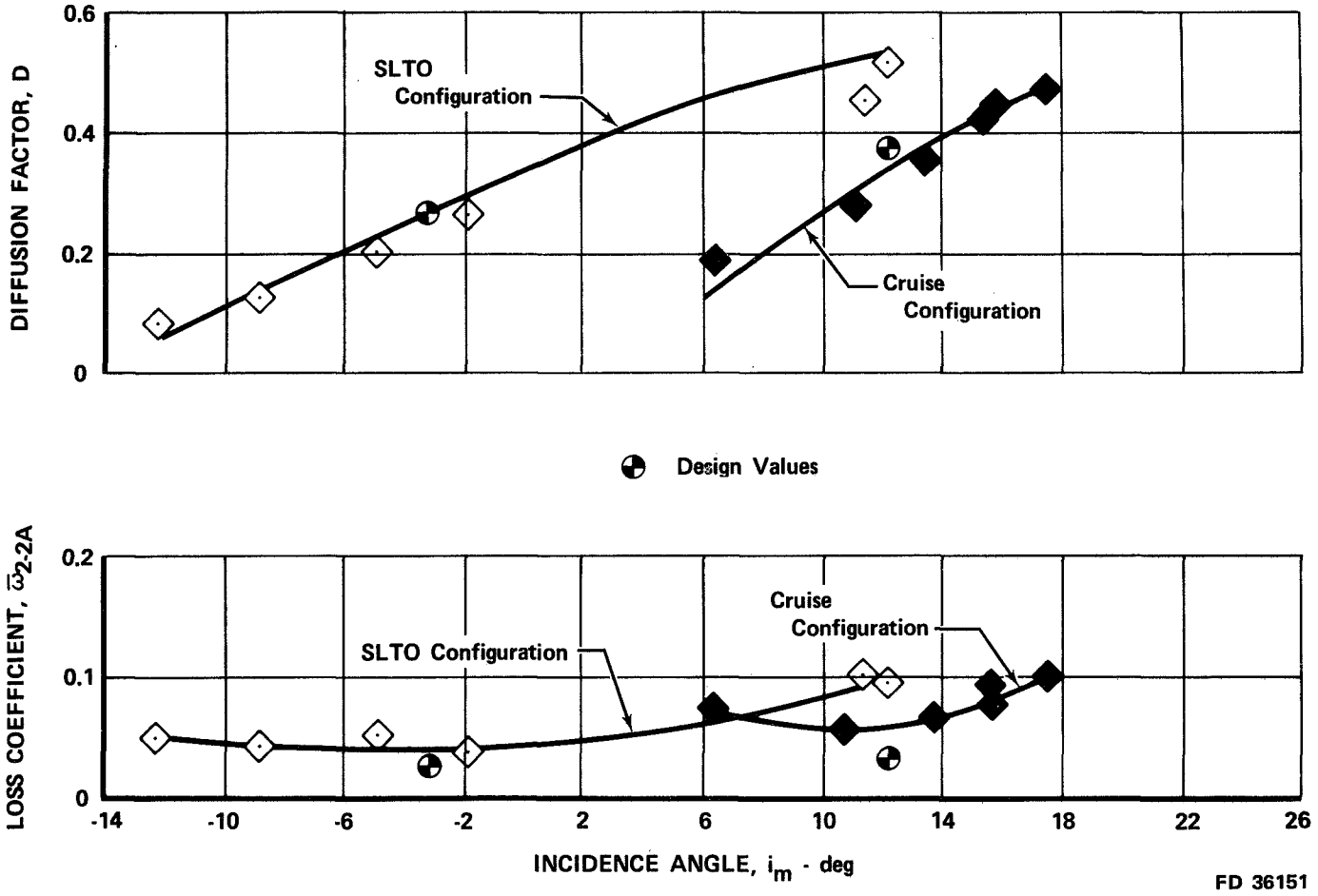

Figure 46. Influence of Stator A Flap on Midspan Diffusion Factor and Loss Coefficient Distributions at Cruise Corrected Rotor Speed

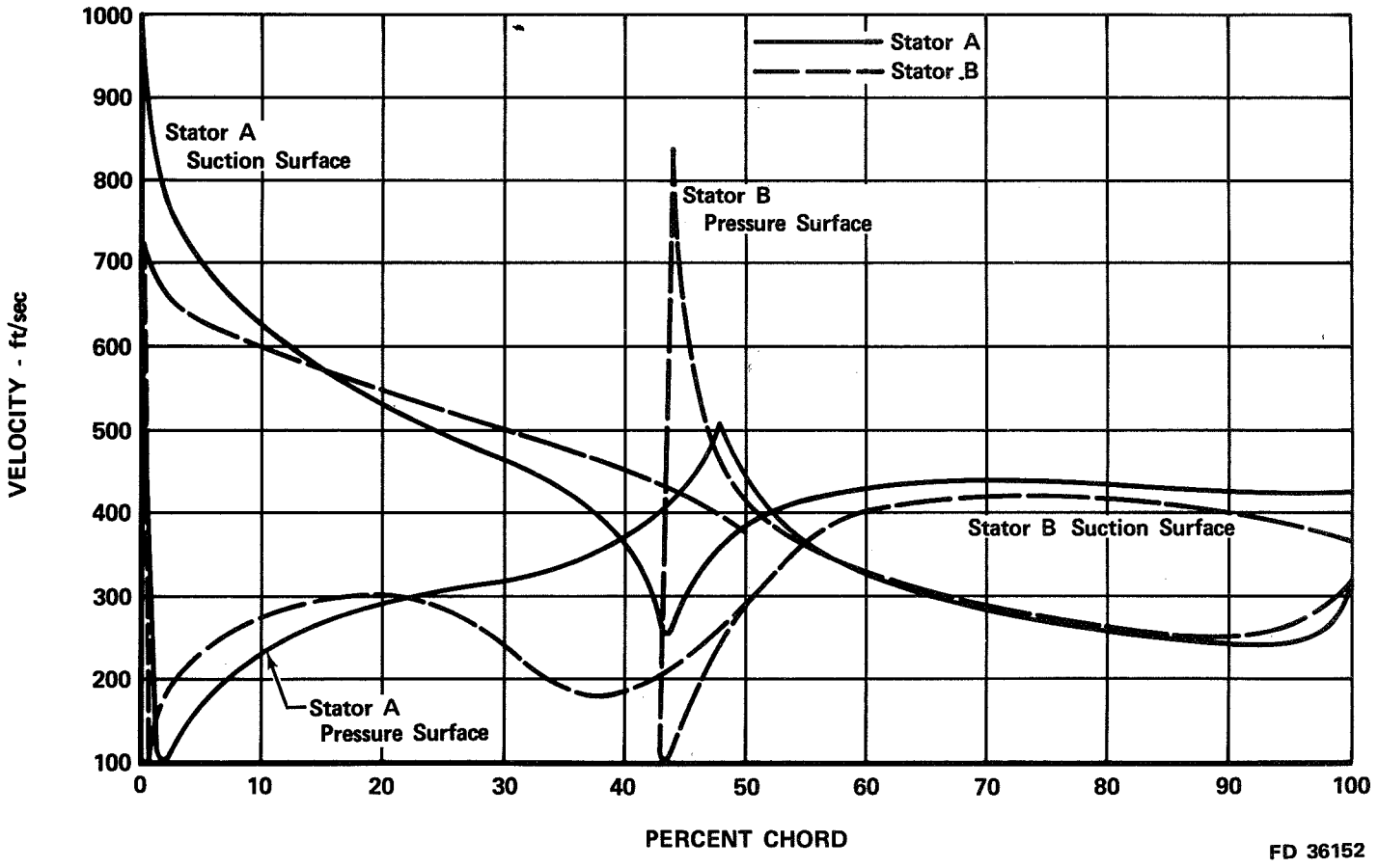

Figure 47. Potential Flow Velocity Distributions for Stator A and Stator B Cruise Configurations at Cruise Design Incidence Angle Conditions

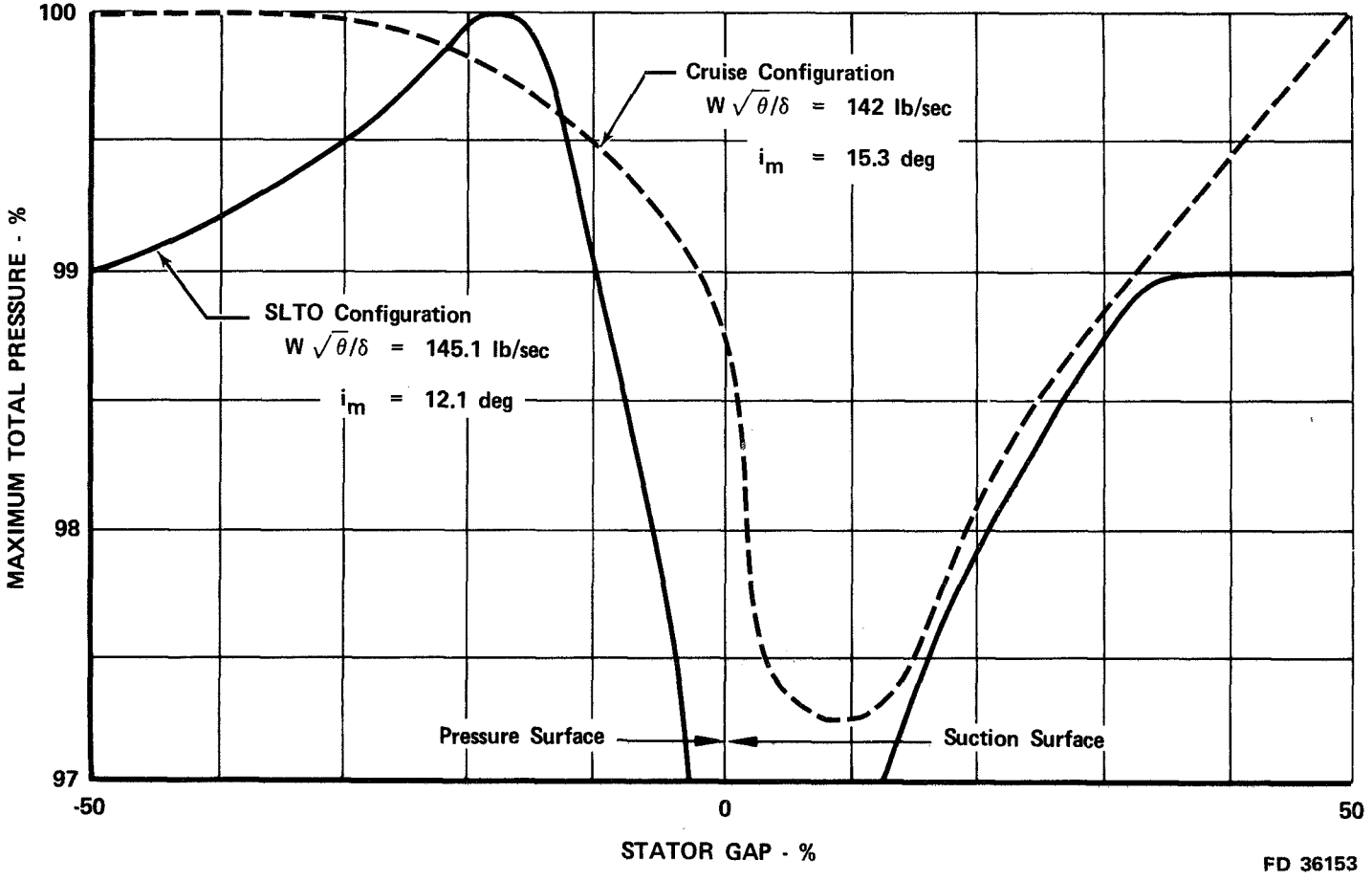

Figure 48. Comparison of Stator A SLTO and Cruise Configuration Midspan Wake Profiles at Near-Cruise Design Flow

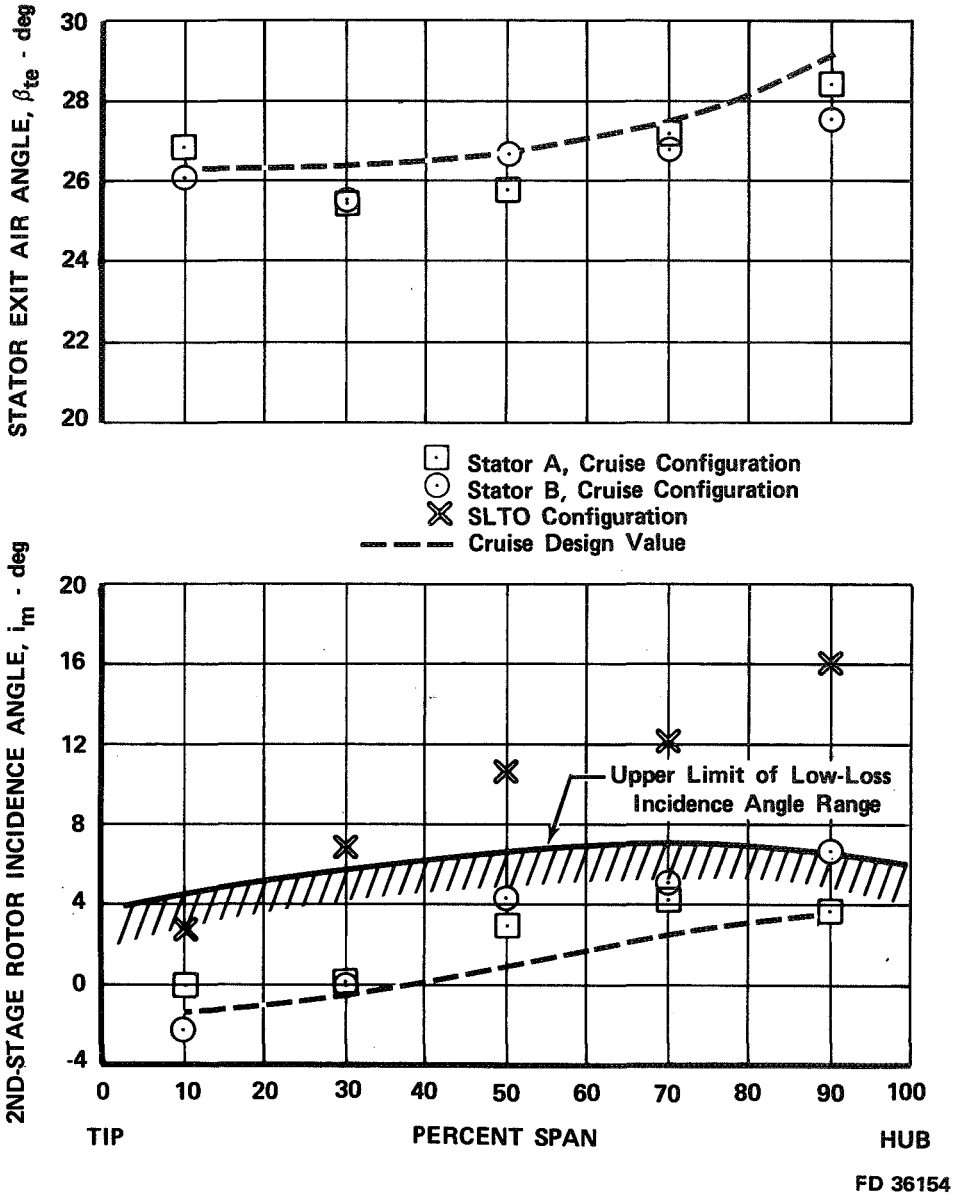

Figure 49. Stator Exit Air Angle and Hypothetical Second-Stage Rotor Incidence Angle for Cruise Configurations Operating at Cruise Corrected Rotor Speed and Flow

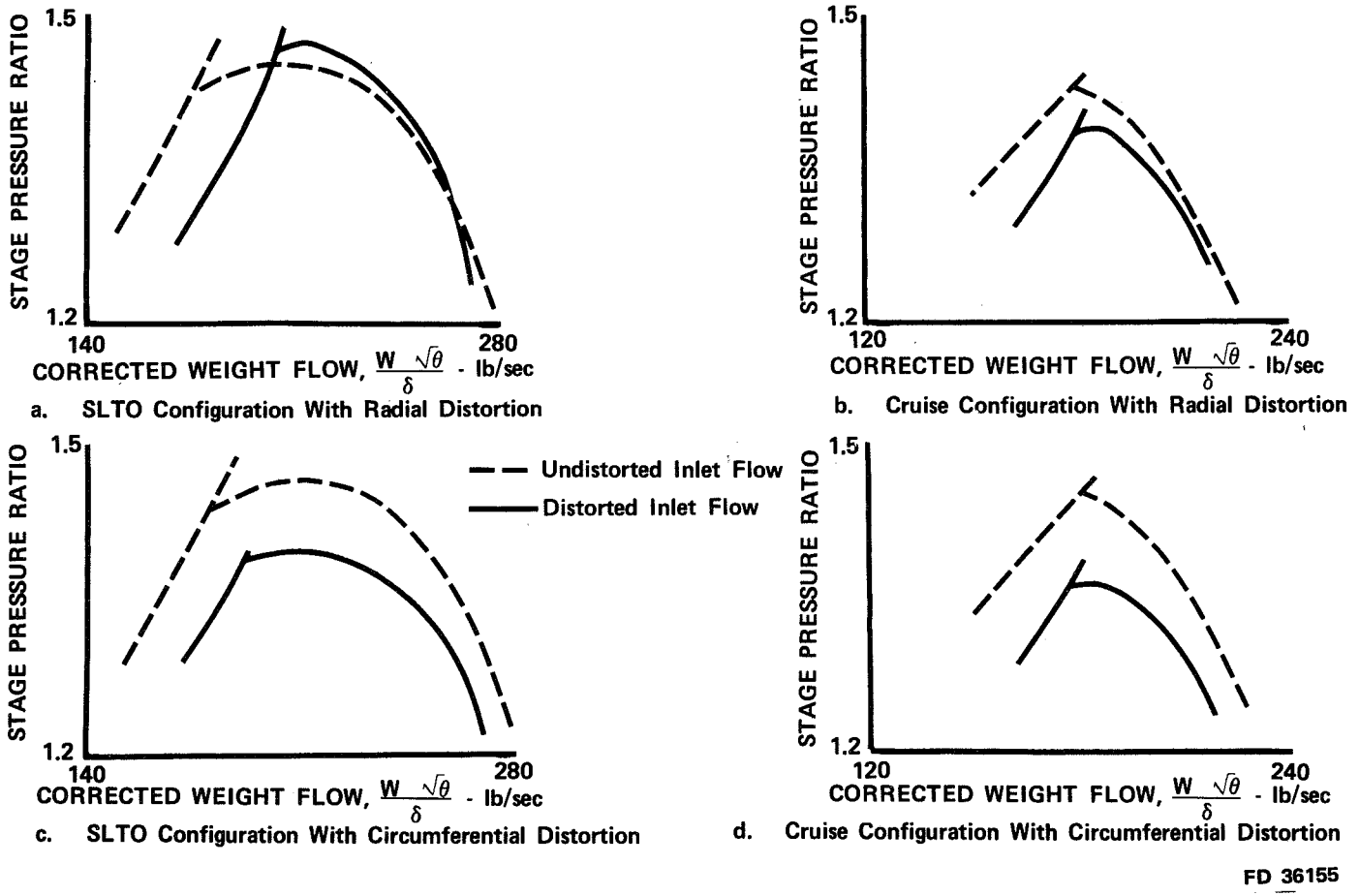

Figure 50. Influence of Radial and Circumferential Distortion on Stall Limit of Stator B Stage at Design Corrected Rotor Speed

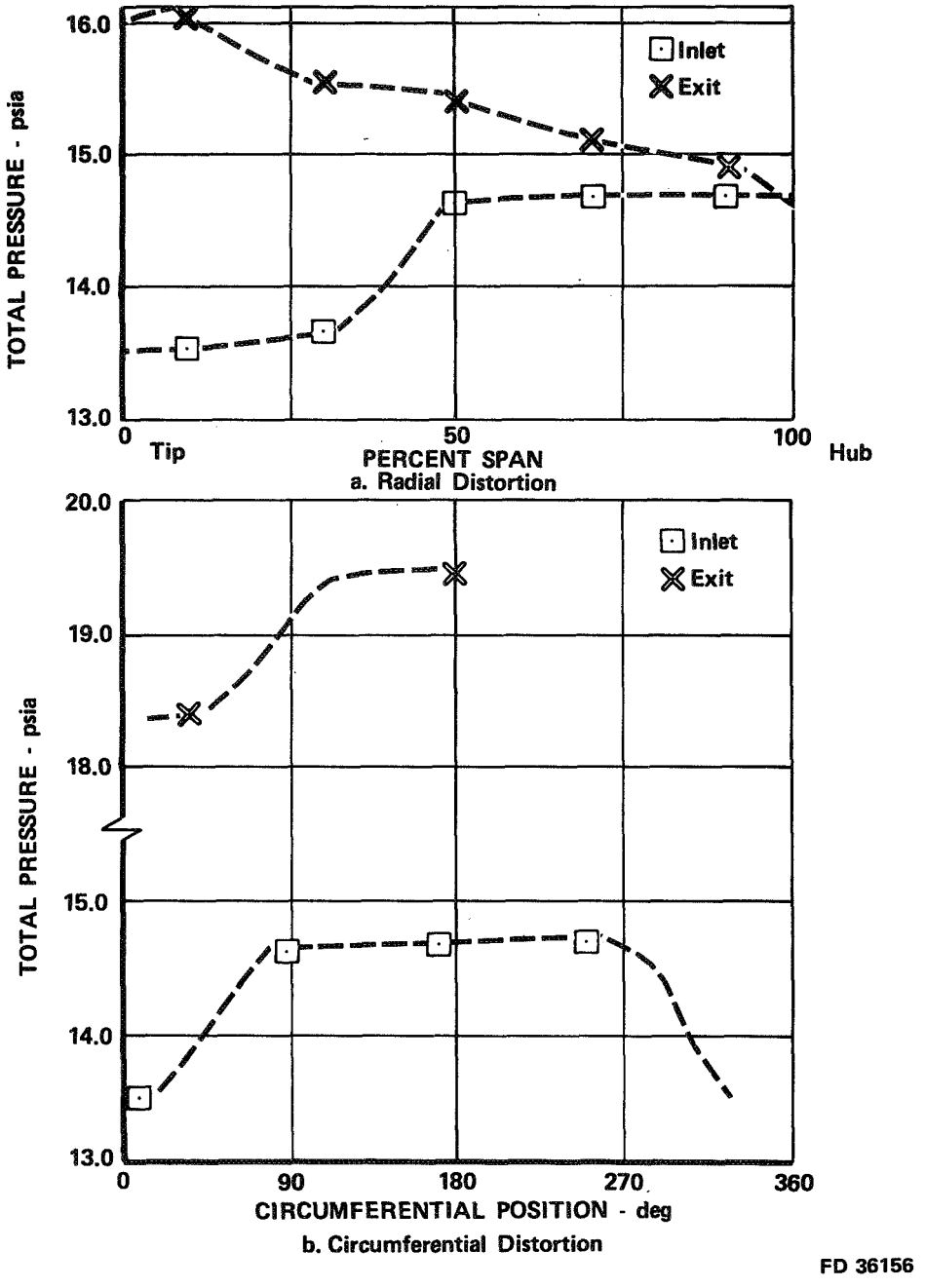

Figure 51. Stage Inlet and Exit Total Pressure Profiles; SLTO Configuration Near SLTO Design Flow Conditions

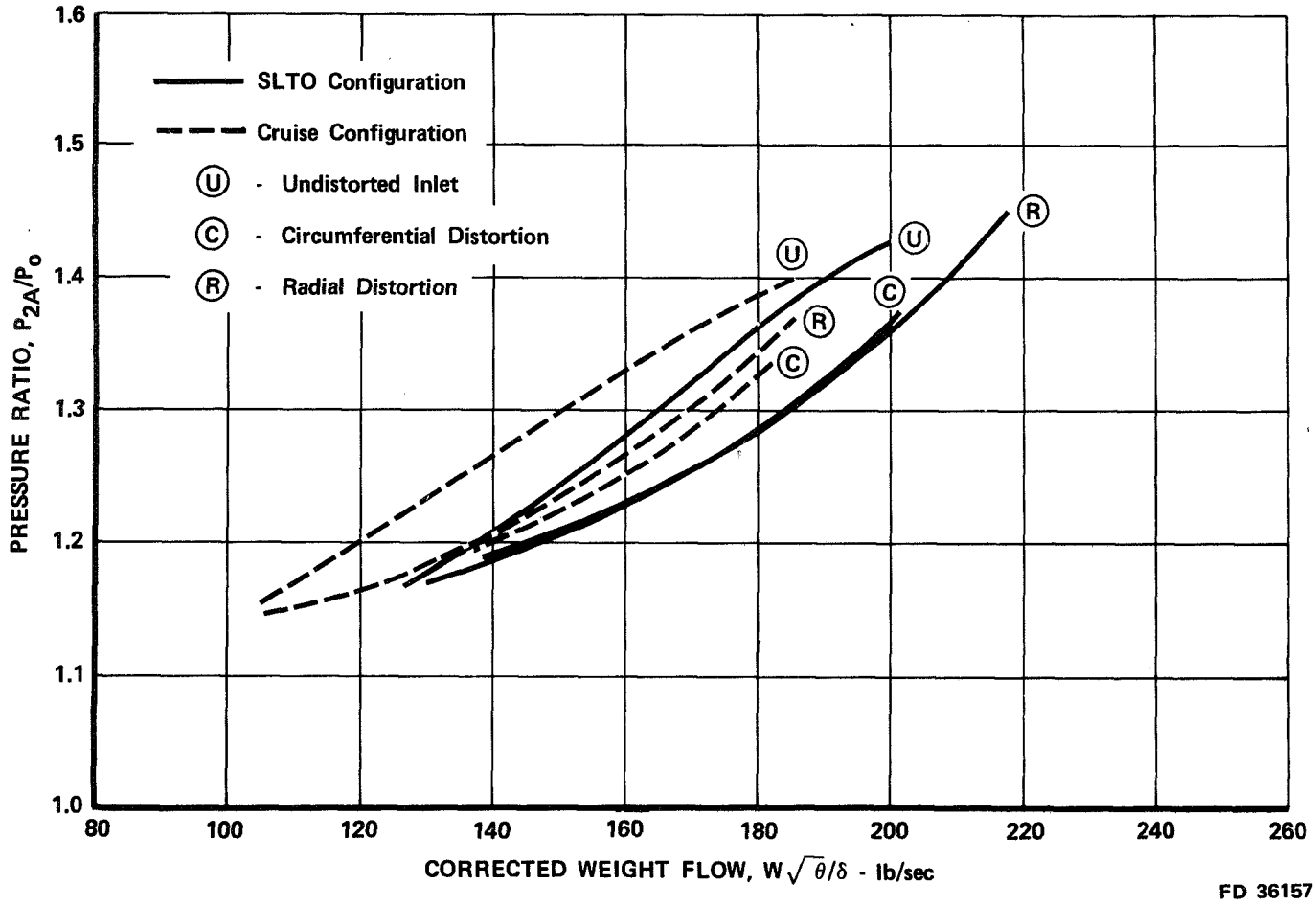

Figure 52. Influence of Inlet Guide Vane Turning on Stall Line; Stator B Stage

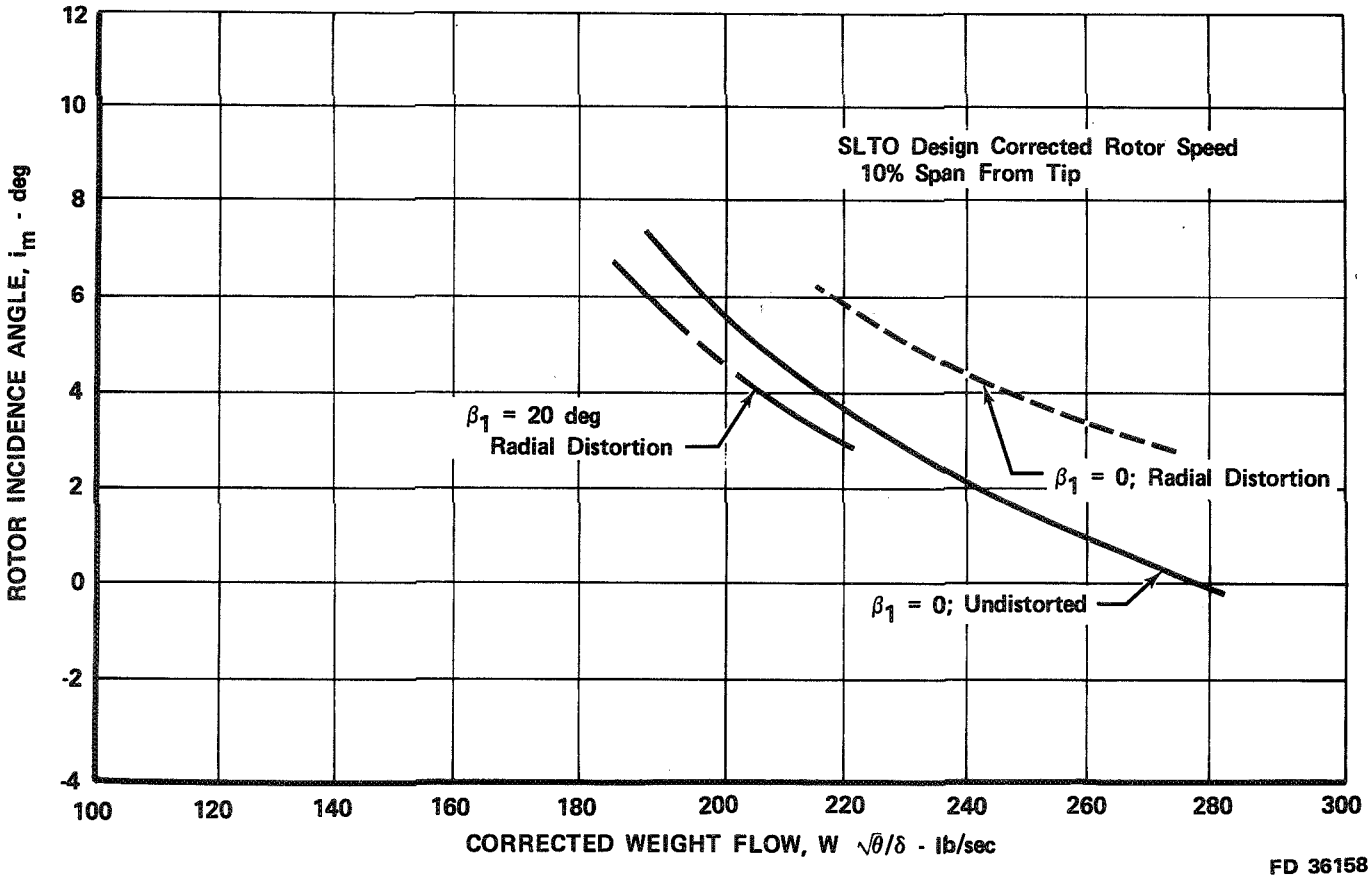

Figure 53. Influence of Guide Vane Tip Turning on Rotor Tip Incidence Angle with Radial Distortion

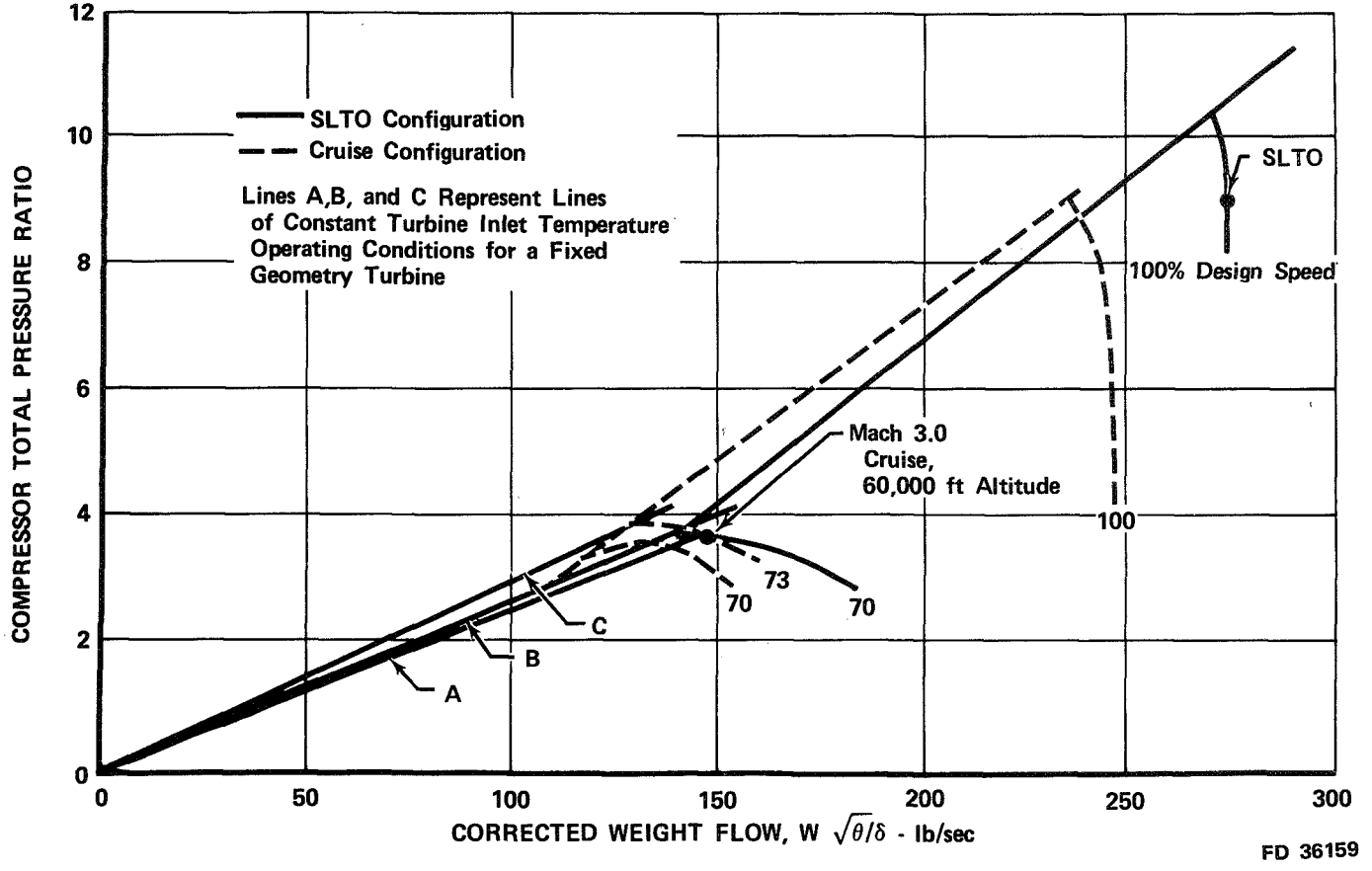

Figure 54. Influence of Variable Geometry Front Stage on Calculated Eight-Stage Compressor Pressure Ratio-Flow Characteristic

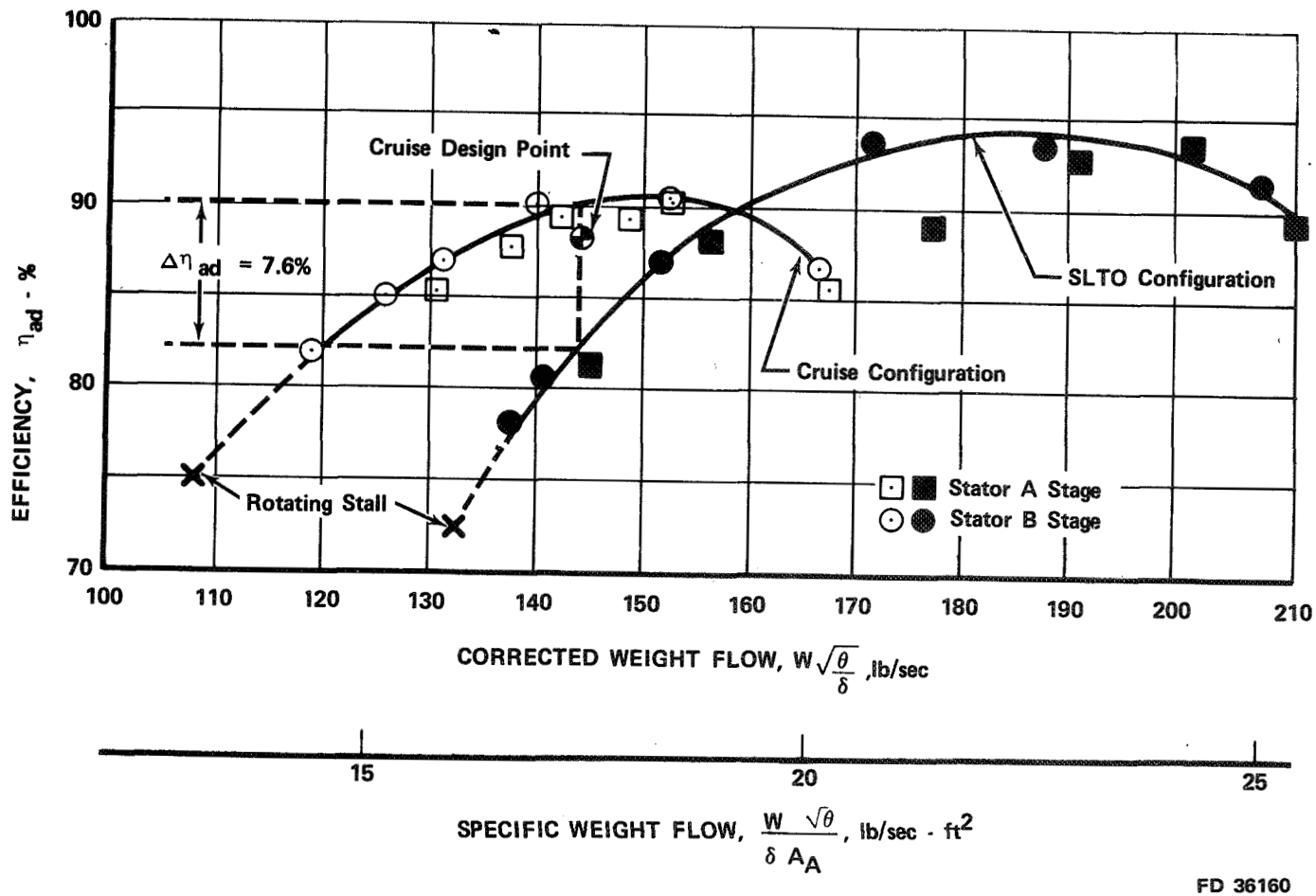

Figure 55. Effect of Variable Geometry Features on Stage Efficiency and Range at Cruise Corrected Rotor Speed

Table 1. Streamline Diameters

Percent Span from Tip at Leading Edge of Blade Row	Inlet Guide Vane		Rotor		Stator	
	Leading Edge	Trailing Edge	Leading Edge	Trailing Edge	Leading Edge	Trailing Edge
0	43.28	43.28	43.050	42.67	42.50	42.10
10	40.75	40.75	40.865	40.45	40.669	40.40
30	35.85	36.10	36.495	36.495	37.007	37.00
50	30.95	31.40	32.125	32.75	33.345	35.70
70	26.05	26.80	27.755	29.10	29.68	30.45
90	21.15	22.20	23.385	25.40	26.02	27.10
100	18.70	19.86	21.200	23.65	24.19	25.61

All dimensions in inches.

Table 2. General Design Performance Data

SLTO Design Point	
Rotor Pressure Ratio, $\bar{P}_2/\bar{P}_1$	1.351
Stage Pressure Ratio, $\bar{P}_{2A}/P_o$	1.321
Rotor Efficiency, η_{ad} - %	92.2
Stage Efficiency, η_{ad} - %	85.1
Corrected Rotor Speed, $N/\sqrt{\theta}$ - rpm	6050.0
Corrected Weight Flow, $W\sqrt{\theta}/\delta$ - lb/sec	265.0
Corrected Specific Weight Flow, $W\sqrt{\theta}/\delta A_A$ - lb/sec-ft^2	32.0
Corrected Rotor Tip Velocity - ft/sec	
Cruise Design Point	
Rotor Pressure Ratio, $\bar{P}_2/\bar{P}_1$	1.137
Stage Pressure Ratio, $\bar{P}_{2A}/P_o$	1.132
Rotor Efficiency, η_{ad} - %	93.5
Stage Efficiency, η_{ad} - %	88.3
Corrected Rotor Speed, $N/\sqrt{\theta}$ - rpm	4235.0
Corrected Weight Flow, $W\sqrt{\theta}/\delta$ - lb/sec	143.3
Corrected Specific Weight Flow, $W\sqrt{\theta}/\delta A_A$ - lb/sec-ft^2	17.28
Corrected Rotor Tip Velocity - ft/sec	

Table 3. Inlet Guide Vane Velocity Diagram Data

Percent Span from Tip at Leading Edge	V_{1e}	β_{mle}	V_{te}	V_{mte}	$V_{\theta te}$	β_{mte}	M_{1e}	$\Delta\beta$	ϵ_{te}
SLTO Design Point									
90	441.0	0.0	475.1	475.1	0.0	0.0	0.400	0.0	12.1
70	460.0	0.0	496.3	496.3	0.0	0.0	0.419	0.0	7.9
50	473.1	0.0	509.2	509.2	0.0	0.0	0.432	0.0	4.2
30	477.6	0.0	514.2	514.2	0.0	0.0	0.435	0.0	1.1
10	477.0	0.0	512.1	512.1	0.0	0.0	0.434	0.0	-1.4
Cruise Design Point									
90	218.9	0.0	293.9	243.8	164.1	33.8	0.199	-33.8	12.1
70	230.9	0.0	288.1	246.9	148.6	31.1	0.208	-31.1	8.1
50	238.3	0.0	283.8	250.4	134.0	28.2	0.215	-28.2	4.8
30	242.3	0.0	279.7	253.5	118.9	25.0	0.218	-25.0	1.8
10	242.4	0.0	274.4	254.3	113.0	21.9	0.218	-21.9	-1.0

Table 4. Inlet Guide Vane Geometry

Airfoil Series: 63
No. of Vanes: 20
Thickness Ratio: 0.09

Diameter, ID: 18.70 in. (Leading Edge)
Diameter, OD: 43.20 in. (Leading Edge)

Percent Span (from Tip)	κ_1	κ_2	ϕ	$\gamma°$	c	σ	$\delta°$
Basic Airfoil*							
90	-19.9(-20.2)**	23.7(25.0)	43.6(45.2)	14.1(13.5)	4.52	1.412	1.4
70	-20.0(-20.2)	22.5(23.3)	42.5(43.5)	13.2(12.6)	4.52	1.245	2.1
50	-20.2(-20.2)	21.2(21.5)	41.4(41.7)	12.2(12.1)	4.52	1.080	2.8
30	-20.4(-20.2)	19.9(19.9)	40.3(40.1)	11.2(11.5)	4.52	0.913	3.5
10	-20.6(-20.2)	18.6(18.0)	39.2(38.2)	10.2(10.5)	4.52	0.748	4.2
SLTO Design Point							
90	-20.2	5.4	*	1.2	4.55	1.412	*
70	-20.2	3.7	*	0.5	4.55	1.245	*
50	-20.2	1.9	*	-0.2	4.55	1.080	*
30	-20.2	0.3	*	-0.9	4.55	0.913	*
10	-20.2	-1.6	*	-1.6	4.55	0.748	*
Cruise Design Point							
90	-20.2	36.0	56.2	21.1	4.47	1.412	2.2
70	-20.2	34.3	54.5	20.5	4.47	1.245	3.2
50	-20.2	32.5	52.7	19.9	4.47	1.080	4.3
30	-20.2	30.9	50.9	19.2	4.47	0.913	5.9
10	-20.2	29.0	49.2	18.5	4.47	0.748	7.1

*See Reference 2, Section II on "Variable Geometry Inlet Guide Vane and Stator Blading."
**Numbers in parentheses refer to modified basic airfoil.

Table 5. Rotor Velocity Diagram Data

Percent Span from Tip at Leading Edge	V'_{le}	V_{mle}	$V'_{\theta le}$	β'_{mle}	V'_{te}	V_{mte}	$V_{\theta te}$	β'_{mte}	U_{le}	U_{te}	M'_{le}	$\Delta\beta$	D_f	ϵ_{le}	ϵ_{te}
SLTO Design Point															
90	804.9	517.8	617.8	50.0	584.8	531.8	239.5	24.9	617.8	670.5	0.738	25.1	0.4787	17.1	16.1
70	908.5	534.4	734.2	53.9	658.2	529.5	396.1	36.8	734.2	769.0	0.832	17.1	0.4371	10.4	9.7
50	1009.2	545.5	849.1	57.3	743.8	522.5	531.0	45.9	849.1	865.5	0.929	11.4	0.4024	5.1	4.6
30	1107.4	548.0	963.9	60.2	826.0	513.3	648.2	51.9	963.9	964.2	1.019	8.3	0.3814	0.8	0.7
10	1208.8	544.0	1080.0	63.2	905.5	497.9	758.9	56.7	1080.0	1071.0	1.110	6.5	0.3721	-2.9	-2.9
Cruise Design Point															
90	378.7	260.8	226.2	46.9	316.3	285.9	131.7	25.0	431.2	567.5	0.341	21.9	0.4040	17.1	16.9
70	450.9	261.9	368.8	54.8	353.5	282.4	210.0	36.8	513.1	536.4	0.409	18.0	0.3808	11.5	11.9
50	531.7	265.0	462.5	60.4	402.7	286.8	284.5	45.0	594.6	604.5	0.482	15.4	0.3933	6.5	7.1
30	618.3	267.1	557.3	64.5	465.5	293.2	361.2	50.9	674.8	673.0	0.560	13.6	0.3874	2.0	2.5
10	702.5	267.8	649.8	67.8	522.0	295.9	431.8	55.4	752.5	744.5	0.635	12.4	0.3965	-2.2	-2.4

Table 6. Rotor Geometry and Performance

Airfoil Series: Circular Arc
No. of Blades: 34
Diameter, ID: 21.20 in. (Leading Edge)
Diameter, OD: 43.05 in. (Leading Edge)

Percent Span (from Tip)	κ_1	κ_2	ϕ	$\gamma°$	c	t/c	σ	i_m	$\delta°$	$\bar{\omega}'$
SLTO Design Point										
90	48.6	18.8	29.8	31.2	3.24	0.075	1.42	1.4	6.1	0.024
70	52.5	32.5	20.0	41.2	3.43	0.065	1.30	1.4	4.3	0.024
50	56.1	42.1	14.0	48.2	3.63	0.055	1.20	1.2	3.8	0.033
30	59.6	48.6	11.0	53.6	3.82	0.045	1.12	0.4	3.3	0.058
10	63.2	52.9	10.3	57.9	4.01	0.035	1.06	0.0	3.8	0.097
Cruise Design Point										
90	48.6	18.8	29.8	31.2	3.24	0.075	1.42	-1.7	6.2	0.030
70	52.5	32.5	20.0	41.2	3.43	0.065	1.30	2.3	4.3	0.018
50	56.1	42.1	14.0	48.2	3.63	0.055	1.20	4.3	2.9	0.030
30	59.6	48.6	11.0	53.6	3.82	0.045	1.12	4.9	2.3	0.064
10	63.2	52.9	10.3	57.9	4.01	0.035	1.06	4.5	2.5	0.125

Table 7. Stator Velocity Diagram Data

Percent Span from Tip at Leading Edge	V_{le}	V_{mle}	$V_{\theta le}$	β_{mle}	V_{te}	V_{mte}	$V_{\theta te}$	β_{mte}	M_{le}	$\Delta\beta$	D_f	ϵ_{le}	ϵ_{te}
SLTO Design Point													
90	696.5	559.2	416.2	36.7	593.9	591.9	43.2	4.1	0.620	32.6	0.362	14.6	6.8
70	661.3	551.5	370.0	33.8	571.9	571.0	26.8	2.6	0.587	31.2	0.350	8.5	3.8
50	634.9	541.2	332.5	31.5	561.0	560.5	19.2	1.8	0.561	29.7	0.335	3.7	1.5
30	617.2	530.0	315.5	30.8	559.7	559.7	18.3	1.8	0.542	29.0	0.319	0.1	0.0
10	604.5	516.5	312.7	31.2	565.9	564.9	20.7	2.1	0.528	28.6	0.298	3.4	-1.6
Cruise Design Point													
90	445.5	298.5	330.0	47.7	313.8	274.0	153.1	29.2	0.400	18.5	0.455	15.5	7.5
70	437.4	294.3	324.5	47.8	333.1	295.1	153.0	27.5	0.392	20.3	0.400	10.6	5.4
50	435.0	297.5	318.1	46.9	351.5	314.1	157.3	26.7	0.388	20.2	0.358	9.8	3.2
30	435.1	301.8	314.5	46.2	370.3	331.8	164.1	26.4	0.388	19.8	0.311	1.4	1.0
10	539.5	303.8	317.4	46.2	392.4	351.5	174.1	26.4	0.389	19.8	0.268	-3.2	1.3

Table 8. Stator Geometry and Performance

Airfoil Series: 65
No. of Vanes: 40
Thickness Ratio: 0.08

Diameter, ID: 24.19 in. (Leading Edge)
Diameter, OD: 42.25 in. (Leading Edge)

Percent Span (from Tip)	κ_1	κ_2	ϕ	$\gamma°$	c	σ	i_m	$\delta°$	$\bar{\omega}'$
SLTO Design Point (Both Stators)									
90	40.9	-8.7	49.6	16.0	2.75	1.28	-4.2	12.8	0.026
70	37.1	-7.5	44.6	14.5	2.88	1.19	-3.3	10.1	0.025
50	34.7	-7.5	42.2	13.5	3.00	1.12	-3.2	9.3	0.026
30	34.0	-8.0	42.0	13.2	3.13	1.07	-3.2	9.8	0.029
10	36.0	-8.9	44.9	13.5	3.27	1.02	-4.8	11.0	0.032
Cruise Design Point (Stator A)									
90	40.9	17.3	-	-	-	1.28	6.8	11.9	0.040*
70	37.1	18.5	-	-	-	1.19	10.7	9.0	0.038
50	34.7	18.5	-	-	-	1.12	12.2	8.2	0.030
30	34.0	18.0	-	-	-	1.07	12.2	8.4	0.024
10	36.0	17.1	-	-	-	1.02	10.2	9.3	0.027
Cruise Design Point (Stator B)									
90	49.9	17.3	-	-	-	1.28	-2.2	11.9	0.040
70	46.1	18.5	-	-	-	1.19	1.7	9.0	0.038
50	43.7	18.5	-	-	-	1.12	3.2	8.2	0.030
30	43.0	18.0	-	-	-	1.07	3.2	8.4	0.024
10	45.0	17.1	-	-	-	1.02	1.2	9.3	0.027

*No loss allowance was made for the effect of high incidence operation on loss coefficient of the single-flap stator.

APPENDIX A

DEFINITION OF CALCULATED PERFORMANCE VARIABLES

Overall Performance Data

Stage Pressure Ratio.

Undistorted Inlet Flow:

$$\frac{\bar{P}_{2A}}{P_o}$$

Distorted Inlet Flow:

$$\frac{\bar{P}_{2A}}{\bar{P}_o}$$

For Circumferential Distortion:

$$\bar{P}_0 = \frac{(3)\ \bar{P}_{0\ \text{undistorted}} + (1)\ \bar{P}_{0\ \text{distorted}}}{4}$$

$$\bar{P}_{2A} = \frac{(3)\ \bar{P}_{2A\ \text{undistorted}} + (1)\ \bar{P}_{2A\ \text{distorted}}}{4}$$

and

$$\bar{T}_{2A} = \frac{(3)\ \bar{T}_{2A\ \text{undistorted}} + (1)\ \bar{T}_{2A\ \text{distorted}}}{4}$$

Corrected Flow.

$$W\sqrt{\theta}\,/\,\delta$$

Corrected Specific Flow.

$$\frac{W\sqrt{\theta}}{\delta A_A}$$

Adiabatic Efficiency.

$$\eta_{ad} = \frac{(\bar{P}_{2A}/P_o)^{\frac{\gamma - 1}{\gamma}} - 1}{\bar{T}_{2A}/T_o}$$

Blade Element Data

Incidence Angle:

$$i_m = \beta_{1e} - \kappa_{1e}$$

Diffusion Factor:

$$\text{Rotor:} \quad D = 1 - \frac{V'_{te}}{V'_{1e}} + \left(\frac{d_{te} V_{\theta te} - d_{1e} V_{\theta 1e}}{\left(d_{1e} + d_{te}\right) \sigma V'_{1e}} \right)$$

$$\text{Stator:} \quad D = 1 - \frac{V_{te}}{V_{1e}} + \left(\frac{d_{1e} V_{\theta 1e} - d_{te} V_{\theta te}}{\left(d_{1e} + d_{te}\right) \sigma V_{1e}} \right)$$

Deviation Angle:

$$\delta^\circ = \beta_{te} - \kappa_{te}$$

Loss Coefficient:

$$\text{IGV:} \quad \bar{\omega} = \frac{P_{fs} - \bar{P}_1}{P_{fs} - P_o}$$

(P_o was found from linear interpolation of inner and outer wall static pressures at Station 0.)

$$\text{Rotor:} \quad \bar{\omega}' = \frac{P'_{2id} - P'_2}{P'_1 - P_1}$$

where:

$$P'_{2id} = P'_1 \left\{ 1 + \frac{\gamma - 1}{2} \left(\frac{U_{te}^2}{a'^2_{0_1}} \right) \left[1 - \left(\frac{d_{1e}}{d_{te}} \right)^2 \right] \right\}^{\frac{\gamma}{\gamma - 1}}$$

P' is found from $p/P' = \left[1 + \frac{\gamma - 1}{2} M'^2\right]^{\frac{\gamma}{\gamma - 1}}$

and M' is calculated using trigonometric functions and the measurements of U, β, P, and p.

Stator: $\bar{\omega} = \frac{P_{fs} - \bar{P}_{2A}}{P_{fs} - P_2}$

APPENDIX B

DEFINITION OF SYMBOLS

A_A	Flowpath annular area, ft^2
a'_{0_1}	Inlet relative stagnation velocity of sound, ft/sec
c	Chord length, in.
c_p	Specific heat of air, 0.24 Btu/lb°F
d	Diameter
D	Diffusion factor
i_m	Incidence angle based on mean camber line, deg (equivalent circular arc mean camber for stators)
Δi	Change in rotor incidence angle
M	Mach number
P	Total pressure, psia
p	Static pressure, psia
q	Pressure equivalent of the velocity head, psia
r	Radius
R	Gas constant for air, 53.3 ft-lb/lb-°R
S	Blade spacing, in.
s	Blade span, in.
T	Total temperature, °R
T_s	Static temperature, °R
t	Blade maximum thickness, in.
U	Rotor speed, ft/sec
V	Velocity, ft/sec

W	Actual flowrate, lb_m/sec
B/r, C, Dr, Er^2	Characteristic tangential velocity distributions (reference 1), where B, C, D, and E are constants
β	Air angle, deg
ϵ	Flow angle in meridional plane
γ	Ratio of specific heats
$\Delta\beta$	Flow turning angle
$\gamma°$	Blade-Chord angle, deg
δ	Ratio of total pressure to NASA standard sea level pressure of 14.696 psia
$\delta°$	Deviation angle, deg
η_{ad}	Adiabatic efficiency
θ	Ratio of total temperature to NASA standard sea level temperature of 518.7°R or guide vane turning angle
κ	Blade metal angle, deg (based on equivalent circular arc for stators)
ρ	Density, lb_m/ft^3
σ	Solidity, c/S
ϕ	Blade camber angle, deg (based on equivalent circular arc for Stator B and on the 0.5% chord and 95% chord for the IGV)
$\bar{\omega}$	Total pressure loss coefficient

Subscripts

0	Compressor inlet instrumentation station
1	Guide vane exit/rotor inlet instrumentation station
2	Rotor exit/stator inlet instrumentation station
2A	Stator exit instrumentation station

fs	Freestream value of guide vane or stator rake total pressure
id	Isentropic condition
le	Leading edge
te	Trailing edge
m	Meridional component
M	Midspan
s	Static condition
z	Axial component
θ	Tangential component

Superscripts

'	Relative to rotor blade
$\bar{}$	Mass average value (used for overall and blade element performance)

REFERENCES

1. Steinke, Ronald J. and James E. Crouse, "Preliminary Analysis of the Effectivieness of Variable-Geometry Guide Vanes to Control Rotor-Inlet Flow Conditions," NASA TN D-3823, January 1967.

2. Jones, B.A. and D.L. Wright, "Single Stage Experimental Evaluation of Variable Geometry Guide Vanes and Stators: Part 1 - Analysis and Design," NASA CR-54554, August 1968.

3. Jones, B.A. and R.P. Oscarson, "Single Stage Experimental Evaluation of Variable Geometry Guide Vanes and Stator Blading: Part III - Data and Performance for Variable Camber Guide Vane and Stator A," NASA CR-54556, December 1968.

4. Jones, B.A. and R.P. Oscarson, "Single Stage Experimental Evaluation of Variable Geometry Guide Vanes and Stator Blading: Part IV - Data and Performance for Variable Camber Guide Vane and Stator B," NASA CR-54557, December 1968.

5. Jones, B.A., R.P. Oscarson and C.E. Clark, "Single Stage Experimental Evaluation of Variable Geometry Guide Vanes and Stator Blading: Part V - Overall Performance for Variable Camber Guide Vane and Stator B with Radial and Circumferential Inlet Flow Distortion," NASA CR-54558, December 1968.

6. "Single Stage Experimental Evaluation of Variable Geometry Guide Vanes and Stator: Part II - Annular Cascade Investigation of Candidate Variable Geometry Designs," NASA CR-54555, July 1967.

7. Dunavant, James C., "Cascade Investigation of a Related Series of 6-Percent-Thick Guide-Vane Profiles and Design Charts," NASA TN-3959, May 1957.

8. "Aerodynamic Design of Axial Flow Compressors (Revised)," NASA SP-36, 1965.

9. "Single Stage Experimental Evaluation of Slotted Rotor and Stator Blading: Part VII - Data and Performance for Slotted Stator 2," NASA CR-54550, September 1967.

10. Abbott, Ira H. and Albert E. Von Doenhoff, "Theory of Wing Sections," Dover Publications, Inc., June 1959.

11. Lieblein, Seymour, Francis C. Schwenk, and Robert L. Broderick, "Diffusion Factor for Estimating Losses and Limiting Blade Loadings in Axial Flow Compressor Blade Elements," NACA RM E53D01, 1953.

12. Mikolajczak, A.A., H.D. Weingold, and J.P. Nikkanen, "Flow Through Cascades of Slotted Compressor Blades," Paper No. 69-GT-6 presented at ASME Gas Turbine Conference, Cleveland, Ohio, March 1969.

13. Katsanis, Theodore and W.D. McNally, "Programs for Computation of Velocities and Streamlines on a Blade-to-Blade Surface of a Turbo-Machine," NASA TN-D5044, March 1969.

14. Reid, C., "The Response of Axial Flow Compressors to Intake Flow Distortion," Paper No. 69-GT-29 presented at the ASME Gas Turbine Conference, Cleveland, Ohio, March 1969.

15. Langston, C.E., "Distortion Tolerance - By Design Instead of By Accident," Paper No. 69-GT-115, presented at the ASME Gas Turbine Conference, Cleveland, Ohio, March 1969.

16. Voit, Charles H., "Investigation of a High Pressure-Ratio Eight-Stage Axial-Flow Research Compressor with Two Transonic Inlet Stages, Part 1: Aerodynamic Design," NACA RM E 53124, December 1953.

17. Voit, Charles H. and Richard P. Geye, "Investigation of a High-Pressure-Ratio Eight-Stage Axial-Flow Research Compressor With Two Transonic Inlet Stages, Part III: Individual Stage Performance Characteristics," NACA RM E 54H17, November 1954.

DISTRIBUTION LIST

Contract NAS3-7604

		Copies
1. NASA-Lewis Research Center 21000 Brookpark Road Cleveland, Ohio 44135 Attention:		
Report Control Officer	MS 5-5	1
Technical Utilization Office	MS 3-19	1
Library	MS 60-3	2
Fluid System Components Division	MS 5-3	1
Pump and Compressor Branch	MS 5-9	6
Dr. B. Lubarsky	MS 3-3	1
A. Ginsburg	MS 5-3	1
M. J. Hartmann	MS 5-9	1
W. A. Benser	MS 5-9	1
D. M. Sandercock	MS 5-9	1
L. J. Herrig	MS 7-1	1
T. F. Gelder	MS 5-9	1
C. L. Ball	MS 5-9	1
L. Reid	MS 5-9	1
L. W. Schopen	MS 77-3	1
S. Lieblein	MS 100-1	1
C. L. Meyer	MS 60-4	1
J. H. Povolny	MS 60-4	1
A. W. Goldstein	MS 7-1	1
J. J. Kramer	MS 7-1	1
W. L. Beede	MS 5-3	1
C. H. Voit	MS 5-3	1
E. E. Bailey	MS 5-9	1
2. NASA Scientific and Technical Information Facility P. O. Box 33 College Park, Maryland 20740 Attention: NASA Representative		6
3. FAA Headquarters 800 Independence Ave., S. W. Washington, D. C. 20553 Attention: Brig. General J. C. Maxwell		1
4. NASA Headquarters Washington, D. C. 20546 Attention: N. F. Rekos (RAP)		1
5. U.S. Army Aviation Material Laboratory Fort Eustes, Virginia Attention: John White		1

		Copies
6.	Headquarters Wright Patterson AFB, Ohio 45433	
	Attention: J. L. Wilkins, SESOS	1
	S. Kobelak, APTP	1
	R. P. Carmichael, SESSP	1
7.	Department of Navy Bureau of Weapons WAshington, D. C. 20525	
	Attention: Robert Brown, RAPP14	1
8.	Department of Navy Bureau of Ships Washington, D. C. 20360	
	Attention: G. L. Graves	1
9.	NASA-Langley Research Center Technical Library Hampton, Virginia 23365	
	Attention: Mark R. Nichols	1
	John V. Becker	1
10.	Boeing Company Commercial Airplane Division P. O. Box 3991 Seattle, Washington 98124	
	Attention: C. J. Schott NS80-66	1
11.	Douglas Aircraft Company 3855 Lakewood Boulevard Long Beach, California 90801	
	Attention: J. E. Merriman	1
	Technical Information Center C1-250	
12.	Pratt & Whitney Aircraft Florida Research & Development Center P. O. Box 2691 West Palm Beach, Florida 33402	
	Attention: R. A. Schmidtke	1
	H. D. Stetson	1
	J. M. Silk	1
	W. R. Alley	1
	R. W. Rockenbach	1
	B. A. Jones	1
	B. S. Savin	1
	J. A. Fligg	1

		Copies
13.	Pratt & Whitney Aircraft 400 Main Street East Hartford, Connecticut	
	Attention: R. E. Palatine	1
	T. G. Slaiby	1
	P. Tramm	1
	M. J. Keenan	1
	B. B. Smyth	1
	A. A. Mikolajczak	1
	Library (UARL)	1
14.	Allison Division, GMC Deparment 8894, Plant 8 P. O. Box 894 Indianapolis, Indiana 46206	
	Attention: J. N. Barney	1
	G. E. Holbrook	1
	B. A. Hopkins	1
	R. J. Loughery	1
	Library	1
	J. L. Dillard	1
15.	Northern Research and Engineering 219 Vassar Street Cambridge 39, Massachusetts	
	Attention: K. Ginwala	1
16.	General Electric Company Flight Propulsion Division Cincinnati 15, Ohio	
	Attention: J. W. Blanton J-19	1
	W. G. Cornell K-49	1
	J. Ringrose H-79	1
	E. E. Hood/J. C. Pirtle J-165	1
	J. F. Klapproth H-42	1
	J. W. McBride H-44	1
	L. H. Smith H-50	1
	S. N. Suciu H-32	1
	J. B. Taylor J-168	1
	Technical Information Center N-32	1
	Marlen Miller H-50	1
17.	General Electric Company 1000 Western Avenue West Lynn, Massachusetts	
	Attention: D. P. Edkins - Bldg. 2-40	1
	F. F. Ehrich - Bldg. 2-40	1
	L. H. King - Bldg. 2-40	1
	R. E. Neitzel - Bldg. 2-40	1
	Dr. C. W. Smith Library Bldg. 2-40M	1

		Copies
18.	Curtiss-Wright Corporation Wright Aeronautical Woodridge, New Jersey Attention: S. Lombardo G. Provenzale J. Wiggins	 1 1 1
19.	Air Research Manufacturing Company 402 South 36th Street Phoenix, Arizona 85034 Attention: Robert O. Bullock John H. Deman	 1 1
20.	Air Research Manufacturing Company 8951 Sepulveda Boulevard Los Angeles, California 90009 Attention: Linwood C. Wright	 1
21.	Union Carbide Corporation Nuclear Division Oak Ridge Gaseous Diffusion Plant P. O. Box "P" Oak Ridge, Tennessee 37830 Attention: R. G. Jordan D. W. Burton, K-1001, K-25	 1 1
22.	Avco Corporation Lycoming Division 550 South Main Street Stratford, Connecticut Attention: Clause W. Bolton	 1
23.	Continental Aviation & Engineering Corp. 12700 Kercheval Detroit, Michigan 48215 Attention: Eli H. Benstein Howard C. Walch	 1 1
24.	Solar San Diego, California 92112 Attention: P. A. Pitt Mrs. L. Walper	 1 1
25.	Goodyear Atomic Corporation Box 628 Piketon, Ohio Attention: C. O. Langebrake	 2
26.	Iowa State University of Science and Technology Ames, Iowa 50010 Attention: Professor George K. Serovy Dept. of Mechanical Engineering	 1

		Copies
27.	Hamilton Standard Division of United Aircraft Corporation Windsor Locks, Connecticut Attention: Mr. Carl Rohrbach Head of Aerodynamics and Hydrodynamics	1
28.	Westinghouse Electric Corporation Small Steam and Gas Turbine Engineering B-4 Lester Branch P. O. Box 9175 Philadelphia, Pennsylvania 19113 Attention: Mr. S. M. DeCorso	1
29.	J. Richard Joy Supervisor, Analytical Section Williams Research Corporation P. O. Box 95 Walled Lake, Michigan	1
30.	Raymond S. Poppe Building 541, Dept. 80-91 Lockheed Missile and Space Company P. O. Box 879 Mountain View, California 94040	1
31.	James D. Raisbeck The Boeing Company 224 N. Wilkinson Dayton, Ohio 45402	1
32.	James Furlong Chrysler Corporation Research Office Dept. 9000 P. O. Box 1118 Detroit, Michigan 48231	1
33.	Elliott Company Jeannette, Pennsylvania 15644 Attention: J. Rodger Schields Director-Engineering	1
34.	R. H. Carmody Dresser Industries Inc. Clark Gas Turbine Division 16530 Peninsula Boulevard P. O. Box 9989 Houston, Texas 77015	1

		Copies
35.	California Institute of Technology Pasadena, California 91109 Attention: Professor Duncan Rannie	1
36.	Massachusetts Institute of Technology Cambridge, Massachusetts 02139 Attention: Dr. J. L. Kerrebrock	1

Requests for copies of this report should be referred to:

National Aeronautics and Space Administration
Scientific and Technical Information Facility
P.O. Box 33
College Park, Md. 20740